Design, Implementation, and Characterization of a Gravity Heat Pipe

by

Janakiraman Boopathy

Department of Mechanical Engineering

McGill University

Montreal, Quebec, Canada

A thesis submitted to McGill University
in partial fulfilment of the requirements for the degree of
Master of Engineering

Abstract

Gravity heat pipes (GHPs) are closed two-phase thermosyphons, which are also referred to as gravity-assisted wickless heat pipes. They are constructed by first evacuating a closed tube and then filling it with an appropriate amount of a chosen working fluid. The bottom portion of the tube is partially or fully filled with the liquid phase of the working fluid, and it is heated to perform as an evaporator. The upper portion of the tube is cooled and serves as a condenser. The central portion of the tube is usually very well insulated and referred to as an adiabatic section. A GHP operates as follows: the heat input to the evaporator causes the liquid contained within it to boil or evaporate; the generated vapor (being lighter than the liquid) moves upwards and then condenses in the condenser section; the condensate returns back to the evaporator under the action of gravity. Due to the latent heat associated with the phase-change processes, GHPs are able to sustain high rates of heat transfer with relatively small temperature differences, and their effective conductance can be significantly greater than copper rods of corresponding dimensions. This feature, along with their operation as a thermal diode (only one-way transfer of heat), simple construction, and wide operating temperature range, have made GHPs attractive for many applications: examples include heating, ventilating, and air-conditioning (HVAC) systems; enhanced latent-heat thermal energy storage units; permafrost preservation systems; geothermal systems for deicing roads and bridges; and cooling of electronic devices and fuel cells. In this work, a GHP was designed and constructed, along with a set-up that allows basic experimental investigations of this device. Water was used as the working fluid in this research. Experiments were conducted for several different combinations of parameters that lead to periodic unsteady and steady-state operation of the GHP. The design considerations and details of this GHP, the experimental investigation, and the results are presented and discussed concisely in this thesis.

Résumé

Les caloducs gravitaires (CG) sont des thermosiphons fermés à deux phases. On les appelle aussi caloducs sans mèche assistés par gravité. Ils sont construits en vidant un tube fermé et en l'emplissant ensuite avec la quantité appropriée d'un fluide choisi. La partie inférieure du tube est remplie, partiellement ou en entier, avec la phase liquide du fluide de travail, puis est chauffée pour agir en tant qu'évaporateur. La partie supérieure du tube est refroidie et sert de condenseur. La portion centrale du tube est généralement très bien isolée et l'on y fait référence comme la section adiabatique. Un CG opère comme suit : l'apport de chaleur à l'évaporateur fait bouillir ou s'évaporer le liquide contenu à l'intérieur; la vapeur obtenue (étant plus légère que le liquide) se déplace vers le haut et se condense dans le condenseur; le condensé retourne dans l'évaporateur sous l'effet de la gravité. Dû à la chaleur latente associée avec le processus de changement de phase, les CG sont en mesure de soutenir des taux élevés de transfert de chaleur avec des différences de températures relativement faibles, et leur conductance effective peut être significativement plus grande que des tiges de cuivre de dimensions similaires. Cette faculté, ainsi que leur fonctionnement en diode thermique (transfert de chaleur en sens unique seulement), leur construction simple et leur possibilité de fonctionnement dans une grande étendue de températures, ont rendu les CG attirants pour de nombreuses applications : les exemples incluent les systèmes de chauffage, ventilation et climatisation (CVC); les unités de stockage d'énergie thermique à chaleur latente accentuée; les systèmes de préservation du pergélisol, les systèmes géothermiques pour déglacer les routes et les ponts; ainsi que le refroidissement d'appareils électroniques et de réservoirs de carburant. Dans cet exercice, un CG a été conçu et construit, de concert avec une configuration qui permet des recherches expérimentales de base de ce dispositif. L'eau a été utilisée comme le fluide de travail dans cette recherche. Des expériences ont été menées avec plusieurs combinaisons différentes de paramètres qui conduisent à un fonctionnement périodique stable et instable du CG. Les circonstances et les détails de ce CG, des expérimentations ainsi que les résultats sont présentés et décrits de façon concise dans cette thèse

Acknowledgements

I would like to express my sincerest gratitude to my supervisor, Professor B. Rabi Baliga, for accepting me to be one of his students, and for offering me such an interesting and challenging thesis project. His continual support and guidance throughout my M.Eng. studies have been greatly appreciated, and I have most certainly learned a great deal from him.

I would also like to thank the Natural Sciences and Engineering Research Council (NSERC) of Canada, for providing financial support for my work through a research grant to my supervisor (Professor B. R. Baliga). I am also grateful to the Department of Mechanical Engineering at McGill University and my supervisor for providing me teaching and research assistantships during my graduate studies.

To my parents and sister, your continual support and encouragement throughout my studies has been a wonderful gift.

This project could not have been completed were it not for Mr. Ariel Kemer and his technical staff and employees at the Exatec Machine Shop, who machined the components required for the experimental setup. I would also like to thank Mr. Chunilal Mistry, his son Bhavesh, and his technical staff and employees at the Bhavesh Machine Shop.

I would like to thank Mr. Mario Iacobaccio, Chief Electronics Technologist of Mechanical Engineering Department at McGill University, for his technical support and inputs.

For help with a number of formalities related to graduate studies at McGill and the thesis-submission tasks, thanks go to Ms. Shirley Baxendale, Ms. Connie Greco, Ms. Mary Fiorilli, Ms. Anne-Marie Pierre, Rev. Gregory Doyle, Ms. Aimee Jabour, and other staff members of the Department of Mechanical Engineering at McGill University.

Last, but not least, I would also like express me sincerest thanks to my colleagues in the Heat Transfer Laboratory James Medvescek, Yuri Lokhmanets, Kelechi Maxwell Damian Ezeji, Osaid Matar, and Massimo Cimmino for their support and help throughout my time here at McGill University.

Table of Contents

Nomenclature

Bo	Bond number
$\{Bo\}_{Evap}$	Bond number in the evaporator section of the GHP
$c_{p,l}$	Liquid specific heat at constant pressure
C_{loss}	Overall heat-loss conductance of the GHP
C_{GHP}	Conductance of the GHP
$C_{s,f}$	Boiling coefficient for the surface-liquid combination (in Rohsenow correlation)
D_i	Inside diameter of the GHP tube
D_o	Outside diameter of the GHP tube
FR	Fill ratio
g	Gravitational acceleration on earth
Gr	Grashof number
Gr_M	Modified Grashof number
Ga	Galileo number
$\{Gr\}_{Evap;Cond}$	Grashof number in the evaporator and condenser sections of the GHP
h	Heat transfer coefficient
h_{fg}	Latent heat of vaporization
$h_{fg}^{'}$	Modified latent heat of vaporization

Ja	Jacob number
$\{Ja\}_{Evap;Cond}$	Jacob number in the evaporator and condenser sections of the GHP
k_l	Thermal conductivity of the liquid
L	Length of the plate
$L_{Adiabatic}$	Length of the adiabatic section of the GHP
$L_{Condenser}$	Length of the condenser section of the GHP
$L_{Evaporator}$	Length of the evaporator section of the GHP
L_{Total}	Total length of the GHP
$\overline{p}^{vapor}_{cond}$	Time-averaged absolute vapor pressure in the condenser section
Pr	Prandtl number
Pr_l	Prandtl number of the liquid
$\{Pr\}_{Evap;Cond}$	Prandtl number in the evaporator and condenser sections of the GHP
q_{in}	Rate of actual heat input to the evaporator section of the GHP
$q_{in,total}$	Rate of total heat input to the evaporator section of the GHP (including losses)
q_{loss}	Rate of heat loss from the GHP to the ambient
q''_{max}	Maximum heat flux
q''_{min}	Minimum heat flux
q''_s	Heat flux at the surface

Re	Reynolds number
Re_{film}	Film Reynolds number
t	Time
t_{period}	Time period
T	Temperature
T_s	Surface temperature
T_{sat}	Saturation temperature
T_{WB}	Time-averaged temperature of the inlet water to the cooling jacket
$\overline{T}_{cond}^{vapor}$	Time-averaged vapor temperature in the condenser section
$\overline{T}_{cond}^{wall}$	Spatial- and time-averaged outer-tube-wall temperature of the condenser section
$\overline{T}_{evap}^{wall}$	Spatial- and time-averaged outer-tube-wall temperature of the evaporator section
$\overline{T}_{evap}^{water}$	Time-averaged temperature of the liquid water in the evaporator section
$T_{\infty,adiab}$	Time-averaged ambient temperature adjacent to the adiabatic section
$T_{\infty,cond}$	Time-averaged ambient temperature adjacent to the condenser section
$T_{\infty,evap}$	Time-averaged ambient temperature adjacent to the evaporator section
$\overline{T}_{\infty}$	Spatial- and time-averaged ambient temperature
ΔT_e	Excess temperature: $(T_s - T_{sat})$
$(\Delta T)_{max}$	Maximum temperature variation on outside wall of the evaporator tube

$\left(Vol\right)_{Evap}$ Volume of the evaporator section of the heat pipe

$\left(Vol\right)_{liquid}$ Volume of the liquid

Greek Notation

Γ Mass flow rate per unit of circumference

θ Angle of tilt of the GHP from the vertical

μ_l Dynamic viscosity of the liquid

ρ_l Density of the liquid

ρ_v Density of the vapor

σ Surface tension at the liquid vapor interface

Chapter 1: Introduction

1.1 Background, Motivation, and Overall Goal

Gravity heat pipes (GHPs) are closed two-phase thermosyphons [Lee and Mittal (1972); Japikse (1973); Chi (1976); Faghri (1995, 2012); Reay et al. (2013); Jafari et al. (2016)]. As their name suggests, each of these devices is contained within a single tube and it functions under the influence of gravity. A schematic illustration of a GHP is given in Fig. 1.1.

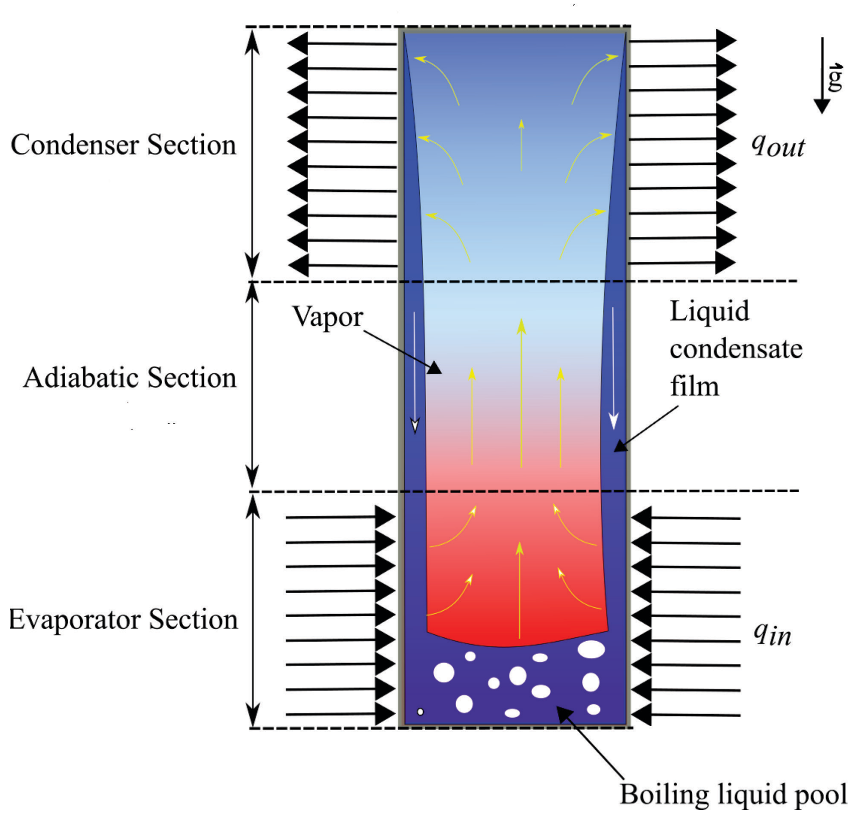

Figure 1.1: Schematic illustration of a gravity heat pipe.

A GHP is usually constructed by first evacuating a closed tube and then filling it with an appropriate amount of a chosen working fluid. As is illustrated in Fig. 1.1, in a GHP, the bottom portion of the tube is partially or fully filled with the liquid phase of the working fluid, it is heated, and performs as an evaporator; the upper portion of the tube is cooled, and it serves as a condenser; and the central portion of the tube is usually very well insulated and referred to as an adiabatic section. A GHP operates continuously (cyclically) as follows: the heat input to the evaporator causes the liquid contained within it to boil or evaporate; the generated vapor (being lighter than the liquid) moves upwards and then condenses in the condenser section; the condensate returns back to the evaporator under the action of gravity; and this cycle continues.

Conventional heat pipes (HPs) [Chi (1976); Faghri (1995, 2012, 2014); Reay et al. (2013)] also consist of a tube filled with a liquid and its vapor, and it (the tube) too has a heated (evaporator), a cooled (condenser), and an effectively adiabatic sections. Furthermore, cyclical liquid-vapor (evaporation) and vapor-liquid (condensation) phase-change phenomena are also involved during the continuous operation of HPs. However, in contrast to GHPs which are contained in simple tubes and rely on gravity for their operation, HPs have a wick structure attached to the inner wall of the tube and they rely on capillary forces generated in the wick at the liquid-vapor interface to drive the liquid condensate in the condenser back to the evaporator. Thus, GHPs are sometimes referred to as gravity-assisted wickless heat pipes. It should be noted here that whereas HPs are designed for continuous operation in any orientation with respect to the gravitational acceleration vector ($\vec{g}$), GHPs are capable of continuous operation only when the evaporator is located below the condenser (the main direction of heat transfer is opposite to that of $\vec{g}$), a characteristic that is often referred to as thermal-diode behavior of these devices.

As the liquid-vapor and vapor-liquid phase-change processes are associated with relatively high latent heat and effectively constant temperatures (for pure substances), GHPs are able to sustain high rates of heat transfer with relatively small temperature differences. Thus, their effective conductance can be significantly greater than solid copper rods of corresponding dimensions. Furthermore, as GPHs are constructed of tubes that are only partially filled with the liquid phase of the working fluid (primarily in the evaporator section), their heat capacity is considerably lower (and thus their thermal response time is also significantly smaller) than that of solid copper rods of corresponding dimensions. These features, along with their thermal-diode behavior, simple construction with no mechanical moving parts, and wide operating temperature range, have made GHPs attractive for use in many engineering systems: examples include heating, ventilating, and air-conditioning (HVAC) and waste heat recovery systems [Azad and Geoola (1984); Azad et al. (1985); Wadowski et al. (1991); Yang et al. (2003); Lin et al. (2005); Danielewicz et al. (2014)]; solar energy systems [Mathioulakis and Belessiostis (2002); Abreu and Colle (2004); Hussein et al. (2006); Du et al. (2012)]; enhanced latent-heat thermal energy storage units [Shabgard et al. (2012)]; permafrost preservation systems [Haynes et al. (1992); Xu and Goering (2008)]; geothermal systems for deicing roads and bridges [Reay et al. (2013)]; temperature regulation in oil wells [Ma et al. (2013); Zhang and Che (2013)]; and cooling of electronic devices and fuel cells [Tsai et al. (2010); Reay et al. (2013)]. Five such applications of GHPs are illustrated in the following figures: Fig. 1.2 (a) [taken with permission from Alyeska Pipeline Service Company, http://www.alyeska-pipe.com]; Figs. 1.2 (b), (c), and (d) [included with permission from Arctic Foundations Inc., http://www.arcticfoundations.com]; and Fig. 1.2 (e) [main ideas adapted from http://long2.eng.sunysb.edu/project/thermosyphon.html].

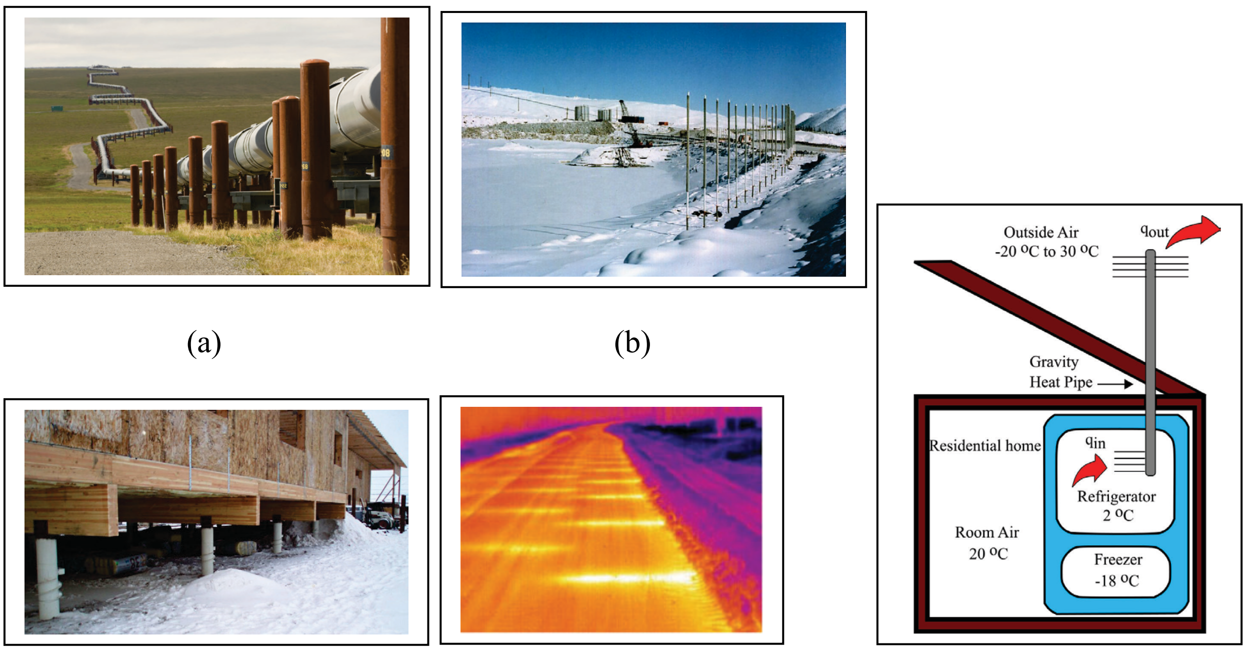

(c) (d) (e)

Figure 1.2: Some examples of the applications of gravity heat pipes and its variants: (a) thermopile support posts of the Trans-Alaska Pipeline (GHPs that are designed to preserve the permafrost); (b) use of GHPs to create a frozen-soil wall for containment of hazardous wastes at the Kubaka gold mine in Russia; (c) thermo-helix-piles (GHPs with spiral plates welded on the outside of the tube for good anchoring in soils) designed to strengthen the building foundation by freezing water in the soil underneath a clinic in Selawik, Alaska; (d) infrared image of road-deicing using fully-buried GHPs for harnessing geothermal energy at the University of Alaska, Fairbanks; and (e) schematic illustration of a GHP-assisted residential refrigerator designed for cold-climate locations (main ideas adapted from a set-up illustrated in the webpage of Professor J. P. Longtin's laboratory at the State University of New York, Stony Brook).

The above-mentioned applications of GHPs demonstrate that they have the potential to provide significant socio-economic and environmental benefits, and thus play an important role in sustainable engineering and design. Such potential benefits of GHPs (coupled with the desire on the part of the author and his supervisor, Professor B. R. Baliga, to contribute to ongoing worldwide efforts directed towards designing efficient, sustainable, and environmentally friendly energy conversion and exchange systems) constitute the main motivation for the work described in this thesis.

The overall goal of the work presented in this thesis was to design and construct a GHP, along with a set-up that allows basic experimental investigations for a characterization of this device. Water was used as the working fluid in this work. Experiments were conducted for several different combinations of the governing parameters, which lead to periodic unsteady and steady-state operations of the GHP. The specific objectives of this work are presented in Section 1.3, after the presentation of the relevant published literature in the next section.

1.2 Literature Review

An exhaustive review of the literature related to GHPs, their various applications, and the related topics is not intended in this section. Rather, this review is only a concise overview of some key books, review articles, and papers on GHPs. As was stated earlier, these devices involve boiling and condensation phenomena, so some of the key articles related to these phenomena and relevant to GHPs are also reviewed briefly in this section.

This section is subdivided into the following subsections: (a) historical developments, books, and review articles related to GHPs; (b) boiling phenomena; (c) condensation phenomena; (d) geyser boiling phenomenon in GHPs; (e) operational limits of GHPs; (f) other analytical, experimental, and numerical investigations of GHPs; and (g) concluding remarks.

1.2.1 Historical developments, books, and review articles related to GHPs

The predecessor of the heat pipe, the Perkins tube, was patented by Perkins (1836). It is a wickless gravity-assisted heat pipe, a closed tube containing a small quantity of water and operating as a two-phase thermosyphon, a design that is closely related to the GHP illustrated in Fig. 1.1. The earliest applications for this type of tube were in locomotive boilers and in locomotive fire-box superheaters. Descriptions of the Perkins tube are available in the works of King (1931) and Reay et al. (2013).

The concepts underlying heat pipes (which are driven by capillary forces produced at the liquid-vapor interface in a wick, or porous lining, attached to the inside surface of the tube) was first put forward by Gaugler (1944) of General Motors Corporation, Ohio, USA, in a patent application published in 1944 and described in the context of a refrigeration system. Grover (1966) coined the term ‘Heat Pipe’ in a patent filed on behalf of US Atomic Energy. Extensive research and development of heat pipes were conducted at the Los Alamos Laboratory, New Mexico, under the supervision of G. M. Grover: several prototype heat pipes were built, the first of which used water as a working fluid, and were soon followed by a heat pipe operating with sodium at temperature of about 1100 K, as reported in Grover et al. (1964). The recognition of the heat pipe as a reliable thermal device was initially due to the preliminary theoretical results and design tools that were reported in a publication by Cotter (1965). Following this publication, research works on heat pipes were initiated around the world, as reported in Reay et al. (2013): the United Kingdom Atomic Energy Laboratory at Harwell started experimenting with sodium heat pipes for use as thermionic diode converters; scientists started conducting similar work at the Joint Research Centre (JCR) in Ispra, Italy, which soon became the most active research centre on heat pipes outside the U.S.; and shortly thereafter, research activities on heat pipes were initiated in Germany, France, the former USSR, and other countries. As the capillary-driven heat pipes can operate in micro-gravity locations, most of the early research and development efforts on these devices were directed toward space applications and the first space flight of such a heat pipe took place in 1967. Today, however, investigators in many countries around the world are actively involved in research, development, and commercialization of heat pipes for space as well as terrestrial applications.

There are many books and review articles on heat pipes (HPs) and GHPs. Examples of such publications include the works of Tien (1975), Chi (1976), Faghri (1995, 2012, 2014), Petersen (1998), Dunn and Reay (2012), Reay et al. (2013), and Jafari et al. (2016).

1.2.2 Boiling phenomena

When evaporation (liquid-vapor phase-change phenomenon) occurs at a solid-liquid interface, it is termed boiling [Rohsenow (1973); Carey (1992); Whalley (1996); Hewitt (1998)]. This phenomenon occurs when the temperature of the surface exceeds the saturation temperature of the liquid. Heat is transferred from the solid surface to the liquid and causes the formation of vapor bubbles (at nucleation sites), which grow and subsequently detach from the surface. These bubbles then rise up through the liquid to the liquid-vapor interface. Extensive discussions of the processes involved in pool and also forced convection boiling in tubes (including the dynamics of bubble formation, growth, and detachment; critical heat flux and burn-out; transition regime, hysteresis, and vapor-film pool boiling; and various modes of forced-convection boiling), and references to publications related to them, are available, for example, in the works of Rohsenow (1973), Carey (1992), Whalley (1996), Hewitt (1998), and Thome (2003).

As is discussed in the seminal work of Nukiyama (1966), first published in 1934 in Japanese, boiling in liquid pools (as in the evaporator section of GHPs akin to the one illustrated schematically in Fig. 1.1) may occur in various modes, such as free-convection, nucleate, transition, and film boiling (some of the related details are presented briefly in Chapter 2 of this thesis). In another seminal work related to nucleate pool boiling, Rohsenow (1952) provided a correlation for the related heat transfer coefficient, and this correlation, with some modifications, is still widely used [Mikic and Rohsenow (1969); Rohsenow (1973); Carey (1992); Hewitt (1998)]. Correlations for free-convection and film modes of pool boiling, and also critical heat flux, are available and discussed, for example, in the works of Rohsenow (1973), Carey (1992), and Hewitt (1998).

Forced-convection boiling in tubes occurs in several successive stages, termed as bubbly-, slug-, churn-, and annular-flow regimes. These forced-convection boiling regimes, the transitions between them, the related parameters, and various correlations for them have been extensively discussed, for example, in the works of Carey (1992), Whalley (1996), Dobson and Chato (1998), Hewitt (1998), and Thome (2003).

Discussions of pool boiling heat transfer phenomena in the evaporator section of closed two-phase thermosyphons or GHPs, including related modelling aspects and critical heat flux, are available, for example, in the works of Casarosa et al. (1983), Imura et al. (1983), Reed and Tien (1987), and Noie (2005). It should also be noted here that extensive research on these phenomena was undertaken in the former Soviet Union: references to some of the related publications and brief reviews of them are available in the work of Casarosa et al. (1983).

1.2.3 Condensation phenomena

Condensation (or vapor-liquid phase-change phenomenon) occurs when the temperature of a vapor is reduced below its saturation temperature [Rohsenow (1985); Marto (1998); Incropera, and DeWitt (2002)]. It can occur in the following modes [Marto (1998)]: surface condensation, which occurs when a vapor comes in contact with a cold surface; homogeneous condensation, where the vapor condenses in form of droplets suspended in a gas (forming a fog or mist); and direct contact condensation, which occurs when the vapor is brought in direct contact with a cold liquid. It is surface condensation that primarily occurs in GHPs. In surface condensation, the latent heat involved in the vapor-liquid phase-change phenomenon is released and transferred to the cooled surface, and a liquid condensate is formed on it. In general, surface condensation can occur in two sub-modes, with the condensing vapor forming either a continuous liquid film or liquid drops on the cold surface: the former is termed as film condensation and the latter as drop-wise condensation [Marto (1998)]. Film condensation is the predominant mode of condensation in most engineering applications [Marto (1998); Incropera and DeWitt (2002)] and also in GHPs. A few key publications related to film condensation are reviewed in the remainder of this subsection, with special emphasis on investigations of its occurrence in GHPs.

The seminal work on the film condensation on surfaces is that of Nusselt (1916). He proposed and solved a mathematical model of laminar film condensation of a saturated vapor of a pure substance on a vertical isothermal cooled surface, assuming that the vapor is stationary far from the surface and the liquid condensate flows down the vertical surface under the action of gravity. Nusselt (1916) also invoked the following additional assumptions in his model: 1) constant thermophysical properties of the condensate (at the arithmetic mean of the temperatures of the saturated vapor and the cooled isothermal surface) and vapor phase (at its saturation temperature); 2) viscous shear stress between the vapor and liquid condensate flowing down the vertical surface is zero (negligibly small); 3) the rates of viscous transport and heat conduction in the vertically downward direction inside the condensate layer are negligible compared to those in the direction normal to it; 4) the rates of advection transport of momentum and heat in the vertically downward direction inside the condensate layer are negligible compared to the rates of viscous transport and heat conduction across it, respectively; and 5) the variation of static pressure across the vertically downward flow of the condensate layer is negligible. Nusselt

(1916) solved his model analytically. His solution provides analytical expressions for the velocity and temperature distributions; the variations of the condensate mass flow rate and layer thickness with the distance along it; and the local and average values of the heat transfer coefficient. Some additional details of the results obtained by Nusselt (1916) are presented in Chapter 2, as it is still the basis many of the latest works on film condensation.

Dhir and Lienhard (1971) have shown that the laminar film condensation model and solution of Nusselt (1916) may also be used for condensation along the upper surface of cooled flat inclined plates, if the gravitational acceleration, g, is replaced by $g\{\cos(\theta)\}$, where θ is the angle between the vertical and the surface, provided the value of θ does not approach 90^{o}. Nusselt's model and solution may also be used for condensation on inner and outer surfaces of vertical tubes, with good accuracy, if the radius of the tube is significantly greater than the condensate film thickness throughout the length of the tube [Rohsenow (1985); Marto (1998)].

The laminar condensate layer in film condensation transitions first to a so-called laminar-wavy regime, and then to turbulent film condensation. A film Reynolds number, based on the mass flow rate inside the condensate layer per unit width of the plate and the dynamic viscosity of the liquid (condensate), is used to characterize conditions that cause the transition from laminar to wavy and then turbulent film condensation: it is generally assumed that when this film Reynolds number is less than or equal to 30, the conditions corresponding to laminar-wavy film condensation; and when this number is greater than or equal to about 1800, the transition from laminar to turbulent film condensation is complete [Incropera and DeWitt (2002)]. Several empirical correlations have been proposed for the heat transfer coefficient in the laminar-wavy and the turbulent regimes of film condensation [Marto (1998); Incropera and DeWitt (2002)].

An adaptation of the work of Nusselt (1916) to laminar film condensation in vertical tubes with upward flow of the vapor is presented in the work of Seban and Hodgson (1982). Extensions of this work to condensation in closed vertical two-phase thermosyphons have been presented by Seban and Faghri (1984) and Chen et al. (1984). An analytical study of the influence of a non-condensable gas on condensation in a two-phase closed thermosyphon, with attention to the retardation of vapor condensation due to both radial and axial diffusion of the gas, has been presented by Huikata et al. (1984). A theoretical analysis and also some experimental studies of film condensation inside vertical and inclined closed two-phase thermosyphons have been presented in the work of Wang and Ma (1991). Models, correlations, and flow pattern maps for condensation in horizontal tubes are available in the works of Carey (1992), Whalley (1996), Dobson and Chato (1998), and El Hajal et al. (2003).

Measurements of condensation heat transfer in a reflux two-phase thermosyphon, using a novel rotating needle contact method, have been presented by Zhou and Collins (1991). Turbulent film condensation was investigated experimentally by Kim and No (2000) for high-pressure steam in a vertical tube, designed to be relevant for applications to passive systems in advanced nuclear power plants. An experimental investigation of film condensation of water in a vertical tube in the laminar, wavy, and turbulent flow regimes, accounting for the influence of counter-current vapor flow, has been presented and discussed by Thumm et al. (2001). Correlations for the heat transfer and friction factor, which specifically account for the effects of the counter-current vapor flow, have also been presented by Thumm et al. (2001). An experimental study of film condensation in a large diameter (200 mm) tube with upward flow of steam has been reported by Pashkevich and Muratov (2015), for the laminar and turbulent flow regimes. Kubin et al. (2016) have presented an experimental investigation of steam condensation in a vertical tube of small diameter (2.0 mm). They showed that the flow of steam causes waves on the surface of the condensate layer, an effect that was not accounted for in the seminal work of Nusselt (1916), and these waves can increase the rate of heat transfer by as much as 20.5 %.

1.2.4 Geyser boiling phenomenon in GHPs

At relatively low heat inputs and ratios of the volume of liquid to the volume of evaporator close to or greater than one (unity), a two-phase thermosiphon could operate intermittently. Periods of relatively quiescent conditions in the liquid pool (corresponding to natural convection, as described in the seminal works of Lighthill [1953] and Martin [1955]) alternate with periods of violent (almost explosive) boiling of the superheated liquid, during which some of the liquid is propelled toward the condenser, almost in the form of a slug. This violent boiling period is followed by a period of very vigorous nucleate boiling that soon ceases, and then the above-mentioned quiescent conditions are re-established. The aforementioned sequence of phenomena then continues in a somewhat chaotic and almost cyclical manner. This mode of boiling in the evaporator during the intermittent operation of two-phase thermosyphons is referred to as geyser boiling in the published literature, after this terminology was introduced in the pioneering works of Murphy (1965) and Casarosa et al. (1983). Some earlier works on the geyser boiling phenomenon, conducted in the former Union of Soviet Socialist Republics (USSR), have been briefly reviewed by Casarosa et al. (1983).

Murphy (1965) has proposed the following description of the geyser boiling phenomena in a long vertical tube, closed at the bottom, filled with a liquid, connected to an open reservoir at the top (partially filled with liquid), and heated on its curved surface. Initially, the heat input to the wall of the tube is transferred to the liquid in the reservoir by means of natural convection. This natural convection process establishes fluid circulation within the tube, and a portion of the heat input is liberated at the liquid surface in the reservoir (by evaporation) and the remainder results in sensible heat gain by the liquid (in the reservoir and the tube). As the heat input to the tube wall continues, the fluid bulk temperature is increased and the liquid in the upper three-quarters (or so) of the tube reaches its saturation condition. Additional heat input to this saturated liquid results in vapor bubble production on the wall of the tube (boiling). These bubbles detach from the tube wall, rise in the liquid, and begin to coalesce and form a larger bubble, which is often referred to as a Taylor bubble. The formation of the Taylor bubble adjacent to the wall of the tube results in a pressure reduction below the bubble, and causes more rapid boiling of the now superheated liquid there. As this sequence of events continues, the vapor forms at a rate that is considerably greater than that which can be removed from the tube wall. Eventually, there is an explosive expulsion upwards of the heated liquid on top of the Taylor bubble; then, colder liquid from the reservoir refills the tube; and the cycle continues. A schematic depiction of this cycle of events during geyser boiling in a closed two-phase thermosyphon, where the expelled liquid hits the closed top of the tube and falls back into the evaporator, has been provided by Khazee et al (2010); an adaptation of their schematic depiction is presented below in Fig. 1.3.

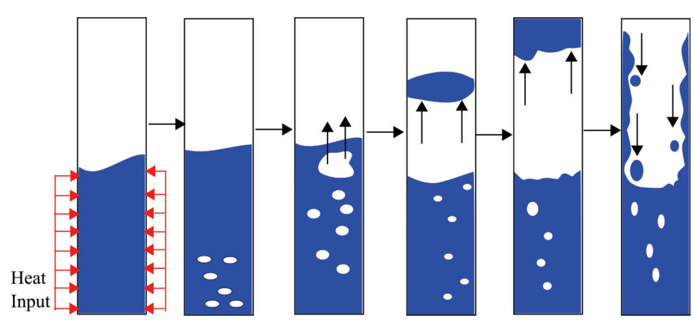

Figure 1.3: A schematic depiction of the geyser boiling phenomena in a closed two-phase thermosyphon with close to 100 % fill ratio [adapted from Khazee et al. (2010)].

Imurra et al. (1983) undertook an experimental study of a closed vertical two-phase thermosyphon, and discussed conditions that lead to geyser and so-called developed (or nucleate) boiling. An experimental investigation of geyser boiling in a vertical annular closed two-phase thermosyphon was undertaken by Lin et al. (1995). They investigated the effects of rate of heat input, condenser temperature, fill ratio, and length of the evaporator on the geyser boiling phenomenon, with water and ethanol as the working fluids. They also carried out flow visualization at low rates of heat input, which clearly showed the process of geyser boiling. Their results also showed that geyser boiling occurs mainly at low rates of heat input, and the time period of this phenomenon is shorter at higher rates of heat input, smaller evaporator length, and lower values of fill ratio. An experimental study of geyser boiling in a closed two-phase thermosyphon has also been presented by Kuncoro et al. (1995), with special emphasis on the underlying mechanisms.

Two modes of hydrodynamic transition in nucleate boiling, the first resulting in a change of the vapor removal process from an intermittent to a continuous one, and the other pertaining to the maximum (or burnout) heat flux, have been investigated experimentally and discussed in the work of Moissis and Berenson (1963). Steady-state characteristics and stability thresholds of closed two-phase thermosyphons have been studied analytically by Dobran (1985). Experimental and theoretical investigations of the transient behavior of a two-phase closed thermosyphon have also been reported by Farsi et al. (2003).

Finally, it is noted here that geysers occur naturally as geothermal phenomena in many parts of the world, and are often very impressive (one of the most famous examples of such geysers is the Old Faithful in the Yellowstone National Park in Wyoming, U.S.A.). The scientific study of naturally occurring geysers and their underlying dynamics, including the importance of hydrostatic pressure on the boiling temperature of water and on the rate of boiling in geyser eruptions, has been the subject of many investigations over almost 170 years. For a review of some of the important publications on this topic and a concise presentation of the related mathematical models and results, the reader is referred to the work of Dowden et al. (1991).

1.2.5 Operational limits of GHPs

GHPs or closed two-phase thermosyphons have several operating limits that depend on the rate of heat input, geometric parameters (such as ratio of the tube length to its diameter; ratios of the lengths of the evaporator and condenser sections to it total tube length; and inclination of the tube from the vertical), fill ratio (ratio of volume of liquid to volume of the evaporator section), and thermophysical properties of the working fluid [Dobran (1985); Dunn and Reay (2012); Jafari et al. (2016)]. These operational limits are referred to in the literature as the dry-out limit, burn-out or critical heat flux limit, flooding or entrainment limit, and sonic limit [Nguyen-Chi and Groll (1981); Dobran (1985); El-Genk and Saber (1997, 1999); Dunn and Reay (2012); Jafari et al. (2016)].

The dry-out limit can occur due to the following conditions [Nguyen-Chi and Groll (1981); Dobran (1985); El-Genk and Saber (1999); Dunn and Reay (2012)]: 1) the amount of working fluid is less than the minimum required for a continuous circulation of the vapor and condensate at a specified rate of heat input to the evaporator; 2) a portion of the liquid condensate flowing down the wall of the tube in the evaporator section at fill ratios below 100 % evaporates at a faster rate than it can be replenished, due to either high input heat fluxes or high condensate-vapor shear stress which hinders the down-flow of the condensate; and 3) the GHP is inclined with respect to the vertical and the condensate film on the wall of the tube is not uniform enough in the cross-section, due to the effects of gravity, causing portions of it to dry out.

At high values of the liquid fill ratio (close to, equal to, or higher than 100 %), when the rate of heat input is high, the operation of the GHP can be limited by the burn-out or critical heat flux limit [Dobran (1985); Dunn and Reay (2012)]. This limit is reached when the rate of vapor formation at the wall of the tube is so high that a vapor film (or blanket) is formed there, and the heat transfer from the wall to the fluid in the evaporator has to occur through this relatively low-thermal-conductivity vapor film. It is similar to the critical heat flux limit in pool boiling [Nukiyama (1966)].

The flooding or entrainment limit can occur at high fill ratios and large rates of heat input. Under these conditions, the vapor flow rate can be quite high and lead to high shear stress at the vapor-condensate interface, causing it to become unstable and wavy. If the heat input is increased further, then liquid in the condensate layer can become entrained into the core vapor flow, causing flooding conditions in the tube, especially if it is of small diameter [Dobran (1985); El-Genk and Saber (1997)].

When liquid metals are used as the working fluid in GHPs and subjected to very high input heat fluxes, then, in principle, the vapor velocity can reach sonic (or supersonic) levels in both start-up and steady-state conditions [Jafari et al. (2016)]. This could lead to choking (or shock waves) in the vapor flow. In practice, however, such a limit has never been reported in the published literature [Dunn and Reay (2012); Jafari et al. (2016)].

Dobran (1985) also discusses an oscillation limit, for conditions in which the input heat flux is increased above the flooding limit, and the GHP starts to operate intermittently. Sometimes, geyser boiling is also considered as an operational limit, as it is highly unsteady and its explosive nature could damage the GHP under extreme conditions [Jafari et al. (2016)].

1.2.6 Other analytical, experimental, and numerical investigations of GHPs

In addition to the publications mentioned above in Subsections 1.2.1 to 1.2.5, there are numerous other publications on analytical, experimental, and numerical investigations of GHPs. Some of these publications are reviewed briefly in the remainder of this subsection.

One of the first comprehensive investigations of GHPs was done by Lee and Mittal (1972) at the University of Ottawa. They conducted an experimental study of the thermofluid aspects of a two-phase closed thermosyphon, along with a simple theoretical analysis to determine its maximum possible rate of heat transfer. Water and Freon-11 were used as the working fluid. The effects of the amount and type of working fluid, ratio of the heated-length to the cooled-length, operating pressure, and input heat flux were investigated.

Shiraishi et al. (1981) conducted an experimental investigation of the heat transfer characteristics of a two-phase closed thermosyphon, with water, ethanol and Freon 113 as the working fluids. The effects of the amount and type of the working fluid, the operating temperature, and input heat flux were studied. The values of heat transfer coefficients in the condenser and the evaporator were estimated from the experimental data. Good agreement was obtained between estimates of the overall thermal resistance of the thermosyphon and the predictions obtained from a simple thermodynamic mathematical model.

Noie (2005) carried out experimental investigations to determine the effects of input heat flux, evaporator length, and fill ratio on the steady-state performance of vertical closed two-phase thermosyphons. Distilled water was used as the working fluid, with fill ratios varying from

30 % to 90 %. The aspect ratios (length of evaporator/ inside diameter of the tube) considered in these experiments were 7.5, 9.8 and 11.8. The boiling heat transfer coefficients were calculated using the experimental measurements, compared with correlations proposed earlier by other investigators, and conclusions were drawn regarding an optimum fill ratio (at which the thermosyphon operates at its best for a given aspect ratio). For the conditions investigated, it was found that the wall of the evaporator was almost isothermal, and the maximum heat transfer rate for different aspect ratios took place at different fill ratios: for an aspect ratio of 11.8, the maximum heat transfer rate occurred when fill ratio was 60 %; while for aspect ratios of 7.45 and 9.8, the corresponding fill ratios for achieving the maximum rate of heat transfer were 90 % and 30 %, respectively.

Li et al. (1991) suggested a method for improving the performance of thermosyphons at low temperature differences. Experiments were carried out on thermosyphons charged with R11, R22, and water, operating at low temperature differences, and the onset of boiling was investigated. It was found that nucleate boiling at relatively low temperature differences between evaporator and condenser can be initiated effectively by using either mechanically agitation of the thermosyphon (by imposed vibrations) or a thermal trigger that involves raising the surface temperature of a small portion of the evaporator section for a short period of time.

Joudi and Witwit (2000) carried out an investigation to improve the conventional gravity-assisted wickless heat pipe (or GHP) for a limited temperature range by modifying its internal structure. The modification was the introduction of a physical barrier at the adiabatic section, suppressing vapor-liquid interaction and resulting in a continuous liquid return to the evaporator. Another modification was also introduced by adding a three-layer, 110 pores per inch, screen wick in the evaporator section only. They investigated the effects of the adiabatic length, inclination angle, and heat flux on the performance or the GHP. The addition of a screen wick in the evaporator raised the evaporator- and adiabatic-section temperatures. The presence of the adiabatic separator also resulted in a marked increase in heat transfer coefficient over those obtained without this separator, with an average increase of approximately 35 %. The introduction of the adiabatic separator also lowered the working temperature and eliminated the effect of inclination angles above 45^{o}; while the addition of the screen wick eliminated the effect of inclination angle but increased the heat-pipe wall temperature.

Hussein et al (2006) carried out an experimental study of the effects of various tube cross-section geometries and fluid fill ratios on GHPs employed in flat-plate solar thermal collectors. Three groups of GHPs having three different cross-section geometries (circular, elliptical, and semi-circular) were designed and manufactured. Each group of these GHPs was charged with distilled water at fill ratios of 10 %, 20 %, and 35 %. Each GHP was then incorporated into a prototype flat-plate solar thermal collector, developed specifically for the purpose of their study. The transient thermal performances of the GHP solar thermal collectors were investigated at different cooling-water inlet temperatures and mass flow rates. The experimental results indicated that the GHPs with the elliptical cross-section tubes had better performance than those with the circular cross-section tubes at low fill ratios. The optimum fill ratio for GHPs with elliptical cross-section tubes was found to be about 10 %, while it was very close to 20 % for those with tubes of circular cross section. The fill ratio corresponding to the flooding limit of the GHPs with the elliptical cross-section tubes was lower than that of the GHPs with circular cross-section tubes. At 20 % fill ratio, GHPs with the semi-circular cross-section tubes showed performance that was not as good as that of GHPs with tubes of the other cross sections.

Amatachaya and Srimuang (2010) also carried out studies to investigate the effects of tube cross-sectional geometries, fill ratio, and aspect ratio on thermal performance of GHPs at different rates of heat input. Two tube cross-sectional geometries (circular and flat) were used. The results indicated that the flat tubes resulted in higher average wall temperature in the evaporator section than those obtained with tubes of circular cross-section. The temperature variation along the wall surface of the evaporator section of the GHPs with circular cross-section tubes was nearly uniform and decreased slightly along the wall of the condenser section. The temperature along the wall surface of the evaporator section of the GHPs with flat tubes increased, due to dry-out effects, and then decreased toward the condenser section. The heat transfer coefficients of GHPs with both the circular and flat cross-section GHPs increased with a decrease in fill ratio. However, the experiments indicated that these coefficients for the GHPs with circular cross-section tubes were significantly higher than those for GHPs with flat cross-section tubes, for all fill ratios investigated.

Wangnippanto (1994) studied the effect of the inclination angle on the heat transfer rate for a copper-water GHP having an inside diameter of 20 mm and a length of 810 mm. In his work, it was found that the highest rate of heat transfer rate occurred when the inclination angle was 22.5° and the fill ratio was 30 %.

Zuo and Gunnerson (1995) studied the heat transfer in an inclined GHP. In their work, the minimum amount of working fluid required to operate the GHP (without dry-out) remained almost constant for inclination angle with respect to the horizontal in the range 20^o to 90^o; however, it increased significantly with decreasing value of this inclination angle below 20^o. They also obtained the highest flooding limit when this inclination angle was between 45^o to 60^o.

Terdtoon et al. (1997) experimentally investigated the effect of the aspect ratio (ratio of evaporator section length to inside diameter of pipe) and Bond number on the heat transfer characteristics of an inclined GHP (two-phase closed thermosyphon). They found that the optimum inclination angle from the horizontal for their GHP, with water as working fluid, was between 70°and 80° from the horizontal. They also found that the value of Qi/Q90 (rate of heat transfer at an inclination angle i / rate of heat transfer for a vertical GHP) gradually decreased with lowering of the inclination angle (below 90^o), for values of aspect ratio less than 10, but it was nearly constant at aspect ratios greater than 10. Correlations to predict the heat transfer characteristics of an inclined closed two-phase thermosyphon have been proposed by Payakaruk et al. (2000).

Noie et al (2007) investigated the effects of the aspect ratio and fill ratio on the thermal performance of an inclined two-phase closed thermosyphon. Their experiments were carried out for fill ratios in range 20 % to 60 % and aspect ratios of 15, 20, and 30, for inclination angle in the range 15° to 90° (from the horizontal). The heat transfer rate, temperature distribution, and condensation heat transfer coefficient of the inclined two-phase closed thermosyphon were measured. The results showed that the best thermal performance of the thermosyphon occurred at an inclination of 60° for all three aspect ratios and several fill ratios. The thermal performance of the inclined thermosyphon with an inclination angle of 60° was best for a fill ratio of 45 %. It was found that highest values of the condensation heat transfer coefficient for all three aspect ratios occurred when the inclination angle was between 30^o and 45^o. It was also found that the effect of the fill ratio on the heat transfer rate was higher when the aspect ratio was lower.

There have also been a few visualization studies to investigate fluid flow phenomena inside GHPs. Shiraishi et al. (1995) carried out a visualization study of the fluid flow phenomena inside an inclined, two-phase, closed thermosyphon at several inclination angles. The fluid flow phenomena were recorded with a video camera and also a still camera, and the corresponding heat transfer rate was also measured. The effect of inclination angle on the heat transfer rate was investigated by using several identical stainless steel thermosyphons with a total length of about 930 mm, with evaporator and adiabatic sections incorporating 13-mm ID glass tubing for flow visualization. Freon 113 was used as the working fluid. Observations of fluid flow phenomena were done at several inclination angles from the horizontal, in the range 90^{o} (vertical orientation) to 5°. Annular flow (condensate layer next to the wall and a vapor core) was recorded in the vertical and very-near-vertical positions, and stratified flow conditions were recorded at other inclination angles. Moreover, for the cases of stratified flow, the occurrence of dry-out on the evaporator wall was observed.

Grooten et al. (2008) carried out a dedicated visualization study of flow patterns in a transparent two-phase thermosyphon (inner diameter 16 mm and total length of 290 mm) to understand the effects of inclination angle (from the vertical) on the heat transfer characteristics. The input heat flux and the angle of inclination were varied. Acetone was used as the working fluid. The results showed that all angles of inclination between 0^{o} and 80^{o}, vapor plugs existed at heat fluxes less than 14 kW/m^2 and an annular condensate film flow with a wavy structure existed between heat fluxes of 14 and 32 kW/m^2. Another interesting result which these authors obtained was that the fill ratio did not have a significant influence on the heat transfer characteristics of their thermosyphon, as long as dry-out of the evaporator was avoided.

Quasi-one-dimensional analytical models of closed two-phase thermosyphons, operating in the steady and transient modes, and their solutions have been proposed by Reed and Tien (1987). Their steady-state solutions agreed well with thermosyphon flooding data from several experimental investigations. No experimental data were available to check out their transient solutions. Nevertheless, it is useful to note here that their results indicate that the governing time scale for system transients in GHPs is a condensate film residence time, which is typically much longer than the times required for viscous and thermal diffusion through the film. Experimental and analytical investigations of a closed two-phase thermosyphon, operating with R-11 as the working fluid and with imposed convection boundary conditions, have been reported by Casarosa and Dobran (1988).

Several numerical solutions of multidimensional models of GHPs (using computational fluid dynamics) are available in the published literature. Representative examples of such investigations include the works of Harley and Faghri (1994), Alizadehdakhel et al. (2010), and Fadhl et al. (2013, 2015).

Finally, it should be noted that many other publications on GHPs have been discussed concisely in review articles and books on this topic. Examples of such publications include the works of Tien (1975), Chi (1976), Faghri (1995, 2012, 2014), Dunn and Reay (2012), Reay et al. (2013), and Jafari et al. (2016).

1.2.7 Concluding remarks

The papers reviewed in the Subsections 1.2.1 – 1.2.6 provide a good physical understanding of the underlying mechanisms and modes of operation of GHPs. However, with respect to designs of GHPs for specific applications, only qualitative guidance can be obtained from these papers, at best, due to the relatively large number of governing parameters, different working fluids (and the variation of their properties with temperature), different boiling regimes and condensation phenomena, and unsteady and steady-state operating regimes.

On the basis of the above-mentioned comments and observations, it was concluded that it would be very useful to set up an experimental facility for obtaining quantitative guidance for particular applications of GHPs. The specific objectives of this work were chosen in this context, and they are presented in the next section of this chapter.

1.3 Objectives

The specific objectives of this work are summarized in pointwise form below:

- Design and construct a GHP for a chosen set of parameters
- Set up an experimental facility that allows investigations of GHPs
- Run experiments and obtain data for characterizing the above-mentioned GHP
- Present and discuss results
- Provide recommendations for extensions of this work

1.4. Overview of the Thesis

In the earlier sections of this chapter (Chapter 1), the following topics were presented and discussed: the background, motivation, and overall goal of this work; a literature review; and the specific objectives of this work. In Chapter 2, some of the theoretical considerations that were used for developing a basic understanding of the various thermofluid processes that occur within GHPs are discussed briefly (they supplement the discussions already presented earlier in Section 1.2). Descriptions of the GHP and the experimental set-up that were designed and constructed for this work, and also the related procedures that were used to run the experiments, are given in Chapter 3. In Chapter 4, the experimental results are presented and discussed. A review of the thesis, a summary of the main contributions of this work, and some recommendations for extensions of this work are presented in Chapter 5.

Chapter 2: Some Theoretical Considerations

In this chapter, some of the theoretical considerations that were used for developing a basic understanding of the various thermofluid processes that occur within GHPs are discussed briefly (these discussions supplement those already presented earlier in Chapter 1, Section 1.2). This chapter is divided into the five sections that address the following topics: 1) the boiling curve of Nukiyama (1966); 2) the correlation of Rohsenow (1952, 1973) for nucleate pool boiling; 3) the laminar film condensation theory of Nusselt (1916) and some extensions of it; 4) some dimensionless parameters that govern GHPs; and 5) concluding remarks.

2.1 Boiling Curve of Nukiyama

An examination of the boiling curve of Nukiyama (1966) is useful for developing an understanding of the underlying physical mechanisms of pool boiling (akin to that which occurs in GHPs) and its various modes. Nukiyama (1966), whose original work was performed in 1934, conducted an experimental investigation of pool boiling by passing electrical current through single nichrome and platinum wires immersed in water. In each case, the heat flux was controlled by the adjusting the electrical voltage across the wire (and hence the current passing through it). The temperature of the wire was determined from its electrical resistance (and a correlation that related electrical resistance of the wire to its temperature). The arrangement used by Nukiyama (1966) is termed power-controlled heating, wherein the excess temperature $\Delta T_e = (T_s - T_{sat})$, where wire temperature is T_s and T_{sat} is the saturation temperature of the water, is the dependent variable and the power input to the wire (and hence the heat flux $q_s^{"}$ from the wire surface to the surrounding water) is the independent variable. Nukiyama (1966) presented the key results of his experiment in a plot which has since come to be known as his pool boiling curve [Rohsenow (1973); Carey (1992); Hewitt (1998); Incropera and DeWitt (2002)]. This curve is presented in Figure 2.1. As is illustrated by the initial portion of this curve, when the applied power input is increased, the heat flux increases, at first slowly and then very rapidly, with excess temperature. Nukiyama (1966) observed that boiling (indicated by the presence of vapor bubbles in his experiment) did not begin until $\Delta T_e \approx 5$ ^{o}C. With further increases in input power, the heat flux increased to very high levels until, for a value slightly larger than $q_{max}^{"}$, the wire temperature jumped to a value that caused the nichrome wire to melt ("burnout").

Nukiyama then switched to the platinum wire, which has a melting point of roughly 2045 K compared to about 1500 K for nichrome wire [Incropera and DeWitt (2002)], and obtained data for the full curve illustrated in Figure 2.1.

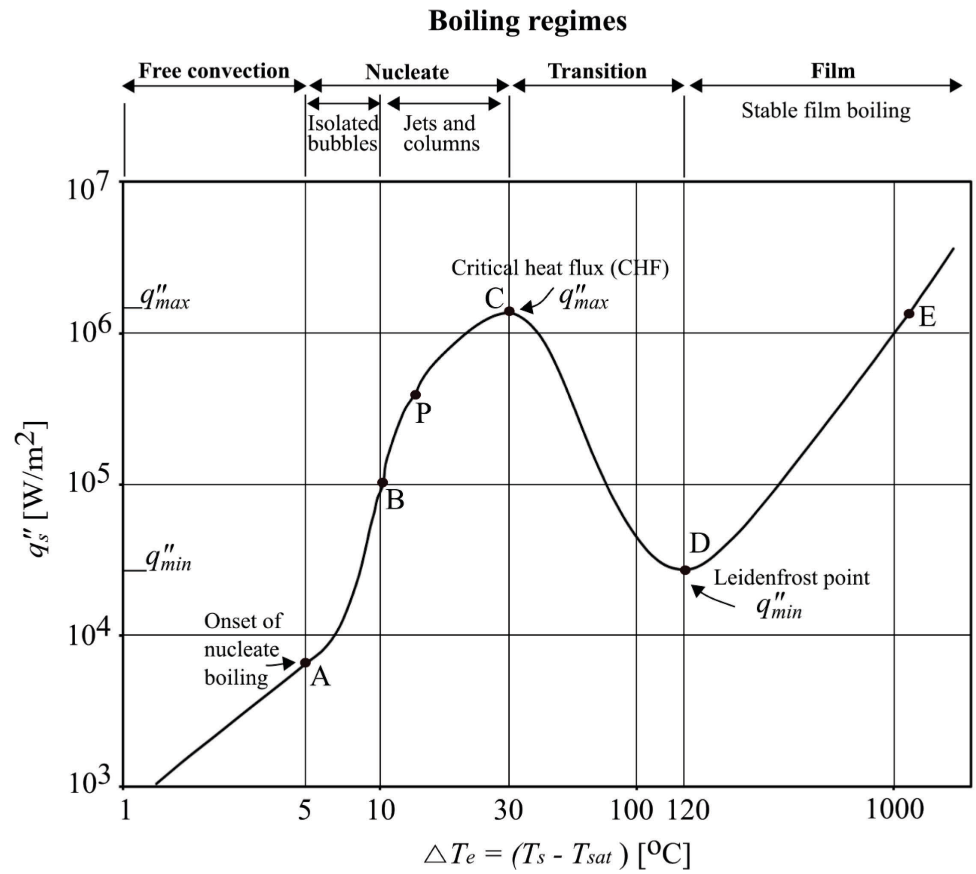

Figure 2.1: The pooling boiling curve of Nukiyama (1966) for water at atmospheric pressure [adapted from a similar curve presented in Incropera and DeWitt (2002)].

Several different regimes (or modes) of pool boiling are identified in the boiling curve shown in Figure 2.1, which pertains to water at atmospheric pressure (similar trends characterize the pool boiling behaviour of other fluids [Rohsenow (1973); Hewitt (1998)]). For increasing heat flux in the region $\Delta T_e \leq \Delta T_{e,A}$ where $\Delta T_{e,A} \sim 5^oC$, heat transfer from the water surface is purely by single-phase natural convection. Superheated liquid rises to the surface of the water pool and evaporation takes place at this surface. As the heat flux is increased beyond the value at 'A', bubbles begin to form on the surface of the wire, depart from its surface and rise through the liquid. This process is referred to as nucleate boiling. Nucleate boiling exists in the range $\Delta T_{e,A} \leq \Delta T_e \leq \Delta T_{e,C}$, where $\Delta T_{e,C} \sim 30^o$ C. In this range, two different boiling regimes may be distinguished: in the region 'A'-'B', isolated bubbles form at nucleation sites, separate from the surface, and induce considerable fluid mixing near the surface, substantially increasing the heat transfer coefficient, h, and $q_s^{"}$. In this regime, most of the heat exchange is through direct transfer from the wire surface to the liquid in motion over this surface, and not through the vapor bubbles rising through the water pool. As ΔT_e increases beyond $\Delta T_{e,B}$, more nucleation sites are created and the increased bubble formation causes bubble interference and coalescence. In the region 'B'-'C', the coalescing vapor bubbles rise through the water pool as jets or columns, which subsequently merge into slugs of the vapor.

The maximum heat flux, $q_{max}^{"}$, is usually termed the critical heat flux. It exceeds the value of 1 MW/m^2 for water at atmospheric pressure. At the point of this maximum, 'C', the significant amount of vapor formation makes it difficult for the liquid to continuously wet the wire surface. The region between point 'C' to point 'D', is termed transition boiling (or unstable film boiling; or partial film boiling), in which the rate of bubble formation is so rapid that a vapor film or blanket begins to form on the wire surface, and the conditions oscillate between film and nucleate boiling; however, the fraction of the total wire surface covered by the vapor film increases with increasing ΔT_e beyond point 'C', and h (and $q_s^{"}$) decreases, as the thermal conductivity of the vapor is much less than that of the liquid. Vapor film boiling exists from point 'D' onwards. At point 'D' of the boiling curve, referred to as the Leidenfrost point [Rohesnow (1973); Hewitt (1998)], the heat flux reaches a local minimum, $q_{min}^{"}$, and the surface of the wire is completely covered by a vapor blanket. Beyond point 'D', heat transfer from the wire surface to the liquid water occurs by conduction and radiation through the vapor film.

The power-controlled arrangement used by Nukiyama (1966), and in many electrical resistance heating devices and also in nuclear reactors, as $q_s^{"}$ is increased beyond $q_{max}^{"}$, the conditions jump suddenly to the vapor film boiling regime, causing a sharp and significant increase in ΔT_e and T_s, often exceeding the melting temperature of the solid, and causing destruction or failure of the heating or power system. Thus, the point 'C' is often referred to as the burnout point or the boiling crisis point.

It is desirable to operate GHPs in the nucleate boiling regime, because of the high values $q_s^{''}$ and h, and also the relatively stable (steady) operating conditions, that characterize this regime.

2.2 Correlation of Rohsenow for Nucleate Pool Boiling

The first and still the most widely used correlation for nucleate pool boiling was proposed by Roshenow (1952). It is usually expressed as follows [Rohsenow(1952); Hewitt (1998)]:

$$q_s^{''} = \mu_l h_{fg} \left[\frac{g(\rho_l - \rho_v)}{\sigma} \right]^{1/2} \left(\frac{c_{p,l} \Delta T_e}{C_{s,f} h_{fg} \Pr_l^n} \right)^3 \tag{2.1}$$

In this equation, all properties are for the saturated liquid, except for ρ_v which is the density of the saturated vapor. The latent heat of evaporation is indicated by h_{fg}; μ_l is the dynamic viscosity of the liquid; g is the acceleration due to gravity; ρ_l is the density of the liquid; $c_{p,l}$ is the liquid specific heat at constant pressure; $\Pr_l$ is the Prandtl number of the liquid; and σ is the surface tension at the liquid-vapor interface (which has a significant effect on bubble formation and development on the surface; and then the vapor pressure inside the bubble and also its size as it rise through the liquid). The coefficient, $C_{s,f}$, and the exponent of the Prandtl number, n, depend on the solid–fluid combination, and representative experimentally determined values are available in literature [Rohsenow (1973); Hewitt (1998)]. The Rohsenow (1952) correlation applies only for clean surfaces. When it is used to estimate the heat flux, the errors can be as high as ± 100 %. However, since the excess temperature is directly proportional to one third of the heat flux, this error is reduced by a factor of 3 when the expression is used to estimate excess temperature from knowledge of heat flux.

It should be noted that correlations for $q_{max}^{''}$, $q_{min}^{''}$, and h in the vapor film boiling regime are available in the work of Hewitt (1998).

2.3 Laminar Film Condensation Theory of Nusselt and Some Extensions

The theory of Nusselt (1916) applies to laminar film condensation on a vertical isothermal surface, with the liquid condensate flowing down the vertical surface under the action of gravity.

Nevertheless, it still provides useful physical insights into condensation processes on the inside surface of tubes and on other curved surfaces, and also turbulent film condensation. The assumptions invoked in the laminar film condensation theory proposed by Nusselt (1916) were already mentioned in Chapter 1 (Subsection 1.2.3). However, they are repeated here (in a slightly different form) for completeness and convenience: 1) the vapor phase is at the saturation condition, and it is stationary (far from the cooled surface); 2) constant thermophysical properties of the condensate (at the arithmetic mean of the temperatures of the saturated vapor and the cooled isothermal surface) and vapor phase (at its saturation temperature); 3) viscous shear stress at the interface between the vapor and the liquid condensate flowing down the vertical surface is zero (negligibly small); 4) the rates of viscous and conduction transport in the vertically downward direction inside the condensate layer are negligible compared to those in the direction normal to it; 5) the rates of advection transport of momentum and enthalpy in the vertically downward direction inside the condensate layer is negligible compared to the conduction transport across it; and 6) the variation of static pressure across the vertically downward flow of the condensate layer is negligible. Nusselt (1916) solved his model analytically.

The analytical solution put forward by Nusselt (1916) provides expressions for the velocity and temperature distributions; the variation with distance of the thickness of the condensate layer; the variation of mass flow rate in the condensate layer with distance; and the local and average values of the heat transfer. Full details are available in the works of Rohsenow (1985), Marto (1998), and Incropera and DeWitt (2002). The local (at a distance *x* downwards from the upper edge of the isothermal flat plate) and average heat transfer coefficients on the vertical isothermal surface are given by the following equations [Incropera and DeWitt (2002)]:

$$h_x = \left[\frac{g\rho_l(\rho_l - \rho_v)h_{fg}k_l^3}{4\mu_l(T_{sat} - T_s)x} \right]^{1/4} \tag{2.2}$$

$$h_{avg} = 0.943\left[\frac{g\rho_l(\rho_l - \rho_v)h_{fg}k_l^3}{4\mu_l(T_{sat} - T_s)\mathrm{L}} \right]^{1/4} \tag{2.3}$$

In Eq. (2.3), L is the total length of the plate.

The relation given by Eq. (2.3) has been found to under-predict most experimental results for laminar film condensation by around 20%. It is therefore customary to use the following equation [Marto (1998)]:

$$h_{avg} = 1.13\left[\frac{g\rho_l(\rho_l - \rho_v)h_{fg}k_l^3}{4\mu_l(T_{sat} - T_s)\mathrm{L}}\right]^{1/4} \tag{2.4}$$

Rohsenow (1985) has shown that thermal advection effects can be incorporated in the theory of Nusselt (1916), using a modified latent heat of vaporization, $h_{fg}^{'}$, in place of h_{fg} in Eqs. (2.2) – (2.4):

$$h_{fg}^{'} = h_{fg} + 0.68\,c_{p,l}\,(T_{sat} - T_s) \tag{2.5}$$

Empirical correlations for turbulent film condensation are available in the works of Marto (1998) and Incropera and DeWitt (2002). Models and correlations for condensation in horizontal, vertical, and inclined tubes, and related discussions, are also available in the published literature, for example, in the works of Seban and Hodgson (1982), Seban and Faghri (1984), Rohsenow (1985), Dobson and Chato (1998), Marto (1998), Thumm et al. (2001), and El Hajal et al. (2003).

2.4 Some Dimensionless Parameters that Govern GHPs

As was discussed in Chapter 1 (Section 1.2) and also in the earlier sections of this chapter, the boiling, condensation, and other thermofluid processes that occur inside GHPs can be quite complex. Thus, there are no generally-applicable and comprehensive mathematical models (governing equations, boundary conditions, and initial conditions) of these processes in the published literature. In the absence of such models, the governing dimensionless parameters can be obtained, in principle, using the Buckingham pi theorem [Fox and McDonald (1985)]. However, this task is made even more complicated when the dependence of the theromophysical properties of the working fluid on the temperature and pressure are taken into account.

Despite the above-mentioned complications in the modelling of GHPs, an attempt was made in this work (using the Buckingham pi theorem) to obtain the dimensionless parameters that govern the particular GHP that was designed, constructed, and used in this work. In this attempt, the dimensionless parameters were based the on the working-fluid thermophysical properties corresponding to the average temperatures and pressures in the evaporator and condenser sections of the GHP. These dimensionless parameters are presented in the remainder of this section, with reference to the notation given in Figure 2.2.

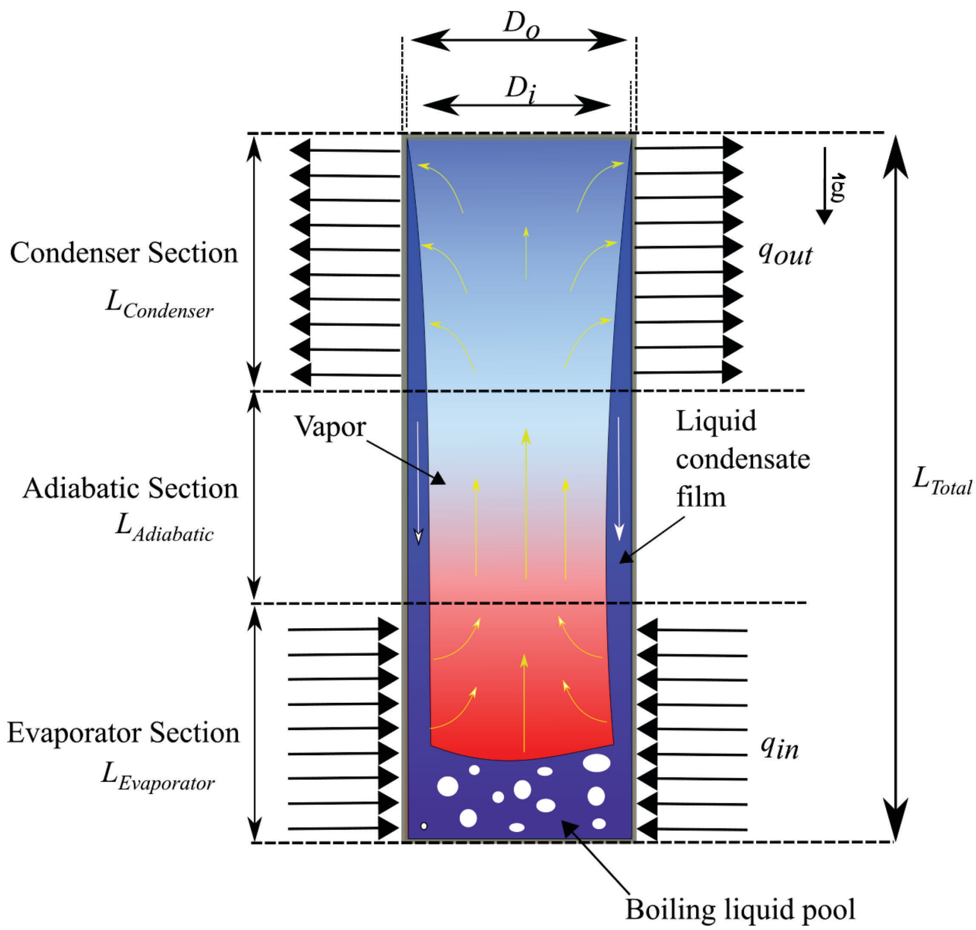

Figure 2.2: Schematic illustration of the GHP in the vertical orientation ($\theta = 0^o$) and some of the notation used in this work.

2.4.1 Geometrical parameters

The dimensionless geometric parameters pertaining to the GHP shown in Figure 2.2 are the following:

$$L_{Evapoartor} / L_{Total} \;\; ; \;\; L_{Condenser} / L_{Total}$$
$$\text{Aspect ratio, } L_{Evaporator} / D_i \;\; ; \;\; (D_o - D_i) / D_i \qquad (2.6)$$
$$\text{Angle of tilt of the GHP from the vertical: } \theta$$

2.4.2 Some thermofluid parameters

Some of the dimensionless thermofluid parameters that govern the operation of the GHP shown in Figure 2.2 are given in this subsection.

Galileo number, Ga, or modified Grashof number, Gr_M, in the evaporator and the condenser (it represents the ratio of buoyancy force, due to the difference in the densities of the liquid and vapor phases of the working fluid, to the viscous force):

$$\{Ga\}_{Evap;\,Cond} = \{Gr_M\}_{Evap;\,Cond} = \{\rho_l g(\rho_l - \rho_v) D_i^3 / \mu_l^2\}_{Evap;\,Cond} \qquad (2.7)$$

Jakob (or Jakov) number, Ja, in the evaporator and the condenser (it represents the ratio of the maximum sensible heat, absorbed by the liquid during condensation and boiling, to the latent heat of vaporization):

$$\{Ja\}_{Evap;\,Cond} = \left\{\frac{c_{p,l}(T_{wall} - T_{sat})}{h_{fg}}\right\}_{Evap;\,Cond}^{Abs} \qquad (2.8)$$

Prandtl number, $\Pr$, in the evaporator and the condenser (it represents the ratio of the rate of diffusion of momentum by viscous action to the rate of diffusion of thermal energy by conduction):

$$\{\Pr\}_{Evap;\,Cond} = \{\mu_l c_{p,l} / k_l\}_{Evap;Cond} \qquad (2.9)$$

Bond number, Bo, in the evaporator (it represents the ratio of the buoyancy force to the surface tension force):

$$\{Bo\}_{Evap} = \{g(\rho_l - \rho_v) D_i^2 / \sigma\}_{Evap} \qquad (2.10)$$

The condensate-film Reynolds number, Re_{film}, in the condenser (it represents the ratio of the inertia to viscous forces in the condensate film, and it is based on the mass flow rate of the condensate per unit perimeter of the inside surface of the tube; it is used to characterize transitions from smooth-laminar to laminar-wavy to turbulent flow regimes):

$$\mathrm{Re}_{film} = 4\Gamma / \mu_l \ \text{; with } \Gamma = (q_{input} / h_{fg}) / (\pi D_i) \qquad (2.11)$$

The fill ratio, FR, which is the ratio of the volume of the liquid in the GHP to the volume of the evaporator section:

$$FR = (Vol)_{liquid} / (Vol)_{Evap} \quad (2.12)$$

The details of the GHP that was designed, constructed, and used in this work are given in Chapter 3; and the experimental data are given in Chapter 4. The properties of water (working fluid) were obtained from Incropera and DeWitt (2002). With respect to these data, the above-mentioned dimensionless parameters had the following values or lay in the following ranges:

$$\begin{array}{l} L_{Evapoartor} / L_{Total} = 0.347 \;\; ; \;\; L_{Condenser} / L_{Total} = 0.365 \\ \text{Aspect ratio, } L_{Evaporator} / D_i = 10.294 \;\; ; \;\; (D_o - D_i) / D_i = 0.0685 \\ \text{Angle of tilt of the GHP from the vertical: } \theta = 0^{\circ},\ 10^{\circ},\ 20^{\circ},\ \text{and } 30^{\circ} \end{array} \quad (2.13)$$

$$\begin{array}{l} \{Ga\}_{Evap;\,Cond} = \{Gr_M\}_{Evap;\,Cond} = \left(3.14 \text{ to } 3.52\right) \text{x} 10^{8} \;\; ; \;\; \left(1.14 \text{ to } 2.31\right) \text{x} 10^{8} \\ \{Ja\}_{Evap;\,Cond} = \left(0.0094 \text{ to } 0.0207\right) \; ; \left(0.0026 \text{ to } 0.018\right) \\ \{\Pr\}_{Evap;\,Cond} = \left(4.25 \text{ to } 3.98\right) ; \left(6.65 \text{ to } 5.04\right) \\ \{Bo\}_{Evap} = \left(79.36 \text{ to } 79.84\right) ; \operatorname{Re}_{film} = \left(1.138 \text{ to } 7.383\right) \\ FR = 40\%,\ 50\%,\ 100\%,\ 150\% \end{array} \quad (2.14)$$

2.5 Concluding Remarks

In conclusion, it is noted again that the theoretical considerations presented in the earlier sections of this chapter were used to develop a basic understanding of the various thermofluid processes that occur within GHPs, and these considerations supplement those already presented earlier in Chapter 1 (Section 1.2).

Furthermore, as was noted in Chapter 1, Subsection 1.2.7, a good physical understanding of the underlying mechanisms and modes of operation of GHPs is provided by the many papers on GHPs in the published literature and the related theoretical considerations (some of which were presented in the earlier sections of this chapter). However, with respect to designs of GHPs for particular applications, only qualitative guidance can be obtained, at best, from the aforementioned papers and theoretical considerations, due to the relatively large number of governing parameters, different working fluids (and the variation of their properties with temperature), various different boiling regimes and condensation phenomena, and unsteady and steady-state operating regimes.

In the light of the above-mentioned comments and observations, it was concluded that it would be very useful to set up an experimental facility for obtaining quantitative guidance for particular specific applications of GHPs. That is the overall goal of this work, as was noted in Chapter 1 (Section 1). Descriptions of the GHP and the related experimental facility that were specially design, constructed and used in this work are provided in the next chapter (Chapter 3).

Chapter 3: Experimental Apparatus and Procedures

Descriptions of the gravity heat pipe (GHP) and the experimental set-up that were designed and constructed for this work, and also the related procedures that were used to run the experiments, are given in this chapter.

The above-mentioned descriptions are presented in the following eight sections of this chapter: 1) overview of the experimental set-up and the GHP; 2) comments on the choice of the working fluid and tube material; 3) condenser section; 4) evaporator section; 5) vacuum circuit and vacuum gauges; 6) working-fluid filling circuit; 7) supporting instrumentation and equipment; and 8) experimental procedures.

The lengths of the various parts of the GHP are presented in this chapter in inches (in) and feet (ft), as these units were used to facilitate fabrication of these GHP parts at machine shops in Montreal and Laval, Quebec, Canada. The equivalent values of these lengths in SI units can be obtained using the following conversion factors: 1 ft = 0.3048 m; and 1 in = 0.0254 m.

3.1 Overview of the Experimental Set-up and the GHP

The overall experimental set-up (including the GHP) that was designed, constructed, and used in this work is schematically illustrated in Figure 3.1. The various parts and subassemblies of this set-up are indicated by the numbers in Figure 3.1 and described briefly in Table 3.1. Isometric views of the main parts of the GHP and its supporting brackets are provided in Figure 3.2.

As is illustrated in Figure 3.2, the GHP has three main parts: evaporator section; adiabatic section; and condenser section. The evaporator and condensers sections were made of two straight stainless steel (SS) 316 tubes of circular cross-section and lengths 9.625 in and 10.125 in, respectively; each had a KF 25 vacuum flange welded to one end. The adiabatic section was a composite straight tube of circular cross-section: a central portion (of length 6.0 in) made of borosilicate glass tube (to allow flow visualization); and two 1-in long tubes, each welded to a KF 25 vacuum flange at one end, all made of Kovar; the other ends of each of these Kovar tubes were fused to the ends of the borosilicate glass tube. Kovar is an iron-nickel-cobalt alloy with a coefficient of linear thermal expansion almost identical to that of borosilicate glass, which enables vacuum-tight fused joints between parts made of these materials. The adiabatic section, made up of the borosilicate glass and Kovar parts, was purchased (prefabricated) from Larson Electronic Glass.

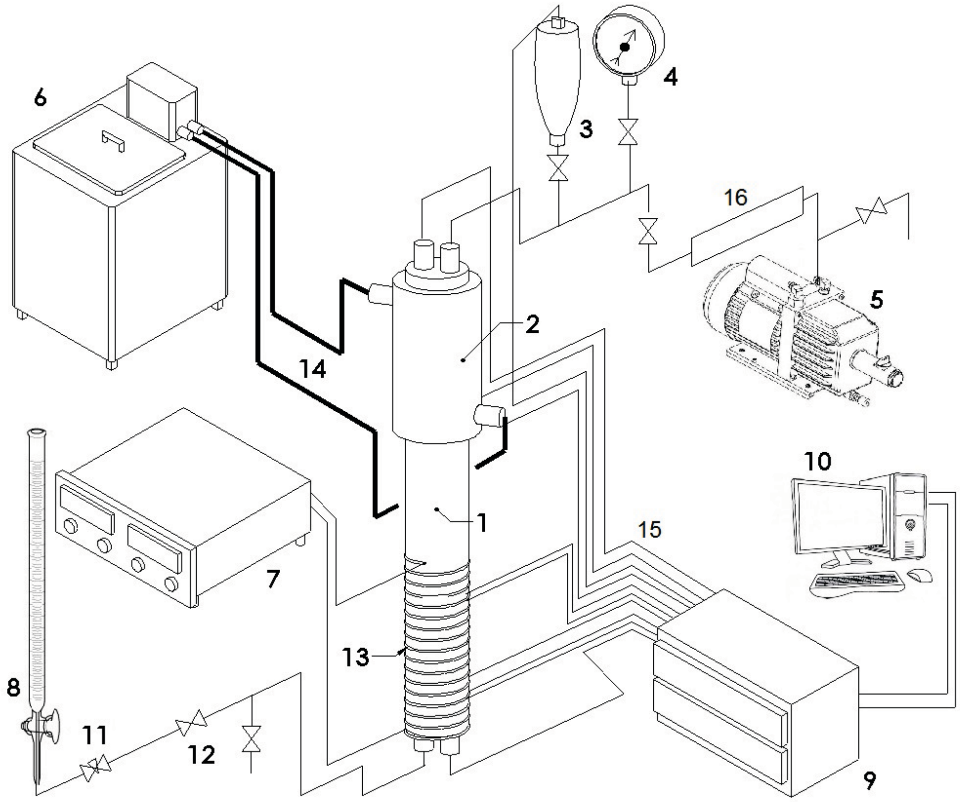

Figure 3.1: Schematic illustration of the overall experimental set-up including the GHP.

Table 3.1: Brief descriptions of the numbered parts and subassemblies indicated in Figure 3.1

1	Gravity heat pipe (GHP)	9	Data acquisition and control system
2	Cooling-water jacket of the GHP	10	PC with USB-GPIB interface
3	Electronic vacuum gauge	11	Needle valve
4	Mechanical vacuum gauge	12	Ball valves
5	Vacuum pump	13	Teflon-coated nichrome heating wire
6	Constant-temperature bath	14	Cooling-water supply line
7	DC power supply	15	Type-E thermocouples
8	Graduated glass burette	16	Flexible metal vacuum hose (SS 316)

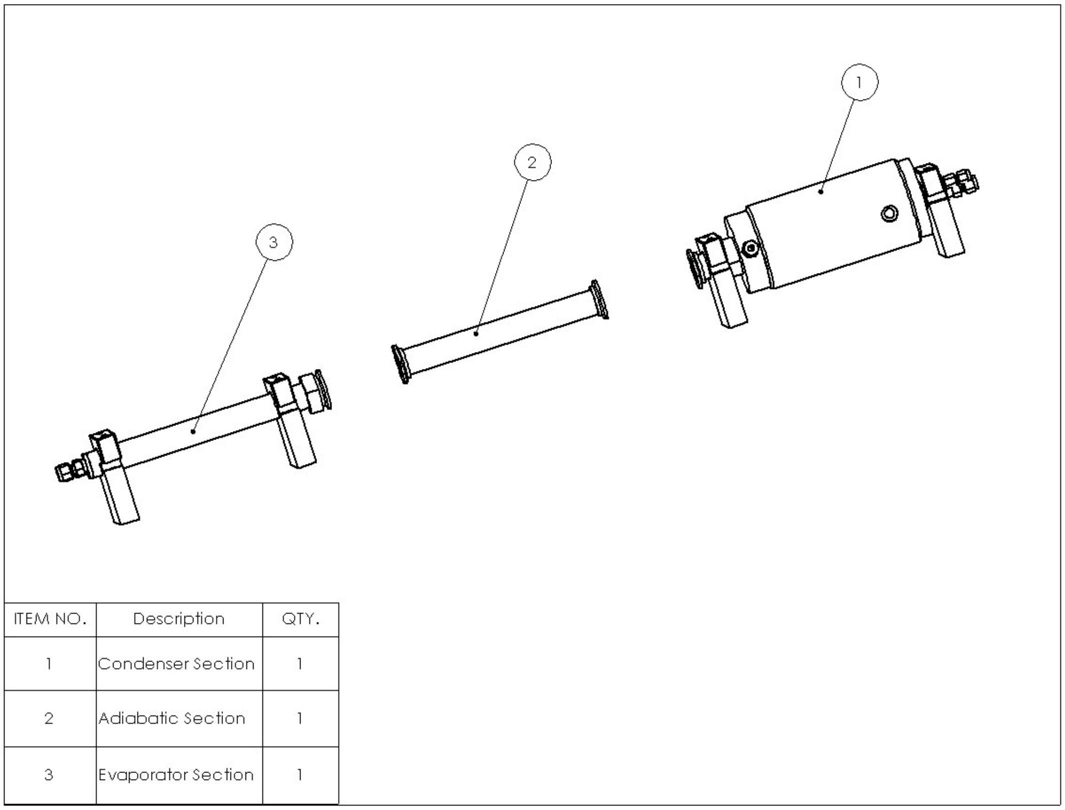

Figure 3.2: Isometric views of the main parts of the GHP and its support brackets.

The tubes in all three sections (evaporator, adiabatic, and condenser) of the GHP shown in Figure 3.2 were of 1-in outside diameter (OD) and 0.93-in inside diameter (ID). The KF 25 vacuum flanges on the ends of the evaporator, condenser, and adiabatic sections were assembled together (in a vacuum-tight manner) by using matching centering rings, fluroelastomer O-rings, and aluminium clamps.

The evaporator section (all metal parts made of SS 316) of the GHP had an active heating length of 8 in. Over this active heating length, a Teflon-covered nichrome wire was tightly (and closely) wound around the outer wall of the evaporator tube and electrically heated to provide an essentially uniform wall-heat-flux boundary condition. The condenser section of the GHP (all metal parts made of SS 361) had an active cooling length of 9 in. This active cooling length was maintained at an essentially constant temperature, 20 ^{o}C nominal, throughout the experiments, using a concentric annular jacket supplied with distilled water as the coolant (from a constant-temperature bath).

The above-mentioned dimensions of the three main sections of the GHP were determined on the basis on the following considerations:

- The work space available in the Heat Transfer Laboratory of the Department of Mechanical Engineering at McGill University
- The machining facilities, instrumentation, and materials that were either available or accessible for this work
- The overall budget for this work
- Assessment of the investigations and results available in the published literature, as described in Chapter 1 (Section 1.2).
- The results of computer simulations based on a rudimentary quasi-one-dimensional model of the GHP.

Swagelok stainless steel (SS 316) tubes (1/8-in nominal), ball and needle valves, and compression fittings were used in the filling and vacuum circuits of the GHP set-up shown in Figure 3.1. The total length of the GHP was 27.75 in. With the above-mentioned dimensions of the evaporator section of the GHP, 88 ml of the working fluid (distilled water was used in this work) was required for a fill ratio (volume of liquid to inside volume of evaporator) of 100 %.

The overall experimental set-up, including the GHP, included the following supporting equipment and parts: a DC power supply for powering the Teflon-insulated nichrome wire wrapped around the active heating section of the evaporator; a calibrated shunt for measuring the electrical current supplied to the aforementioned heating wire; a safety cutoff circuit, including a relay and a power supply, to switch off the main electrical power to the nichrome wire when the temperatures in the GHP exceeded user-selected values; a constant-temperature bath for providing cooling water to the concentric jacket surrounding the active cooling portion of the condenser section; a circuit for filling desired amounts of the working fluid into the GHP; a vacuum pump (along with the tubings, fittings, and valves) for creating a vacuum in the GHP before charging it with the working fluid; and a layer of *Armaflex* insulation over the outer surfaces of the various components of the GHP, coolant supply lines, and some parts of the filling circuit to minimize heat loses to (or gains from) the ambient environment.

Ten thermocouples were used for measuring temperatures at selected points on the outer surface of the active heating length of the evaporator section; and another ten thermocouples were used for measuring temperature at selected points on the outer surface of the active cooling length of the condenser section. Three thermocouples were used to measure the ambient temperature at locations adjacent to the evaporator, adiabatic, and condenser sections of the GHP throughout all of the experimental runs. Six thermocouples were used to record temperatures at selected locations of the vacuum circuit. Two sheathed (SS 304 sheath material) thermocouples were inserted inside the GHP, one each from the end-plates of the top (condenser) and bottom (evaporator) sections. Two thermocouples were used to measure the cooling-water temperature at the inlet and exit ports of the annular jacket of the condenser section. All thermocouples were calibrated to an accuracy of ± 0.05 ^{o}C over the temperature range 2 ^{o}C to 65 ^{o}C. Electronic and mechanical vacuum gauges were used to monitor the absolute pressure inside the GHP, before filling it with the working fluid and also throughout the course of each experimental run. A data acquisition and control system, connected to a personal computer (PC) via a USB-GPIB interface, and a computer program (written using LabVIEW) were used for monitoring, recording, and saving the experimental data from the above-mentioned supporting instrumentation and equipment.

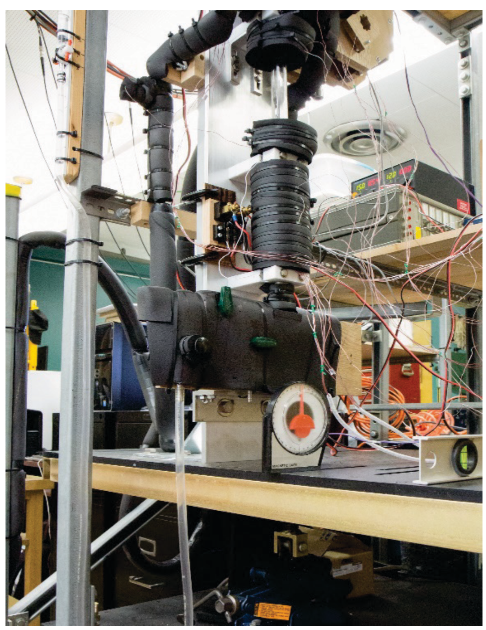

Figure 3.3: Photograph showing some portions of the GHP mounted on an aluminium support-plate anchored to a tilt table.

Four Teflon brackets (design and machined specially for this work) were used to mount the GHP on an aluminum support-plate (4-ft long; 6-in wide; and 1/4-in thick). This aluminum support plate was anchored to a tilt table, using a cast iron angle bracket. The tilt table allowed for investigations of the GHP at various inclination angles (from the vertical) in the range 0^o to 30^o. A photograph showing the insulated evaporator and adiabatic sections of the GHP (with the flow visualization section exposed), the aluminum support plate, the tilt table, and a portion of the filling circuit (insulated, except for the glass burette and connecting Tygon tube) is given in Figure 3.3.

Additional details of the condenser and evaporator sections of the GHP are presented in Sections 3.3 and 3.4, respectively. The vacuum circuit, the working-fluid filling circuit, and some of the supporting instrumentation and equipment are discussed in Sections 3.5, 3.6, and 3.7, respectively. The procedures that were designed and used to run the experiments are summarized in Section 3.8.

3.2 Comments of the Choice of the Working Fluid and the Tube Material

Within the estimated operating temperature range of any GHP, some of the characteristics that must be examined to determine the most acceptable working fluids for the particular application of interest are the following [Reay et al. (2013)]: 1) good stability of the fluid properties on repeated thermal cycling in the temperature range of interest; 2) good wetting of the wall material; 3) vapor pressure not too high or too low in the operating temperature range; 4) good chemical compatibility with the wall material; 5) safety (nontoxicity) to humans; 6) high thermal conductivity; 7) high latent heat of vaporization; 8) low dynamic viscosity of both the liquid and the vapor phases; and 9) acceptable freezing and boiling points.

Ammonia, acetone, methanol, ethanol, and water were some of fluids that were considered for use as the working fluid in this work. Based on the various selection characteristics given above, and also factors such as cost and availability, water was selected as the working fluid for use in the GHP designed, constructed, and investigated in this work.

The function of the tube of the GHP is to isolate the working fluid from the outside environment. Therefore, it has to be leak-proof, maintain the inside-to-outside pressure differential across its walls, and enable a good rate of heat transfer to and from the working fluid. Some of the other considerations that go into the selection of the tube material are the following

[Reay et al. (2013)]: 1) compatibility and wettability with respect to the working fluid in the operating temperature range; 2) good strength-to-weight characteristic; 3) high thermal conductivity; 4) good machinability and weldability; 5) ready availability and low cost; and 6) maintenance of non-brittleness and strength with repeated thermal cycling.

Possible materials for the tube include aluminum, stainless steel, copper, brass, and titanium. In this work, stainless steel 316 L was selected as the tube material, mainly because of its availability, strength, resistance to corrosion and brittleness, good machinability, and excellent weldability.

The combination of water as the working fluid and SS 316 as the tube material, although quite commonly used, is not without its flaws. Ever since heat pipes were first conceived, difficulties have been experienced while operating a water-steel combination, mainly because of the generation and accumulation of hydrogen in the tube over time [Reay et al. (2103)]. This hydrogen generation and accumulation usually manifests itself as a cold plug of non-condensible gas in the condenser section of the heat pipe. However, this problem is present only at the elevated operating temperatures (~250 ^{o}C or higher) in the presence of metal oxides. As the operating temperature range in the GHP experiments undertaken in this work was 20 ^{o}C to 80 ^{o}C (maximum in a few cases), the pros of the water-steel combination far outweighed the cons.

3.3 Condenser Section

The condenser section of the thermosyphon spanned a 10.125-in long segment of the top (upper) portion of the GHP. It consisted of a stainless steel SS 316 L tube, having inner and outer diameters of 1 in and 0.935 in, respectively, and a 9-in total active cooling length. The active cooling length had a concentric annular cooling-water jacket on its outside surface; and distilled water supplied from a constant-temperature bath (at a nominal temperature of 20 ^{o}C; and almost constant volume and mass flow rates of 63.6 ml/s and 0.0635 kg/s, respectively) was circulated through this jacket. The condenser-section assembly and an exploded view of its various components are presented in Figures 3.4 and 3.5, respectively.

The outer tube of the concentric annular cooling-water jacket was also made of stainless steel SS 316: it was approximately 9-in long, its outer diameter was 3.4 in, and it had four *Swagelok* compression fittings welded into holes drilled in its curved surface. This annular cooling-water jacket was mounted on the GHP using specially designed end plates and four O-rings. The cooling water was fed into this annular jacket through a port at the lower end and taken out through another port at its upper end, using 3/8-in *Swagelok* compression fittings. A photograph of these and also some other parts of the GHP is given in Figure 3.6.

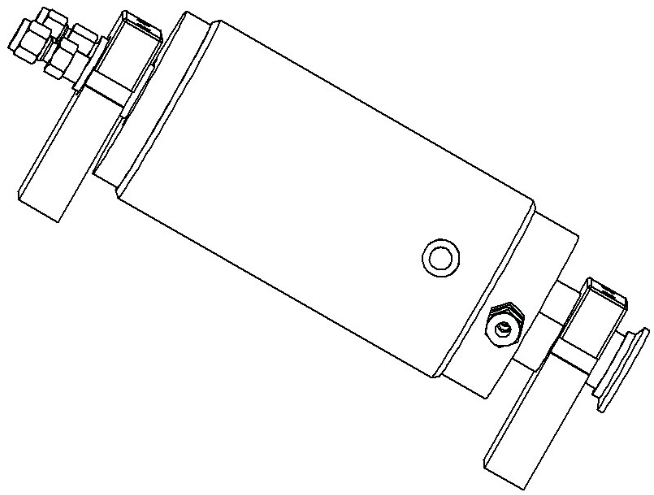

Figure 3.4: Schematic illustration of the assembled condenser section of the GHP.

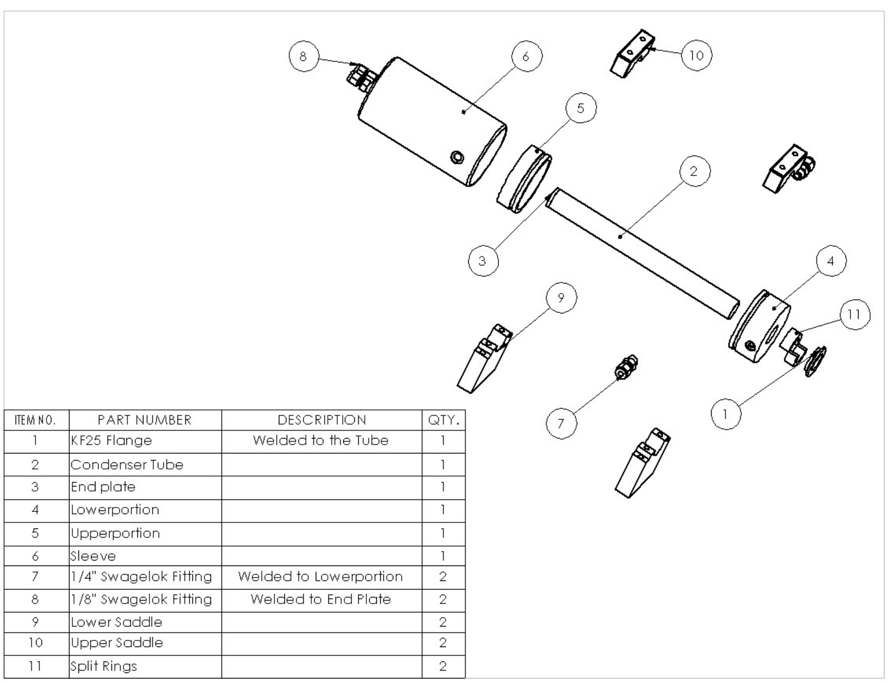

ITEM NO.	PART NUMBER	DESCRIPTION	QTY.
1	KF25 Flange	Welded to the Tube	1
2	Condenser Tube		1
3	End plate		1
4	Lowerportion		1
5	Upperportion		1
6	Sleeve		1
7	1/4" Swagelok Fitting	Welded to Lowerportion	2
8	1/8" Swagelok Fitting	Welded to End Plate	2
9	Lower Saddle		2
10	Upper Saddle		2
11	Split Rings		2

Figure 3.5: Exploded view of the condenser section, showing its various components.

Figure 3.6: Photograph of various parts of the GHP. The adiabatic section is the tube with a transparent borosilicate glass portion in its central region (it was used for flow visualization). A spool of Teflon-covered nichorme heating wire, which was later wrapped around the tube of the evaporator section, is shown in the left-hand side of this photograph.

Two T-junction *Swagelok* connectors were attached to the inlet and outlet cooling-water ports of the above-mentioned annular jacket, to insert thermocouples which were previously calibrated in accordance with a procedure described later in Section 3.7.1. These thermocouples were used to measure the inlet and outlet temperatures of the cooling water. It should be noted here that the above-mentioned volume and mass flow rates (63.6 ml/s and 0.0635 kg/s, respectively) of the cooling water through the annular jacket were high enough to make the difference between the two aforementioned temperatures negligibly small.

Two 1/8-in *Swagelok* adapter fittings were welded into holes drilled in the lower end-plate of the annular cooling-water jacket, and used for inserting 10 calibrated thermocouples. These thermocouples were attached to the outer wall of the condenser-section tube, in a helical arrangement, to measure its temperature at 10 chosen locations. Two 1/8-in bore-through *Swagelok* adapter fittings were welded into holes drilled in the upper end-plate of the GHP condenser section: one of these fittings was used to insert and hold a 6-in long calibrated sheathed (SS 316) thermocouple, with its tip approximately 4 in inside the condenser section (this thermocouple was used to measure the temperature of the water vapor inside the condenser section of the GHP during its operation); the other fitting was used to connect the condenser section to the vacuum pump via a vacuum circuit (described later in Section 3.5). The other (lower) end of the condenser-section tube (SS 316) was welded to a KF 25 vacuum flange (SS 316), as shown in the previous figures. The components of the KF 25 vacuum-flange assembly are shown in Figure 3.7. Apart from allowing easy connect and disconnect procedures, these flanges have a vacuum rating of $1\text{x}10^{-8}$ Torr and reusable centering rings and O-rings. Photographs of some of the other parts of the condenser section and the cooling-water jacket are shown in Figure 3.8.

Figure 3.7: Photograph of the clamps, centering rings, and O-rings of K 25 vacuum flanges.

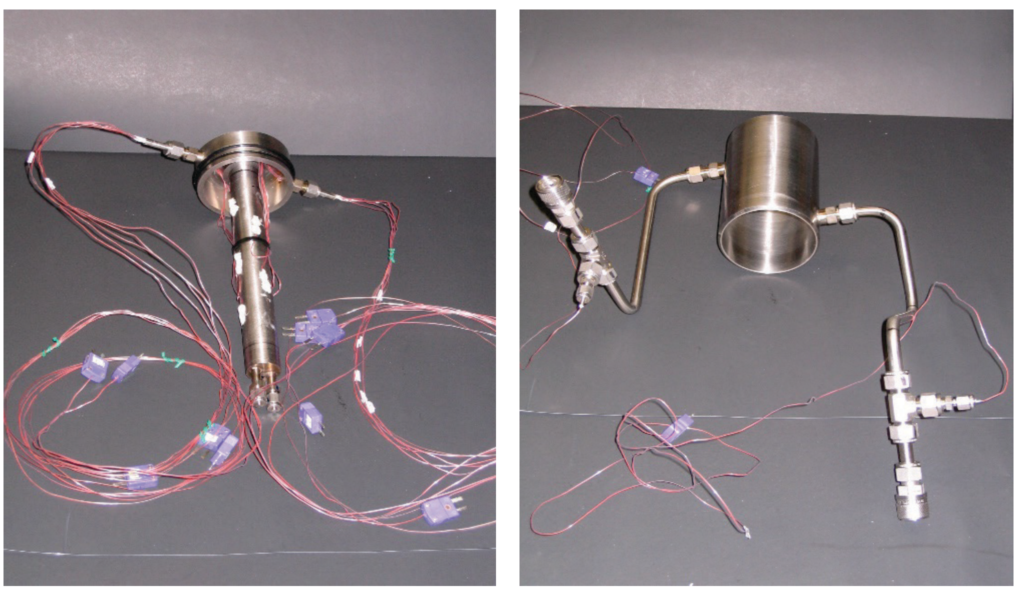

Figure 3.8: Photographs of the condenser-section tube with the attached thermocouples (left); and (right) outer tube of the annular cooling-water jacket, with the inlet and outlet ports and tubes, *Swagelok* T-junctions, quick-connect fittings, and the inserted thermocouples.

After cleaning and drying of the machined components, the lower end-plate of the annular cooling-water jacket (with the O-rings inserted) was slipped onto the condenser tube from the top. Then, five calibrated thermocouples (made from 30 AWG *Omega* TT-E-30 Teflon-insulated thermocouple wire) were routed through each of the 1/4-in *Swagelok* fittings and attached on the outer surface of the condenser-tube in the helical pattern mentioned earlier. The beads of these thermocouples were coated with a high-thermal-conductivity glue (*Omegabond 101*), and a marine glue was used to attach the coated beads of these thermocouples to the outer surface of the condenser-section tube.

Suitably bent 3/8-in tubes (SS 316) were connected to the inlet and outlet cooling-water ports (see Figure 3.8). These bent tubes ensured the appropriate layout of the cooling-water circuit. Each one of these two bent cooling-water tubes was connected at the other end to one of the two straight portions of a *Swagelok* T-junction (SS 316); a 1/8-in tube, with a calibrated thermocouple inserted and glued within it, was connected through the T-portion of this junction; and the other straight portion of the T-junction was connected to a *Swagelok* quick-connect fitting (SS 316). These assemblies are shown in the right-side photograph given in Figure 3.8.

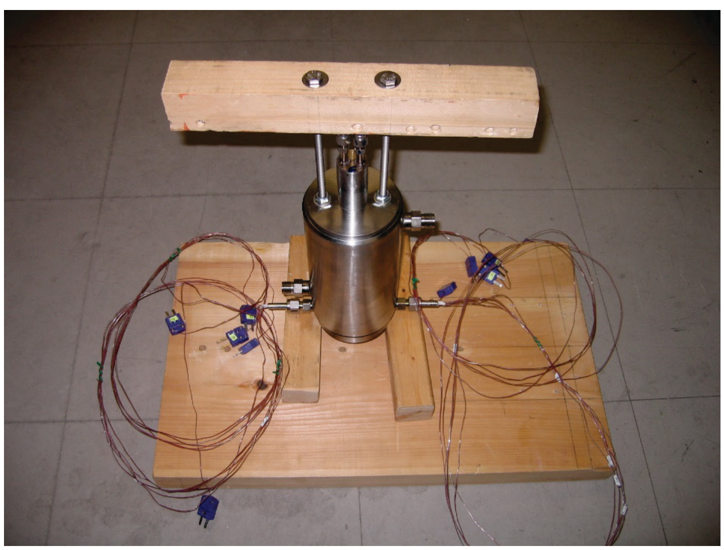

Figure 3.9: Photograph of the assembled condenser section of the GHP, with a specially designed jig attached to the upper end-plate of the annular cooling-water jacket.

The upper end-plate of the annular cooling-water jacket was introduced concentrically onto the condenser-section tube and into the outer sleeve of this jacket using a specially designed jig. This jig ensured proper assembly and disassembly of the condenser section of the GHP. A photograph of this jig, attached to the assembled condenser section, is given in Figure 3.9.

After assembly and mounting of the entire GHP (as described in Section 3.1), the outer surfaces of the entire condenser section, including its active cooling portion, were insulated with a layer of *Armaflex* pipe insulation. The outer diameter of this insulation on the cooling-water jacket was approximately equal to 4.5 in. The quick-connect fittings attached to the bent tubes of the cooling-water jacket were connected to a constant-temperature bath (*NESLAB* Endocal LT 50) using flexible *Neoprene* tubes having 3/8-in and 5/8-in inner and outer diameters, respectively. These flexible tubes were insulated with *Armaflex* pipe insulation (1/2-in thick).

3.4 Evaporator Section

As was mentioned earlier, the active heating section of the closed-loop thermosyphon consisted of a stainless steel tube having 0.93-in and 1-in inner and outer diameters, respectively, and a 9.625-in total length. The bottom end-plate of the evaporator had two 1/8-in *Swagelok* bore-through adapter fittings welded to it: one of these was used to insert and hold a calibrated sheathed (SS 316) thermocouple, with its tip approximately 4 in inside the evaporator section (this thermocouple was used to measure the liquid-pool temperature inside the evaporator section of the GHP); and the other fitting was connected to the filling circuit, which was used to fill the GHP with working fluid (and also drain it), when required. The other end of the evaporator-section tube was welded to a KF 25 vacuum flange (photograph given in Figure 3.7).

A total of 10 calibrated Type-E thermocouples were attached to the outer surface of the tube (SS 316) of the active heating section. The beads of these thermocouples (coated with *Omegabond 101*) were positioned in a helical pattern at regular intervals along the length of the tube. The fabrication and calibration of these thermocouples (and also the other thermocouples used in the experimental investigation) are discussed later in this chapter (Subsection 3.7.1).

A Teflon-coated nichrome heating wire (27 AWG wire; with 0.3 mm thickness of Teflon coating) was wound tightly and closely (contiguously, without overlapping) around the outer surface of the tube of the active heating section. Electrical power input (from a DC power supply) to this nichrome wire was used to obtain an essentially uniform heat flux on the outer surface of the tube of the active heating section. The Teflon coating ensured that there was no direct electrical contact between the nichrome wire and the outer surface of the stainless steel tube. This Teflon-coated nichrome wire was wound on top of the coated thermocouple beads, in successive short portions (1.5-in long), using a specially designed and constructed jig and procedure (details given later in this section).

Prior to the attachment of the beads of the above-mentioned 10 thermocouples and the winding of the Teflon-coated nichrome wire, a thin layer of a high-thermal-conductivity paste (*Omegatherm* 201; thermal conductivity of 2.31 W/m°C) was applied on the outer surface of the active heating portion of the stainless steel tube. This paste was used to reduce the thermal contact resistance between the Teflon-coated nichrome wire, and also the thermocouples beads, and the outer surface of the stainless steel tube of the active heating section. Once the nichrome wire was tightly and closely wound around the stainless steel tubing and the thermocouple beads, the outer surface of this assembly was wrapped with thin Teflon sheets, to contain any excess high-thermal-conductivity paste and provide a clean outer surface that could be conveniently handled during the final assembly of the GHP. Electrical bus-bar terminals were attached near one of the Teflon supports of the GHP, and the extremities of the nichrome wire (stripped off the Teflon coating) were fastened to these terminals. Larger-gauge insulated copper wires (of per-unit-length electrical resistance very much lower than that of the nichrome wire) were used to connect these terminals to the main DC power supply.

Figure 3.10: Photograph of a special jig designed to facilitate the attachment of thermocouples and winding of the Teflon-coated nichrome heating wire on the evaporator-section steel tube.

A specially designed and constructed jig was used to wind the Teflon-coated nichrome wire on the outer surface of the evaporator-section steel tube. A photograph of this jig is provided in Figure 3.10. The stainless steel tube was held in place horizontally near its ends by two supports. A crank and a straight support frame were temporarily fastened to one end of the stainless steel tube. The crank was used to rotate the tube; and the support was used to hold the lead wires of the calibrated thermocouples, and prevent them from tangling up during the winding of the nichrome wire on the stainless steel tube. A spool of the Teflon-coated nichrome wire was supported on a metal rod whose longitudinal axis was maintained parallel to the axis of the stainless steel tube of the active heating section (as can be seen in Fig. 3.10).

The bead of each of the 10 calibrated thermocouples was attached (sequentially, in 1.5-in long sectors or portions) to the outer surface of the evaporator-section tube in the following manner: 1) the thermocouple bead was properly located on the outer surface of the stainless steel tube a helical pattern; 2) the thermocouple was secured in place temporarily using electrical tape, about 15 mm behind the bead, 3) each 1.5-in long tube sector and the thermocouple beads were covered with a high-thermal-conductivity paste (*Omegatherm* 201); 4) the Teflon-coated nichrome wire was wound tightly and closely around this 1.5-in long section of the tube, over the thermocouple bead and wire; 5) a tie-wrap was used to temporarily hold the coiled nichrome wire in place; 6) the electrical tape holding the thermocouple lead wire on the outer surface of the tube was removed; and 7) the thermocouple lead wire was bent away from the outer surface of the tube and secured to the frame (of a jig) fixed at one end of the tube (see Fig. 3.10). This procedure was repeated sequentially until the beads of all 10 thermocouples were attached and the winding of the Teflon-coated nichrome wire was completed.

The above-mentioned procedure for attaching the beads of the thermocouples and winding the Teflon-coated nichrome wire on the outer surface of the tube (of the active heating portion of the evaporator section) was performed by two persons: one turned the crank of the special jig (see Figure 3.10) slowly and locked it in place when needed; and the other attached the thermocouples, applied the high-thermal-conductivity paste, and ensured that the Teflon-coated nichrome wire was wound tightly and closely, without any overlap, on the outer surface of the tube. Once this procedure was completed, the previously mentioned tie-wraps were sequentially removed, and thin Teflon sheets were wrapped around the outer surface of the nichrome wire coil and kept in place using new tie-wraps.

Once the above-mentioned procedures were completed, the evaporator section of the GHP was finalized. The whole evaporator-section assembly was then insulated with a layer of *Armaflex* foam pipe insulation (having a thermal conductivity of approximately 0.04 W/m°C). The outer diameter of this insulation was approximately equal to 2 inches. After complete assembly and insulation of the active heating section, the evaporator section of the thermosyphon was mounted vertically on Teflon brackets which were fastened on an aluminum frame. The evaporator section was then connected to the adiabatic section of the GHP using the KF 25 vacuum flange. The GHP was then ready to be connected to the vacuum, filling, and electrical circuits.

3.5 Vacuum Circuit and Vacuum Gauges

The GHP was vacuumed as thoroughly as possible (roughly 2 x 10^{-3} mbar with the equipment available) before filling it with the desired amount of working fluid. A vacuum circuit was designed and implemented to create this vacuum and carry out the following operations:

- Leak testing of the experimental set-up prior to filling the GHP with the working fluid
- Degassing of the all inner surfaces of the GHP
- Degassing of the working fluid
- Removal of non-condensable gases from within the GHP and filling and vacuum lines
- Assisting with the filling and metering of the working fluid

A schematic illustration of the vacuum circuit and the vacuum gauges used in this work is given in Figure 3.11. Before describing the vacuum circuit and its operation, it is worth mentioning some important considerations taken in its construction. The circuit was made of suitable lengths of 1/8-in SS 316 *Swagelok* tubes and PTFE seated *Swagelok* ball valves (body made of SS 316). The circuit was assembled together using suitable Swagelok compression fittings; and the vacuum gauges were attached to it using KF 16 vacuum flange assemblies.

A two-stage oil-sealed rotary-vane vacuum pump (*Edwards* RV8) was used in this work. It offered vacuum conditions that were quite adequate for this work, in both high-vacuum and high-throughput modes, and with or without the gas-ballast mode. The gas-ballast mode of operation of this vacuum pump is required when the air being vacuumed has water vapor mixed in it: this mode prevents the water vapor from condensing in the oil filled in the vacuum pump, and thus avoids reduced vacuum performance, corrosion, and pump seizure. The gas-ballast mode ensures that the water vapor entering the vacuum pump stays and exits in the vapor state, and thus keeps the oil unadulterated, increasing the life and ensuring the performance of the pump. A photograph of the vacuum pump used in this work is given in Figure 3.12, and its main characteristics are presented in Table 3.2.

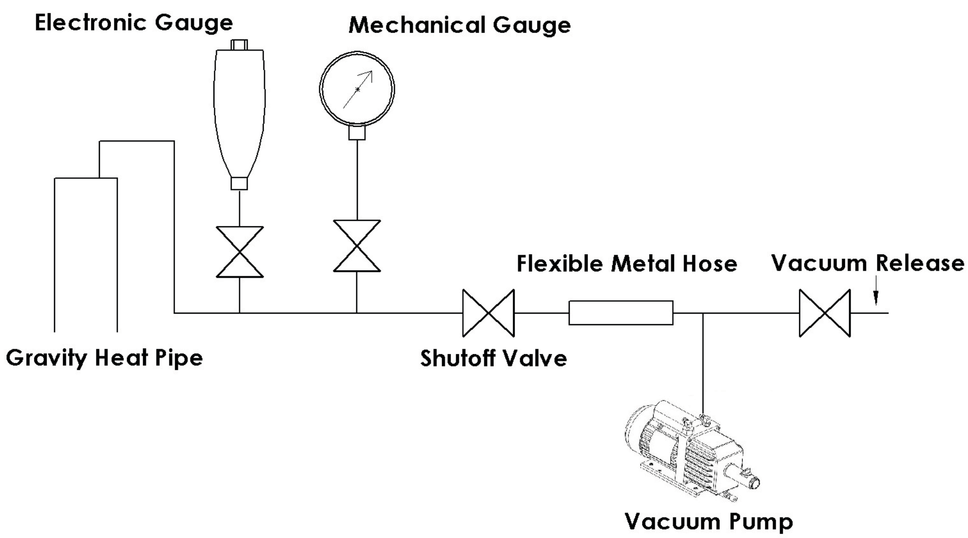

Figure 3.11: Schematic illustration of the vacuum circuit and the vacuum gauges.

Figure 3.12: Photograph of the vacuum pump used in this work.

Table 3.2: Main characteristics of the vacuum pump used in this work.

Edwards RV8 Vacuum Pump	
Ultimate Pressure	2 x 10^{-3} mbar
Ultimate Pressure (Gas Ballast Mode)	3 x 10^{-2} mbar
Maximum Allowed Inlet Pressure	1500 mbar

The vacuum pump was connected to the vacuum circuit via a K 25 vacuum flange assembly, a short length of 3/8-in *Swagelok* SS 316 tubing, and a 3/8-in *Swagelok* SS 316 T-junction (see Figure 3.11). One end of the straight potion of this T-junction was connected to a shutoff ball valve that was used readmit air into the GHP and the vacuum circuit, when desired; the other end of the straight portion of the T-junction was connected to one end of a 6-ft long flexible vacuum hose (made of SS 316; manufactured by *Swagelok*) via a 3/8-in *Swagelok* SS 316 quick-connect fitting. The other end of this flexible vacuum hose was connected to the rest of the vacuum circuit via another 3/8-in *Swagelok* SS 316 quick-connect fitting and a shutoff ball valve, which allowed isolation of the vacuum pump after the creation of the desired vacuum conditions inside the GHP.

Edwards CG16K Dail Gauge   Inficon CDG020D Gauge

Figure 3.13: Photographs of the mechanical (left) and electronic (right) vacuum gauges.

Table 3.3: Specifications of the mechanical (Edwards) and electronic (Inficon) vacuum gauges.

Gauge	Range	Accuracy	Resolution	End Connection
Edwards CG16K	0 - 125 mbar	±2 % of FS	0.5 mbar	KF 16
Inficon CDG020D	0 – 1000 Torr	±0.5 % of Reading	0.05 % FS	KF 16

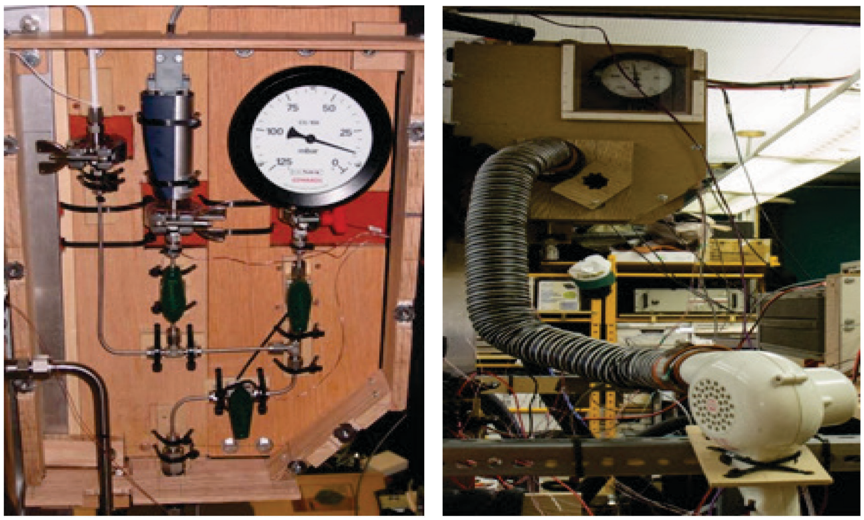

Figure 3.14: Photographs of a portion of the vacuum circuit, the electronic and mechanical vacuum gauges, and a wooden box or cabinet (left and right); and the hair dryer and the flexible hose that were used provide heated air to the aforementioned wooden box (right).

The vacuum circuit was connected to the GHP through one of the two 1/8-in *Swagelok* fittings welded to the top end-plate of the condenser-section tube (as was mentioned in Section 3.3). Two vacuum gauges were included in the vacuum circuit (see Figures 3.11, 3.13, and 3.14) to measure the absolute pressure in the GHP before and after it was filled with the working fluid, and also during the experiments. These two vacuum gauges, one a mechanical Bourdon-tube gauge (*Edwards* CG16K) and the other an electronic capacitance-type diaphragm gauge (*Inficon* CDG020D), were connected in parallel as shown in Figures 3.11 and 3.14. The mechanical gauge allowed a quick and convenient visual check of the vacuum conditions inside the GHP; the electronic gauge provided the desired accuracy in the absolute pressure data and also allowed computer-based acquisition of this data; and the two gauges also allowed quick and continuous cross-checking of the pressure data measured by each of them. As shown in Figures 3.11 and

3.14 (left side), each gauge was connected to the vacuum circuit via a K 16 vacuum flange assembly (which allowed easy installation and replacement of the gauge, if needed) and a shutoff ball valve (which allowed isolation of the gauge in case defects or leaks were detected or suspected during the experiments). Photographs of these two gauges are given in Figures 3.13 and 3.14 (left side); and their main specifications are provided in Table 3.3.

Substantial portions of the vacuum circuit were exposed to the ambient room temperature; which varied from 21 ^{o}C to 24 ^{o}C. During the experiments on the GHP, the average temperature of the water vapor inside the condenser section varied between 21 ^{o}C to 37 ^{o}C, and the average temperature of the water in the evaporator section varied between 23 ^{o}C to 53 ^{o}C. Under these operating conditions, special design features had to be incorporated into the overall experimental set-up to prevent the water vapor from condensing inside the lines, fittings, and gauges of the vacuum circuit. Such condensation of the water vapor, if it were allowed to occur, would have severely compromised the accuracy and reliability of the absolute pressure measurements yielded by the aforementioned vacuum gauges, and also adversely affected their service life.

To ensure that water vapor did not condense inside the lines, fittings, and gauges of the vacuum circuit, they were all maintained at temperatures that were between 55 ^{o}C to 70 ^{o}C. The vacuum gauges selected for this work (see Table 3.3) could operate reliably at temperatures up to 75 ^{o}C. The elevated temperatures of the aforementioned components of the vacuum circuit were achieved by enclosing them inside a wooden box (cabinet) that was supplied with hot air from a common hair dryer, via a special flexible hose (that could handle temperatures up to 90 ^{o}C). The hair dryer chosen for this task had several different 'heat' settings, and specially designed adjustable ventilation slots were built into the wooden box. These features of the hot-air arrangement were used to control the steady-state temperatures achieved by the aforementioned components of the vacuum circuit and ensure that they were in the desired range. The photographs in Figure 3.14 show the aforementioned wooden box, the hair dryer, and the flexible hose. In addition to this hot-air arrangement, the vacuum line coming directly out of the top end-plate GHP condenser section was also heated by passing electrical current through a Teflon-coated nichrome wire wound tightly and closely around it. The temperatures of the aforementioned components of the vacuum circuit were continuously monitored during the experiments on the GHP; and these temperatures were maintained in the desired range (55 ^{o}C to 70 ^{o}C) by adjusting the aforementioned heating arrangements.

3.6 Filling Circuit

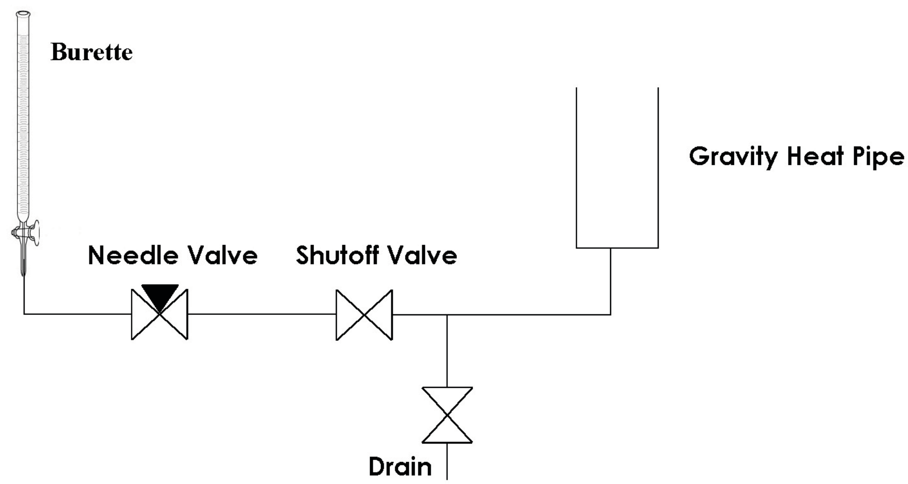

Figure 3.15: Schematic illustration of the filling circuit and the glass burette.

The filling circuit is schematically illustrated in Figure 3.15. This circuit was made up of a graduated 100-ml glass (borosilicate) burette with a stopcock; a *Swagelok* needle valve (SS 316 body and 1/8-in compression fittings at each end; PTFE seat for the stem); two *Swagelok* shutoff ball valves (SS 316 body and 1/8-in compression fitting at each end; PTFE seals); 1/8-in diameter SS 316 tubing; and a *Swagelok* 1/8-in T-junction with compression fittings at each of its three ends. The glass burette was connected to a 1/4-in-hose-barb-1/8-in-tube reducer (attached to one end of the needle valve) using a flexible *Tygon* tube (1/4-in ID; 7/16-in OD). The filling circuit was attached to the GHP using a 1/8-in SS 316 tube connected one end to the above-mentioned T-junction and at the other end to one of the two *Swagelok* 1/8-in bore-through compression fittings adapters welded to the bottom end-plate of the evaporator section.

The glass burette was used to hold the degassed working fluid and also to determine the amount of the working fluid that was metered into the GHP in a controlled manner using the needle valve. The shutoff valves were used to isolate the GHP from the burette, needle valve, and the outside air during the initial vacuuming procedure; the shutoff valve connected to the drain pipe (see Figure 3.15) was kept closed during the filling procedure, and opened when draining of the working fluid from the GHP was desired.

3.7 Supporting Instrumentation and Equipment

The thermocouples, DC power supplies, constant temperature water bath, data acquisition system, and an overheat-safeguard system that were used in this work are described concisely in this section.

3.7.1 Thermocouples

Eighty thermocouples were calibrated for use in the experiments. Of these, 70 were fabricated in the laboratory from 6-ft lengths of Teflon-coated 30 AWG Type-E (chromel-constantan) thermocouple wire (*Omega* TT-E-30); and the other 10 were prefabricated 6-in long, 1/8-in diameter, sheathed (SS 304) Type-E thermocouples (ungrounded) with a miniature male connector at the open end of the sheath (*Omega* E-MQ-SS-125-U-6). The 70 thermocouples fabricated in the laboratory were made by spark-welding the exposed ends of the chromel and constantan wires. After fabrication, the beaded end of each of these 70 thermocouples was coated with a high-thermal-conductivity glue (*Omegabond* 101); and the other end was attached to a miniature male connector (*Omega* SMPW-E-M). Each of the 10 sheathed thermocouples was connected to 6-ft long thermocouple 24 AWG Type-E extension wire (*Omega* EXTT-E-24), attached to miniature female and male connectors at its ends (*Omega* SMPW-E-F and SMPW-E-M, respectively).

It should be noted that of the above-mentioned 70 thermocouples fabricated in the laboratory, only 31 were used in the GHP experiments; and of the 10 prefabricated sheathed thermocouples purchased from Omega, only two were used in the GHP experiments.

Each of the far-end miniature male connectors of the above-mentioned 80 thermocouples was plugged into miniature Type-E female connectors mounted in 19-in panels (*Omega* 19MJP-2-40-E) fitted on specially fabricated wooden relay boxes. Each of the 80 Type-E female connectors were attached to one end of a 3-ft long thermocouple 24 AWG Type-E extension wire (*Omega* EXTT-E-24); the other end of this 3-ft extension wire was connected to the socket-pair of a selected input channel, of a 80-channel data acquisition/control unit (*Hewlett-Packard* 3497A; fitted with four twenty-channel hardware-compensated relay multiplexer temperature-measurement cards, Option 020). This data acquisition/control unit contains a 5½-digit electronic voltmeter that provides a resolution of 1 μV and an accuracy of ±3 μV when reading voltages in the range from 0 to 0.1V. This voltmeter was used to read the output voltages of the thermocouples; and the data acquisition/control unit was used to acquire these voltages and store them on a personal computer connected to it. A computer program, specially designed and written using the NI LabVIEW software, was used to perform all of the aforementioned data acquisition and control tasks.

Each of the above-mentioned 80 thermocouples was calibrated using a quartz thermometer as a secondary standard (*Hewlett-Packard* 2804A; it was previously precision calibrated to an accuracy of ±0.005 ^{o}C over the temperature range 0 ^{o}C to 95 ^{o}C, using a platinum resistance thermometer, at the Physics Division of the National Research Council in Ottawa). The calibration of the 80 thermocouples was performed for temperatures in the range from 2 ^{o}C to 60 ^{o}C, at intervals of 2 ^{o}C in this range. The procedure that was used for acquiring and storing the calibration data from the thermocouples is summarized below:

1. The probe (sensor) of the quartz thermometer and the coated beads of the 70 fabricated thermocouples and the tips of the 10 prefabricated sheathed thermocouples were inserted into blind holes machined in a copper block (75 mm diameter, 50 mm high). During the calibration, this copper block ensured that the probe of the quartz thermometer and the beads/tips of the thermocouples were maintained at essentially the same temperature (to within ± 0.02 ºC)

2. The above-mentioned copper block with the inserted (and secured) beads/tips of the thermocouples was placed in a constant-temperature bath (*NESLAB* RTE-221; which can maintain the set temperature to within ± 0.01 ºC or better) filled with distilled water, and fitted with a special insulating lid that closed the opening of the bath, but allowed the passage of the lead wires of the thermocouples and the stainless steel shaft of the quartz-thermometer probe. The calibration runs were started by setting the bath temperature to 2 ºC, the lowest temperature of the calibration range. The quartz thermometer was connected to the personal computer using a USB-GPIB interface. All electronic equipment (data acquisition and control system, quartz thermometer, and the personal computer) were then turned on and allowed to warm up for at least two hours.

3. For each setting of the constant-temperature bath, the voltages from the quartz thermometer and the thermocouples were continuously monitored. Once the copper block (along with the inserted quartz-thermometer probe and thermocouples) had

reached a steady-state temperature (assumed to be reached when variations in the temperature measured by the quartz thermometer were less than ± 0.02 ^{o}C for at least 15 minutes), all data were recorded using the above-mentioned LabVIEW program. Each set of these data consisted of a reading from the quartz thermometer, followed by a sequential reading of each of the 80 thermocouples, and then one more reading from the quartz thermometer. Each set of such data was recorded 40 times; and the average of these 40 data sets was taken as the final set of readings for the chosen temperature. For each setting of the constant-temperature bath, the procedure to acquire and store the aforementioned final averaged set of data took approximately 20 minutes to complete.

4. After the acquisition and storage of the above-mentioned averaged data set was completed for one selected setting of the constant-temperature bath, it was set to the next desired value of the temperature. This overall procedure was used repeatedly until the whole range of desired temperatures was covered.

Type-E thermocouples have the highest voltage output (and hence provide the highest accuracy) compared to thermocouples of any other type for temperatures in range of interest in this work (2 ^{o}C to 60 ^{o}C). That is why they were chosen for this work. Also, since these thermocouples are designed to provide a voltage-temperature response that is close to linear (a straight line), once all of the calibration data were acquired and saved, they were arranged in a tabular form. In the experiments with GHP, the temperatures of interest were deduced from the voltages output of each thermocouple using a linear interpolation of the aforementioned tabulated calibration data for that thermocouple, as follows:

$$y = y_0 + (y_1 - y_0)\left\{\frac{x - x_0}{x_1 - x_0}\right\} \tag{3.1}$$

In this equation, x is the voltage output of the thermocouple (in mV); y_0 and y_1 are temperatures corresponding to the voltages x_o and x_1, respectively, immediately below and above x, or equal to it, in the tabulated calibration data ($x_0 \le x \le x_1$); and the temperature of interest is given by y.

3.7.2 Power supplies and related measurements

Three different DC power supplies were used in this work: a *Sorensen* DCR 300-3B power supply (0-300 V, 0-3 A), to power the Teflon-coated nichrome wire wrapped around the active-heating portion of the GHP evaporator-section tube; a single-channel *Hewlett Packard* E3612A power supply (0-60 V, 0-0.5 A; or 0-120 V, 0-0.25 A), to provide DC power to the electronic vacuum gauge; and a dual-channel *Xantrex* LXQ 30-2 power supply (each channel 0-30 V, 0-2 A), with one channel powering a Teflon-coated nichrome wire wrapped around a portion of the vacuum circuit adjacent to the top end-plate of the GHP condenser section, and the other channel powering a relay that was used in an overheat-protection circuit (described later in this chapter). These three DC power supplies are shown in the photographs presented in Figure 3.16.

Figure 3.16: Photographs of the *Sorenson* (left), *Hewlett Packard* (center), and *Xantrex* (right) DC power supplies that were used in this work.

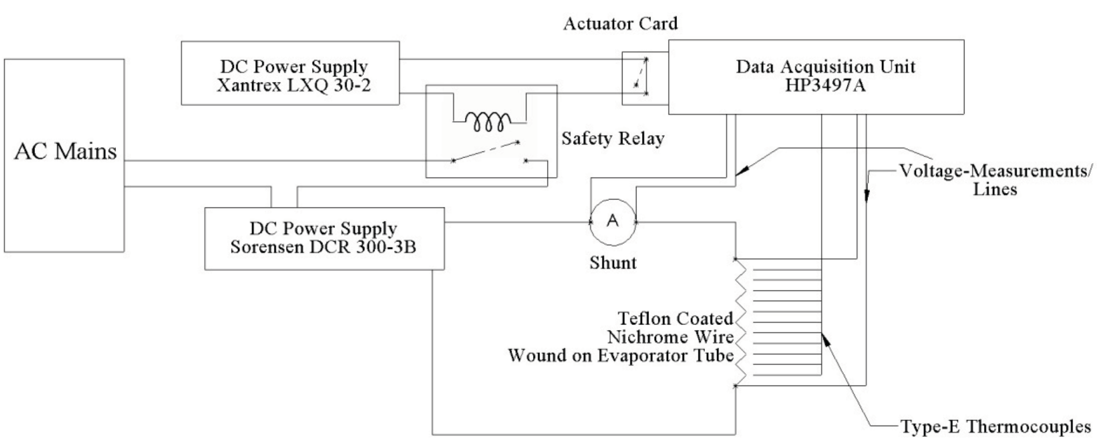

Figure 3.17: Schematic illustration of some of the electrical circuits used in this work.

Some the electrical circuits that were used in the overall experimental set-up are illustrated in Figure 3.17. The electric current supplied to the main nichrome wire wrapped around the active-heating portion of the GHP evaporator-section tube was determined by measuring the voltage drop across the terminals of a high-accuracy shunt (a 0.01Ω manganin resistor, connected in series with the nichrome wire). The resistance of this shunt remained effectively unchanged in all of the GHP experiments undertaken in this work. Thus, the DC voltage drop across this shunt and could be related directly to the electrical current flowing through it.

About halfway through the series of experiments on the GHP, the above-mentioned *Sorensen* DC power supply failed. This power supply was then replaced with two *Kepco* ATE 100-10M DC power supplies (each 0-100 V, 0-10 A) connected in series. A photograph of these two *Kepco* DC power supplies is given below in Figure 3.18.

Figure 3.18: Photograph of the two *Kepco* DC power supplies that were used in this work.

3.7.3 Data acquisition and control

A data acquisition and control unit (*Hewlett Packard* HP3497A), fitted with three temperature-measurement multiplexer cards (20 channels each; with internal hardware compensation for Type-E thermocouples; Option 020), was used to read data from 31 thermocouples (taken from the 70 thermocouples that were fabricated and calibrated in this work) and two sheathed thermocouples (taken from the 10 sheathed thermocouples that were purchased prefabricated from *Omega* and then calibrated in this work) employed in this work (these thermocouples and the related calibration procedures were described earlier in Subsection 3.7.1). The three temperature-measurement multiplexor cards were used to sequentially acquire data from the aforementioned total of 33 thermocouples, when required. In addition to these three temperature-measurement multiplexor cards, a 20-channel voltage-measurement multiplexer card (Option 010) and a 16-channel actuator card (Option 110) were also inserted into the data acquisition unit. The 20-channel voltage-measurement multiplexor card was used for the following measurements: the voltage drop across the Teflon-coated nichrome wire wrapped around the active-heating portion of the GHP evaporator-section tube; the voltage drop across the shunt shown in Figure 3.17; and the output from the electronic vacuum gauge (see Figures 3.11, 3.13, and 3.14). The 16-channel actuator card was used for triggering a relay used in an overheat-protection circuit (see Figure 3.17). All these voltages (including those from the aforementioned 33 thermocouples) were read using a digital voltmeter (DVM) that was integrated in the aforementioned *Hewlett Packard* data acquisition unit. These digitized voltage reading were transmitted to a personal computer (PC), using a GPIB interface on the data acquisition unit and a USB-GPIB interface attached to the PC, and then stored in ASCII format in specially designated files on a hard-disk in the PC, when required.

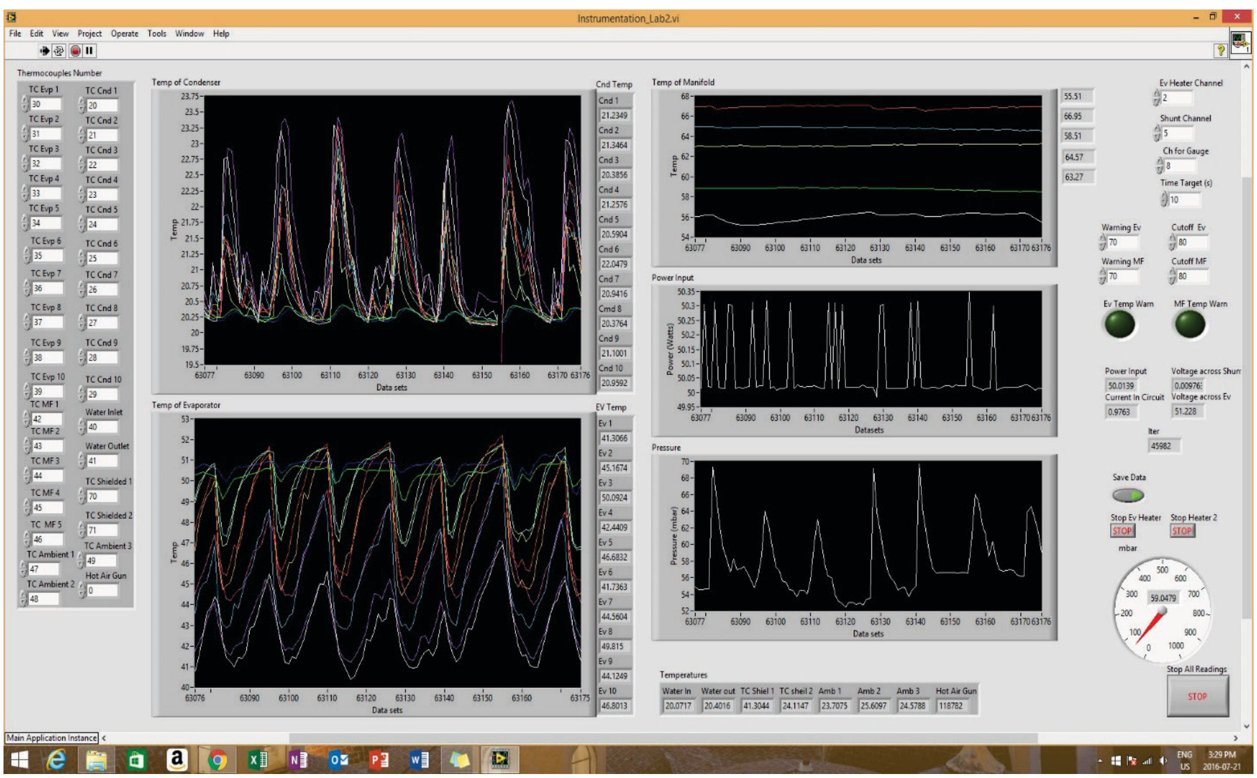

Figure 3.19: Screen-capture picture of the virtual control panel displayed on a PC monitor screen by a program (written using the National Instruments LabView software) for data acquisition and control.

The data acquisition and control tasks were managed by a program that was run on the personal computer (PC). This program was specially designed to present the data and input instructions on a virtual control panel displayed on the PC monitor screen; and it was written using the National Instruments LabVIEW software. The electrical power input to the active-heating portion of the GHP evaporator section was calculated using the corresponding voltage drop across the Teflon-coated nichrome wire and the electrical current flowing through it. The output from the electronic pressure gauge was converted to mbar and presented in a window on the virtual control panel, in digital form and also a dial-type icon. During the GHP experiments, the complete aforementioned set of data was sampled every 4.206 seconds; after these data were processed by the LabVIEW computer program, there were stored (appended) to an ASCII file, along with the corresponding time and date stamps. In addition to data displays and monitoring graphics displayed on the virtual control panel, the display also included indicators which warned the user if the measured temperatures on the surfaces of the evaporator-section tube and the chosen elements of the vacuum-circuit exceeded user-defined limits. A screen-capture picture of this virtual control panel displayed on the PC monitor screen is shown in Figure 3.19.

3.7.4 Overheat protection

During the GHP experiments, there was the possibility that the temperatures in the evaporator section could rise to unacceptably high levels (> 70 ^{o}C), due to dry-out conditions (or other operational limits of GHPs discussed in Chapter 1) in the evaporator or malfunctioning (or incorrect settings) of the main DC power supply. In order to prevent damage to the GHP, the above-mentioned 16-channel actuator card (fitted inside the data acquisition/control unit) and the LabVIEW computer program were set-up to activate an electro-mechanical relay (see Figure 3.17) if any of the measured temperatures exceeded the set limit (of 70 ^{o}C). This relay was powered using one of the two channels of the *Xantrex* LXQ 30-2 DC power supply (set to 12 V). Under normal operating conditions, this relay was closed and it completed the circuit that provided the powered to the Teflon-coated nichrome wire wrapped around the active heating portion of the GHP evaporator section; and this relay opened and cut off power to the nichrome heating wire when it was triggered by the aforementioned overheat-protection arrangement.

The second channel of the dual-channel *Xantrex* LXQ 30-2 DC power supply was used to power the Teflon-coated nichrome wire wrapped around a portion of the vacuum circuit adjacent to the top end-plate of the GHP condenser section. Its voltage was adjusted (based on several preliminary experiments) to ensure that the temperatures of the related elements did not exceed the chosen limit (70 ^{o}C). Nevertheless, an indicator light (icon) was activated on the virtual control panel displayed on PC monitor screen if these temperatures exceeded 70 ºC, prompting corrective action from the person conducting the GHP experiment.

3.7.5 Constant-temperature baths

In the main GHP experiments, a *Neslab* Endocal LT-50 constant-temperature bath (see Figure 3.20) was used to supply the cooling water to the annular jacket around the active-cooling portion of the GHP condenser section (described earlier in Section 3.3). The characteristics of this constant-temperature bath are the following: temperature stability of ± 0.02 ^{o}C; maximum cooling capacity of 250 W at the 20 ^{o}C setting; bath volume of 20.5 L; and a maximum pumping capacity of 15 litres per minute. The inlet and outlet ports of the bath were connected to those of the active cooling section using two 40-ft long *Neoprene* tubes (3/8-in ID and 5/8-in OD) enclosed in *Armaflex* pipe insulation of 1/2-in thickness. As was mentioned previously, the cooling water flowed through the annular jacket around the active-cooling portion of the GHP condenser section at almost constant volume and mass flow rates of 63.6 ml/s and 0.0635 kg/s, respectively, at the set nominal temperature of 20 ^{o}C.

Neslab Endocal LT 50 Neslab RTE-221

Figure 3.20: Photographs of the constant-temperature baths used in this work.

A *Neslab* RTE-221 constant-temperature bath (see Figure 3.20) was used in auxiliary experiments for calibrating the thermocouples used in this work (as was discussed in Subsection 3.7.1). The characteristics of this constant-temperature bath are the following: temperature stability of ± 0.01 °C; maximum cooling capacity of 500 W at the 20 ^{o}C setting; bath volume of 20.5 L; and a maximum pumping capacity of 15 litres per minute.

3.8 Experimental Procedures

The following experimental procedures are summarised in this section: leak testing of the GHP and the vacuum circuit; determination of an overall heat-loss conductance for the GHP; filling of the GHP with the working fluid; GHP experiments; and draining of the GHP.

3.8.1 Leak testing of the GHP and the vacuum circuit

The leak testing of the GHP and the vacuum circuit was carried out as follows:

1. After completing the assembly of the GHP, the filling and vacuum circuits, and the rest of the experimental set-up, switch on the power supplies, the data acquisition system, and the electronic vacuum gauge. Switch on the personal computer and monitor; and run the LabVIEW program written for data acquisition and control. Leave all these systems turned on and running for at least two hours (to allow them to stabilize and achieve reliable operating conditions).
2. Close all the valves in the vacuum and filling circuits (see Figures 3.11 and 3.15). Turn on the vacuum pump in the half-open gas ballast mode, and let it run in this mode for at least 1/2 hour (this ensures that it warms up properly; and any moisture, air, or other gases in the vacuum pump and some of the connecting lines will be expelled).
3. Open the ball valve connecting the vacuum pump to the vacuum circuit. Also open the ball valves connected to the electronic and mechanical vacuum gauges (see Figure 3.11). Monitor the vacuum level using these gauges. If there are any major leaks present in the set-up, they would not allow high-vacuum levels; if such major leaks are detected, try to locate and fix them by sequentially checking and eliminating the related possibilities.
4. Once the vacuum reaches less than 12 mbar absolute, completely close the gas ballast on the vacuum pump and continue running it in the high-vacuum mode.

5. Once the vacuum level is better than 2 mbar, switch off the vacuum pump and isolate it from the experimental set-up, by closing the shutoff ball valve connecting it to the vacuum circuit. Hold the vacuum conditions in the GHP and vacuum circuit for at least 12 hrs, and then note down the vacuum level (measured using aforementioned gauges). It would be normal at this stage for the vacuum level to go up to about 15 mbar, due to the outgassing from the materials of the vacuum circuit elements and the GHP.
6. Open the shutoff valve connecting the GHP and vacuum circuit to the vacuum pump; and then open the vacuum release valve connected to the T junction in the vacuum circuit (Figure 3.11).
7. Repeat steps 2 to 6 three times to allow thorough outgassing of the materials of the GHP and the vacuum circuit elements.
8. Run steps 2 and 4 and then continue running the vacuum pump in high-vacuum mode until the vacuum level in the GHP and vacuum circuit reaches 0.1 mbar or less. Shut off the ball valve that connects the vacuum pump to the vacuum circuit; and then switch off the vacuum pump. Hold the vacuum in the GHP and vacuum circuit for about 12 hrs. At this time, if the vacuum level is more than 2 mbar, then the GHP and vacuum circuit can be assumed to be effectively free of any leaks for experiments such as those undertaken in this work. It this condition is not achieved, then try to locate and fix the possible leaks by sequentially checking and eliminating the possibilities in this regard. Once this leak test is successfully completed, the GHP is ready for all of the other experiments.

3.8.2 Determination of an overall heat-loss conductance of the GHP

An overall heat-loss conductance, C_{loss} [W/^{o}C], was determined (by undertaking auxiliary experiments after the completion of the leak tests) and then used in this work to estimate the rate of heat loss, $q_{loss} \triangleq C_{loss}(\overline{T}_{evap}^{wall} - \overline{T}_{\infty})$, from the GHP to the ambient environment in each of the final experiments. The procedure that was used in the auxiliary experiments that were undertaken to determine this overall heat-loss conductance of the GHP is presented in pointwise form below:

1. Switch on the power supplies, the data acquisition system, and the electronic vacuum gauge. Switch on the personal computer and monitor; and run the LabVIEW program written for data acquisition and control. Turn on the cooling-water flow to the condenser

section of the GHP. Leave all these systems turned on and running for at least two hours (to allow them to stabilize and achieve reliable operating conditions).

2. Bring the GHP to a vertical position (tilt angle θ = 0^{o}) by adjusting the tilt table to the horizontal position. Drain any remaining working fluid in the GHP. Close the shutoff valves in the filling circuit (Figure 3.15). Evacuate the GHP to a vacuum level of 0.1 mbar or less using steps akin to some of those listed in Section 3.8.1 (leak testing procedure). Then close the shutoff ball between the vacuum pump and the vacuum circuit (Figure 3.11). Then shut off the vacuum pump.
3. Turn on the power supply to the active heating portion of the evaporator section of the GHP; and then adjust its output voltage to get the desired average wall temperature in the evaporator section (start with 40 ^{o}C, nominal).
4. Maintain the condition described in previous step for at least six hours, so that the temperatures in the evaporator section reach a steady value. Then record the all data (power input; all temperatures; and reading from the electronic vacuum gauge) by clicking on "Save Data" button on the virtual control panel displayed on the computer monitor. Record the data for approximately 30 mins (at least 100 sets of data points). The LabVIEW program saves this data in a specially created ASCII file. Copy this data from this ASCII file into another appropriately labelled data file, for further processing later, and clear the original ASCII file for accepting data from the next run.
5. Increase the power input to achieve the next desired average wall temperature in the evaporator section. Then repeat steps 3 and 4. Continue this procedure until the runs for evaporator-section average wall temperatures of 40 ^{o}C, 50 ^{o}C, and 60 ^{o}C (nominal) have all been covered.
6. Shut off the power input to the active heating portion of the evaporator section, and allow all wall temperatures in this section to cool down to below 40 ^{o}C. Then repeat steps 3 – 5, to obtain data that would serve as repeatability checks.

In these experiments, as there is no working fluid in the GHP, all of the power supplied to the active portion of the evaporator section is essentially lost to the ambient. The recorded data for each of the chosen values of the power input can be used to obtain the corresponding values of the total power or rate of heat input, $q_{in,total,vacuum\ conditions\ in\ GHP}$, the spatial- and time-averaged evaporator-tube wall temperature, $\overline{T}_{evap}^{wall}$, and the spatial- and time-averaged ambient temperature, $\overline{T}_{\infty}$. These data were used to calculate the overall heat loss coefficient, C_{loss}, as follows:

$$C_{loss} \triangleq (q_{in,total,vacuum\ conditions\ in\ GHP}) / (\overline{T}_{evap}^{wall} - \overline{T}_{\infty}) \tag{3.2}$$

The corresponding experimental data and results are summarized in Table 3.4. The arithmetic mean of the first six C_{loss} values presented in this table was taken as the overall heat-loss conductance of the GHP in the final series of experiments. This value is C_{loss} = 0.078 W/ ^{o}C.

Table 3.4: Data and results obtained from auxiliary experiments that were conducted to determine the overall heat-loss conductance of the GHP.

$q_{in,total}$ vacuum conditions in GHP **[W]**	$\overline{T}_{evap}^{wall}$ [^{o}C]	$\overline{T}_{\infty}$ [^{o}C]	C_{loss} **[W/ ^{o}C)]**
1.42	39.95	21.79	0.078
1.42	39.94	21.73	0.078
2.21	48.94	21.14	0.079
2.20	48.98	21.13	0.078
2.81	61.71	25.37	0.077
3.45	68.93	24.18	0.078
Average value of C_{loss}			0.078

3.8.3 Filling of the GHP with the working fluid

The following procedure was followed for filling the GHP with the working fluid:

1. Determine the amount of working fluid required for the desired fill ratio. Note that 88 ml of the working fluid is required for a 100 % fill ratio of the GHP used in this work.
2. Vigorously boil about 250 ml of the working fluid (double-distilled distilled water was used in this work) in a clean vessel (a glass electric kettle was used in this work) for at least 30 minutes. This level of boiling is sufficient to adequately expel the dissolved gases form the working fluid. Store this boiled (degassed) water in a clean glass bottle with an air-tight lid.

3. With the needle valve and ball valves closed in the filling circuit (Figure 3.15), carefully pour the working fluid into the graduated burette with the stopcock in open position, until it reaches a level just below the maximum (100 ml) position. Open the two shutoff ball vales in the filling circuit (Figure 3.15) and use the needle valve to very slowly prime the filling circuit (but not the GHP) with the working fluid; also allow some of this fluid to drip out through the drain and then close its shutoff ball valve. Close the other shutoff ball valves and the needle valve in the filling circuit. Top-up the working fluid in the glass burette to a level just below the maximum (100 ml) position.
4. Evacuate the GHP and vacuum circuit to a vacuum level better than 0.1 mbar, using steps akin to some of those listed in the Subsection 3.8.1 (the leak testing procedure).
5. Close the shutoff ball valve connecting the vacuum pump to the vacuum circuit (Figure 3.11). Then shut off the vacuum pump.
6. Turn on the hair dryer and the rest of the arrangement for heating the vacuum circuit and the vacuum gauges (Figure 3.11), in accordance with the discussion given in Section 3.5.
7. Open the needle valve in the filling circuit to about the half-way point. Then open the shutoff ball valve located in between needle valve and the GHP in the filling circuit (Figure 3.11). Carefully monitor the working fluid level in the glass burette and meter the rate at which it flows into the GHP. Fully close the needle valve after the desired amount of the working fluid is filled into the GHP (and the desired fill ratio is achieved). Then close the aforementioned shutoff ball valve, to isolate the needle valve and the burette from the GHP.
8. Wait till the pressure and temperatures in the GHP reach stable values. The GHP is now ready for the next series of experiments with the chosen fill ratio.

3.8.4 GHP experiments

After the procedures for the leak testing, determination of the overall loss coefficient, and filling of the GHP with the working fluid discussed in the previous three subsections were successfully completed, the following procedure was used to run the GHP experiments, and acquire and save the related data:

1. With the GHP prepared for the experiment with the chosen fill ratio (in accordance with the procedure described in Subsection 3.8.3; start with a fill ratio of 50 %), switch on the power supplies, the data acquisition system, and the electronic vacuum gauge. Switch on the personal computer and monitor; and run the LabVIEW program written for data acquisition and control. Turn on the cooling-water flow to the condenser section of the GHP and set the corresponding water bath temperature to 20 ^{o}C. Also ensure that the hair dryer and the rest of the arrangement for heating the vacuum circuit and the vacuum gauges (Figure 3.11) are turned on and appropriately adjusted in accordance with the discussions given in Section 3.5. Leave all these systems turned on and running for at least two hours (to allow them to stabilize and achieve reliable operating conditions).
2. Start with the GHP in the desired tilt position (start with zero tilt angle, $\theta = 0^{o}$, which corresponds to the horizontal position of the tilt table) and no (zero) power input to the active heating portion of the evaporator section.
3. Slowly increase power input to the active heating portion of the evaporator section to the desired level (start with 50 W, nominal), by increasing the voltage applied by the DC power supply across the Teflon-coated nichrome wire wrapped around the tube of this section. Then wait for at least two hours or until all monitored temperatures have reached effectively steady-state values.
4. Click the "Save Data" button on the virtual control panel displayed on the computer monitor. Record the data for approximately 30 mins (at least 100 sets of data points). The LabVIEW program saves this data in a specially created ASCII file.
5. Once the data has been recorded in the above-mentioned ASCII file, copy the data from this ASCII file into another appropriately labelled data file, for further processing later. Then clear the original ASCII file for accepting data from the next experimental run.
6. Repeat steps 3 to 5 with the next desired level of power input to the active heating section. Do this for power inputs of 50 W, 100 W, 150 W, 200 W and 250 W (nominal).
7. Once the runs are completed for all of the desired power levels at $\theta = 0^{o}$, change the tilt angle to the next desired value and repeat steps 3 to 6. Do this until all of the desired values of the tilt angel, $\theta = 0^{o}$, 10^{o}, 20^{o}, and 30^{o}, have been covered.
8. After completing the experimental runs for all of the desired power input levels at each of the above-mentioned tilt angles, slowly bring back the GHP to zero tilt angle ($\theta = 0^{o}$) .

9. Repeat steps 1 to 8 for all desired values of the fill ratio (50 %, 100 % and 150 %).

3.8.5 Draining of the GHP

After a set of runs was completed for a chosen fill ratio, the GHP was fully drained and completely evacuated before filling it with the working fluid to achieve the next desired fill ratio. The draining of the GHP after each set of experimental runs was carried out in the following manner:

1. Set the tilt angle of the GHP to zero ($\theta = 0^o$), by bringing the tilt table to the horizontal position. Reduce the power input to the active heating portion of the evaporator section of the GHP to 0 W; and then wait until the monitored temperatures of the GHP reach either the room-air or the cooling-water temperatures (roughly 20 ^oC).
2. Open the ball valve connecting the vacuum pump to the vacuum circuit; and then open the vacuum-release valve (Figure 3.11). Wait for the pressure values in the GHP to stabilize at the prevailing atmospheric value.
3. Place a beaker (of appropriate volume) under the drain pipe in the filling circuit and then open the drain valve (Figure 3.15). Wait for the working fluid in the GHP to drain fully, and then close the drain valve. Evacuate the GHP fully again using steps akin to those described in Subsection 3.8.1; and keep the vacuum pump on for at least 12 hours to fully evacuate all air and moisture from the GHP. Then release the vacuum and leave the GHP filled with air at atmospheric pressure.

Chapter 4: Results and Discussion

In this chapter, the results obtained using the experimental apparatus and procedures described in Chapter 3 are presented and discussed in the following sections: 1) overview of GHP experiments and results; 2) overview of repeatability tests and uncertainties in the experimental results; 3) variation of GHP conductance with fill ratio and power input; 4) variation of GHP conductance with power input and tilt angle; 5) variations of time-period and maximum change of evaporator-wall temperature with power input and tilt angle during geyser boiling; and 6) variations of time-period and maximum change of evaporator-wall temperature with power input and fill ratio during geyser boiling.

4.1 Overview of GHP Experiments and Results

After many preliminary runs of the GHP experiments, undertaken to gain experience with the experimental apparatus and the characteristics of the GHP, a total of 50 final runs (labelled as Runs # 1-50) were conducted. A summary of the experimental settings and conditions, and the corresponding results, are presented in Table 4.1 for Runs # 1-27 and in Table 4.2 for Runs # 28-50. The repeatability of the experimental results and the associated uncertainties are presented and discussed in Section 4.2.

For FR = 40 %, values of $q_{in,total}$ > 50 W (nominal) could not be used because of the dry-out limit. For FR = 50 %, values of $q_{in,total}$ > 50 W (nominal) lead to the dry-out limit for values of $\theta \geq 10^{o}$; however, values of $q_{in,total}$ in the range 50 W (nominal) $\leq q_{in,total} \leq$ 250 W (nominal) could be used without any difficulties for $\theta = 0^{o}$. For FR = 100 % and 150 %, values of $q_{in,total}$ in the range 50 W (nominal) $\leq q_{in,total} \leq$ 250 W (nominal) and $\theta = 0^{o}$, 10^{o}, 20^{o}, and 30^{o} were possible without encountering dry-out conditions. The results for the dry-out-free conditions are reported in Tables 4.1 and 4.2.

In the columns of Tables 4.1 and 4.2 pertaining to experimental settings and conditions, the values of the constant-temperature water bath setting, T_{WB}, and the ambient temperatures adjacent to the evaporator, adiabatic, and condenser sections, $T_{\infty,evap}$, $T_{\infty,adiab}$, and $T_{\infty,cond}$, respectively, all correspond to temporal (time) averages.

Experimental settings and conditions								Experimental results								
Run #	FR [%]	θ [°]	$q_{in,total}$ [W]	T_{WB} [°C]	$T_{\infty,evap}$ [°C]	$T_{\infty,adiab}$ [°C]	$T_{\infty,cond}$ [°C]	q_{loss} [W]	q_{in} [W]	$\overline{T}_{evap}^{wall}$ [°C]	$\overline{T}_{evap}^{water}$ [°C]	$\overline{T}_{cond}^{wall}$ [°C]	$\overline{T}_{cond}^{vapor}$ [°C]	$\overline{p}_{cond}^{vapor}$ [mbar]	C_{GHP} [W/°C]	Boiling in evap
1	40	0	49.20	20.06	23.20	24.03	24.23	0.655	48.55	32.34	23.36	20.62	21.43	27.67	4.143	Geyser
2	50	0	51.48	20.03	24.71	24.09	24.14	0.668	50.82	32.95	24.27	20.65	21.74	28.49	4.128	Geyser
3	50	0	100.9	20.07	20.89	22.57	22.37	1.192	99.75	37.35	26.39	21.34	24.32	32.26	6.231	Geyser
4	50	0	125.2	20.06	22.05	23.79	23.39	1.189	123.9	38.49	27.26	21.68	25.97	34.52	7.379	Geyser
5	50	0	150.7	20.09	21.21	23.11	22.94	1.531	149.2	42.30	30.07	22.11	28.30	41.03	7.386	Nucleate
6	50	0	201.0	20.07	22.10	24.41	23.89	1.618	199.4	44.55	30.62	22.84	29.78	42.10	9.185	Nucleate
7	50	0	250.6	20.06	21.44	23.77	23.51	1.951	248.7	48.20	32.99	23.48	32.03	48.03	10.07	Nucleate
8	50	10	51.49	20.02	25.18	29.00	26.38	0.363	51.13	31.51	23.96	20.62	21.83	28.08	4.692	Geyser
9	50	20	51.49	20.02	26.12	28.66	27.03	0.317	51.17	31.49	24.10	20.62	21.90	28.14	4.709	Geyser
10	50	30	51.49	20.02	28.15	33.41	29.91	0.114	51.38	31.87	25.08	20.63	21.90	29.81	4.573	Geyser
11	100	0	50.62	20.01	25.66	25.09	24.58	1.331	49.29	42.36	38.05	20.72	22.79	54.90	2.281	Geyser
12	100	0	100.8	20.01	26.40	25.64	25.09	1.581	99.31	46.19	39.99	21.61	25.93	64.81	4.037	Geyser
13	100	0	150.9	20.00	26.35	25.53	24.58	1.883	149.1	49.91	42.03	22.42	29.29	73.52	5.422	Nucleate
14	100	0	199.5	19.99	28.49	28.40	27.11	2.077	197.4	54.96	45.16	23.23	32.12	87.06	6.223	Nucleate
15	100	0	249.4	20.14	28.78	28.14	27.52	2.552	246.9	61.31	49.40	24.14	36.09	108.9	6.641	Nucleate
16	100	10	50.58	19.99	26.13	30.24	28.22	1.091	49.48	42.41	38.30	20.70	22.06	58.76	2.283	Geyser
17	100	10	100.6	20.00	27.18	29.59	28.14	1.501	99.19	47.82	41.40	21.44	24.19	71.65	3.757	Geyser
18	100	10	150.9	20.00	26.09	29.60	27.37	1.947	148.9	53.03	44.48	22.15	27.35	85.57	4.831	Nucleate
19	100	10	199.2	20.01	27.38	30.25	28.77	2.208	197.1	57.45	47.23	22.97	30.80	99.27	5.714	Nucleate
20	100	10	249.2	20.07	28.11	31.34	29.68	2.492	246.7	62.10	49.86	23.69	32.85	113.3	6.418	Nucleate
21	100	20	50.62	20.03	25.09	26.04	24.78	1.427	49.20	43.73	39.80	20.65	21.73	65.21	2.129	Geyser
22	100	20	100.8	20.01	27.80	30.00	28.69	1.529	99.28	48.72	42.49	21.39	23.35	76.46	3.631	Geyser
23	100	20	150.9	20.03	27.30	29.41	28.01	1.971	149.0	53.86	45.44	22.13	27.41	90.90	4.704	Nucleate
24	100	20	199.2	20.02	29.71	32.48	30.85	2.204	197.0	59.63	49.36	22.87	30.91	111.3	5.363	Nucleate
25	100	20	249.2	20.02	27.39	31.28	29.88	2.721	246.6	64.83	52.58	23.56	32.96	130.9	5.969	Nucleate
26	100	30	50.66	20.03	28.69	33.35	29.16	1.077	49.59	44.36	40.64	20.66	21.36	69.10	2.091	Geyser
27	100	30	100.8	20.02	31.16	36.26	31.17	1.271	99.60	49.29	43.24	21.40	23.02	80.71	3.568	Geyser

Table 4.1: Summary of the experimental setting and conditions, and the corresponding results, obtained in Runs # 1-27 of the GHP experiments.

Experimental settings and conditions								Experimental results								
Run #	FR [%]	θ [°]	$q_{in,total}$ [W]	T_{WB} [°C]	$T_{\infty,evap}$ [°C]	$T_{\infty,adiab}$ [°C]	$T_{\infty,cond}$ [°C]	q_{loss} [W]	q_{in} [W]	$\overline{T}_{evap}^{wall}$ [°C]	$\overline{T}_{evap}^{water}$ [°C]	$\overline{T}_{cond}^{wall}$ [°C]	$\overline{T}_{cond}^{vapor}$ [°C]	$\overline{p}_{cond}^{vapor}$ [mbar]	C_{GHP} [W/°C]	Boiling in evap
28	100	30	150.9	20.00	31.67	36.07	31.76	1.693	149.3	55.06	46.86	22.18	27.42	98.72	4.541	Nucleate
29	100	30	199.4	20.01	34.36	35.41	31.42	2.104	197.3	61.05	50.88	22.88	31.20	121.6	5.173	Nucleate
30	100	30	249.2	20.00	33.32	35.98	29.14	2.486	246.8	65.11	52.82	23.67	33.35	134.2	5.946	Nucleate
31	150	0	50.63	20.07	22.85	23.96	23.38	1.778	48.85	46.51	41.69	20.75	22.27	54.52	1.901	Geyser
32	150	0	100.2	20.06	22.52	23.80	23.10	1.858	98.40	47.35	40.64	21.52	24.74	57.63	3.813	Geyser
33	150	0	149.6	20.03	24.15	23.52	22.50	2.267	147.4	52.82	44.89	22.11	26.21	75.53	4.802	Nucleate
34	150	0	200.4	20.01	24.40	24.23	23.13	2.503	197.9	56.40	46.41	22.96	31.19	82.42	5.919	Nucleate
35	150	0	250.9	20.03	28.98	35.37	27.66	2.489	248.5	62.98	50.54	23.72	31.85	110.8	6.327	Nucleate
36	150	10	50.22	20.03	25.37	29.99	26.64	2.033	48.19	53.70	49.14	20.62	21.13	94.42	1.458	Geyser
37	150	10	100.5	20.01	25.86	27.76	26.53	2.138	98.40	54.51	47.82	21.42	22.19	92.58	2.971	Geyser
38	150	10	149.9	20.03	24.14	27.87	24.84	2.313	147.6	55.66	47.47	22.15	24.42	91.38	4.404	Nucleate
39	150	10	200.5	20.03	25.03	28.15	26.58	2.478	198.1	58.81	48.62	22.89	28.34	96.88	5.518	Nucleate
40	150	10	248.2	20.03	24.66	28.02	26.24	2.827	245.4	63.06	51.01	23.66	32.26	109.6	6.227	Nucleate
41	150	20	50.24	20.05	25.12	27.60	25.95	2.167	48.07	54.41	49.71	20.62	21.17	100.1	1.419	Geyser
42	150	20	100.4	20.02	26.27	28.35	26.79	2.079	98.37	54.12	47.36	21.43	22.31	91.76	3.014	Geyser
43	150	20	149.8	20.04	24.54	25.95	24.64	2.441	147.4	56.79	48.55	22.19	24.05	98.94	4.257	Nucleate
44	150	20	200.5	20.03	25.83	27.06	25.85	2.482	198.0	58.48	48.12	22.94	28.31	96.07	5.568	Nucleate
45	150	20	251.1	20.03	25.45	26.34	25.64	2.864	248.3	62.96	50.57	23.76	32.65	109.0	6.342	Nucleate
46	150	30	50.22	20.04	28.22	36.91	28.11	1.791	48.43	54.39	50.17	20.60	20.65	107.6	1.432	Geyser
47	150	30	100.4	20.03	29.08	35.84	28.42	1.748	98.72	53.84	47.30	21.43	22.08	93.25	3.047	Geyser
48	150	30	149.9	20.05	28.28	33.06	28.17	2.037	147.9	56.31	48.16	22.21	24.21	97.74	4.336	Nucleate
49	150	30	200.4	20.02	28.66	35.19	27.79	2.191	198.3	58.93	48.66	22.91	27.58	100.2	5.511	Nucleate
50	150	30	250.9	20.03	28.98	35.37	27.66	2.486	248.5	62.98	50.54	23.72	31.85	110.8	6.334	Nucleate

Table 4.2: Summary of the experimental setting and conditions, and the corresponding results, obtained in Runs # 28-50 of the GHP experiments.

4.1.1 Rates of heat loss and power input to the evaporator

The rates of heat loss, q_{loss}, were computed for each experimental run using the data obtained for the average (spatial and temporal) of the temperatures of the evaporator wall ($\overline{T}_{evap}^{wall}$), the ambient temperature, $\overline{T}_{\infty} = (T_{\infty,evap} + T_{\infty,adiab} + T_{\infty,cond})/3$, and the overall heat-loss conductance of the GHP, $C_{loss} = 0.078$ W/ ^{o}C (discussed in Chapter 3, Subsection 3.8.2): $q_{loss} \triangleq C_{loss}(\overline{T}_{evap} - \overline{T}_{\infty})$. Then, for each experimental run, the aforementioned rate of heat loss, q_{loss}, was subtracted from the total power input to the Teflon-coated nichrome wrire wrapped around the evaporator tube, $q_{in,total}$, to obtained the actual power input to the evaporator section of the GHP, $q_{in} = (q_{in,total} - q_{loss})$. These results for q_{loss} and q_{in} for each of the 50 final runs are shown in Tables 4.1 (Runs # 1-27) and 4.2 (Runs # 28-50). The values of q_{loss} ranged from 0.114 W (Run # 10) to 2.864 W (Run # 45); and the values of q_{in} ranged from 48.55 W (Run # 1) to 248.7 W (Run # 7). In all cases, q_{loss} was less than 1.5 % of q_{in}.

4.1.2 Average outer-tube-wall and water temperatures in the evaporator section

The average outer-tube-wall and water temperatures in the evaporator section, $\overline{T}_{evap}^{wall}$ (spatial and temporal average) and $\overline{T}_{evap}^{water}$ (temporal average), respectively, were in the following ranges: 31.51 ^{o}C (Run # 8) $\le \overline{T}_{evap}^{wall} \le$ 64.83 ^{o}C (Run # 25) and 23.36 ^{o}C (Run # 1) $\le \overline{T}_{evap}^{water} \le$ 52.58 ^{o}C (Run # 25).

As was to be expected, for each set of values of the fill ratio (*FR*) and the tilt angle (θ), the low values of $\overline{T}_{evap}^{wall}$ and $\overline{T}_{evap}^{water}$ correspond to the low values of the power input to the evaporator, q_{in}; and the high values of these temperatures correspond to the high values of q_{in}.

4.1.3 Average outer-tube-wall and vapor temperatures and pressure in the condenser section

The average outer-tube-wall and vapor temperatures and pressure in the condenser section, $\overline{T}_{cond}^{wall}$ (spatial and temporal average), $\overline{T}_{cond}^{vapor}$ (temporal average), and $\overline{p}_{cond}^{vapor}$ (temporal average), respectively, were in the following ranges: 20.60 ^{o}C (Run # 45) $\leq \overline{T}_{cond}^{wall} \leq$ 23.76 ^{o}C (Run # 45); 21.17 ^{o}C (Run # 41) $\leq \overline{T}_{cond}^{vapor} \leq$ 33.35 ^{o}C (Run # 30); and 27.67 mbar (Run # 1) $\leq \overline{p}_{cond}^{vapor} \leq$ 134.2 mbar (Run # 30).

Again, as was to be expected, for each set of values of the fill ratio (*FR*) and the tilt angle (θ), the low values of $\overline{T}_{cond}^{wall}$, $\overline{T}_{cond}^{vapor}$, and $\overline{p}_{cond}^{vapor}$ correspond to the low values of the power input to the evaporator, q_{in}; and the high values of these temperatures and pressure correspond to the high values of q_{in}.

4.1.4 Conductance of the GHP

The average conductance of the GHP is defined as follows:

$$C_{GHP} \triangleq (q_{in}) / (\overline{T}_{evap}^{wall} - \overline{T}_{cond}^{wall}) \tag{4.1}$$

The values of C_{GHP} were in the following range: 1.419 W/^{o}C (Run # 41) $\leq \overline{T}_{cond}^{wall} \leq$ 10.07 W/^{o}C (Run # 7). In contrast, the overall conductance of a solid copper rod (thermal conductivity k = 400 W/m-^{o}C) of diameter and length equal to the inner diameter and total length of the GHP is 0.251 W/^{o}C. Thus, the overall conductance of the GHP designed and constructed in this work, for the experimental settings and conditions investigated (as reported in Tables 4.1 and 4.2), was 5.65 to 40.1 times higher than that of the aforementioned solid copper rod of corresponding dimensions. These 5- to 40-fold increases in the overall conductance of the GHP over that of an equivalent copper rod are impressive. However, these increases would be even more impressive for longer lengths of the adiabatic section of the GHP: as the overall conductance of the GHP would not be significantly affected by the length of its adiabatic section (as long as the flooding or entrainment limits are not reached); however, the overall conductance of a solid copper rod is inversely proportional to its length [Incropera and DeWitt (2002)].

In all cases, for fixed values of *FR* and θ, the value of C_{GHP} increases with increasing values of q_{in}, for the settings and conditions investigated in this work (see Tables 4.1 and 4.2). This is because as q_{in} increases from 50 W (nominal) to 250 W (nominal), the boiling phenomena in the evaporator goes from intermittent (and somewhat chaotic) geyser boiling regime to vigorous (and effectively steady) nucleate pool boiling regime, with corresponding increases in the boiling heat transfer coefficient on the inner surface of the evaporator-tube wall.

The highest value of C_{GHP} was obtained for FR = 50 %, and not 100 % and 150 %. This results can be explained by noting that when FR = 50 %, the vapor production is due to boiling in the liquid pool and also evaporation at the surface of the condensate-vapor interface (which covers a substantial portion of the inner surface of the evaporator tube), leading to very high values of the heat transfer coefficient and not too high values of the tube-wall temperature in the evaporator; whereas for FR = 100 % and 150 %, the vapor production is mainly due to boiling in the liquid pool and also, to some extent, evaporation at the surface of the condensate-vapor interface (which does not cover any part of the inner surface of the evaporator tube), leading to still high values of the heat transfer coefficient in the evaporator, but not as high as those for FR = 50 %, and higher tube-wall temperatures than those FR = 50 %.

For the experimental settings and conditions considered here (see Tables 4.1 and 4.2), the highest values of C_{GHP} were obtained for cases in which the GHP was oriented vertically (θ = 0^o). This finding seems reasonable, as in the vertical orientation, the inner surfaces of the tubes in the evaporator and condenser sections of the GHP participate fully in the overall heat transfer process; whereas for the tilted GHP ($\theta > 0^o$), the upper portions of the inner surfaces of the tubes in the evaporator and condensers sections would be starved of the liquid (pool or condensate film), as it would tend to flow down and pool in the lower portions, under the influence of gravity. However, this finding is in marked contrast to some of the results reported in the published literature (see discussions in Chapter 1, Section 1.2), where the optimum operating conditions (highest values of C_{GHP}) were found for values of θ between 10^o and 30^o.

Graphical representations of some of the above-mentioned results are presented in Sections 4.3 and 4.4.

4.1.5 Boiling regimes in the evaporator

As indicated in the last column of both Tables 4.1 and 4.2, the geyser boiling regime (see related description and discussions presented in Chapter 1, Subsection 1.2.4) prevailed in the evaporator section of the GHP for values of q_{in} below 140 W (nominal); for values of q_{in} above 150 W (nominal), nucleate boiling conditions prevailed in the evaporator section of the GHP; and the transition between these two boiling regimes occurred (somewhat intermittently or haphazardly) in the range 140 W (nominal) $\leq q_{in} \leq$ 150 W (nominal). Similar results have been reported in the published literature (see discussions in Chapter 1, Subsection 1.2.4).

Flow visualization pictures for *FR* = 150 % and conditions corresponding to geyser and nucleate boiling in the evaporator section of the GHP (Runs # 31 and 35) are presented in Figures 4.1 and 4.2, respectively. These pictures were obtained by using a frame-capturing technique on video recordings of the related phenomena, as viewed through the borosilicate glass section of the adiabatic section of the GHP. In Figure 4.1, which corresponds to geyser boiling conditions (Run # 31), the pictures show a quiescent liquid-vapor interface in the lower half of the left-most picture at time t = 0 s, then chaotic eruptions of the liquid for times 8.5 s $\leq t \leq$ 34 s, and back to a quiescent liquid-vapor interface at time t = 43.5 s. These pictures are somewhat similar to the schematic illustrations of the geyser boiling phenomenon depicted schematically in Figure 1.3, which was borrowed from the work of Khazee et al. (2010). In Figure 4.2, which corresponds to nucleate boiling conditions (Run # 35), the visualizations pictures show an effectively steady (unchanged) condensate film flowing down the inner surface of the borosilicate glass tube and a vapor core (thus, pictures corresponding only to t = 0 s, 1 s, 2 s, 3 s, 4 s, and 5 s are shown in this figure).

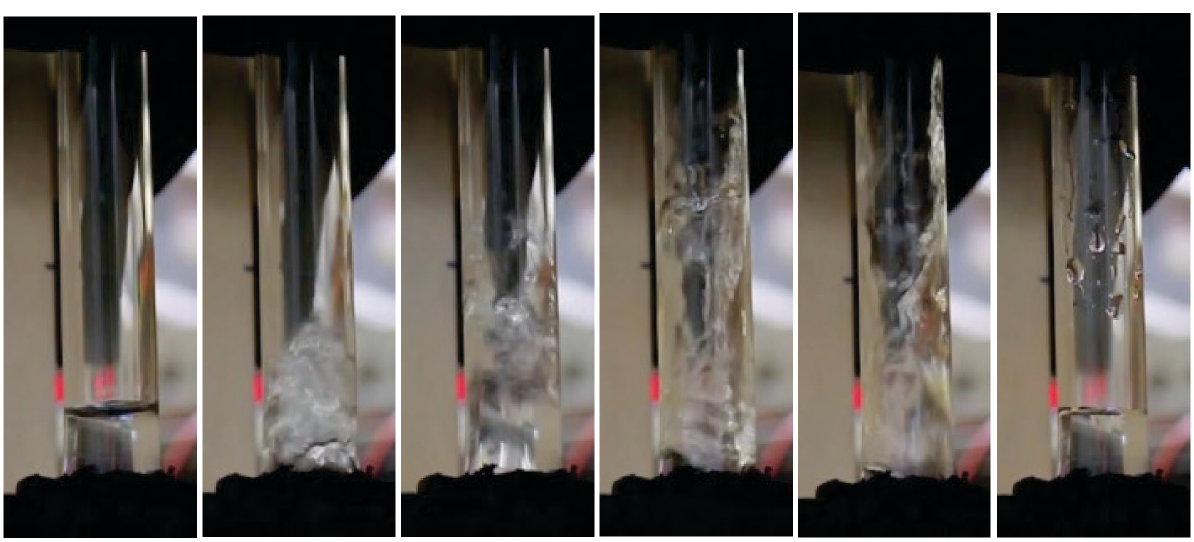

t = 0 s ***t = 8.5 s*** ***t = 17 s*** ***t = 25.5 s*** ***t = 34 s*** ***t = 43.5 s***

Figure 4.1: Sequence of flow visualization pictures at selected times during one cycle of geyser boiling in the evaporator for Run # 31: *FR* = 150 %, θ = 0°, and q_{in} = 50 W (nominal).

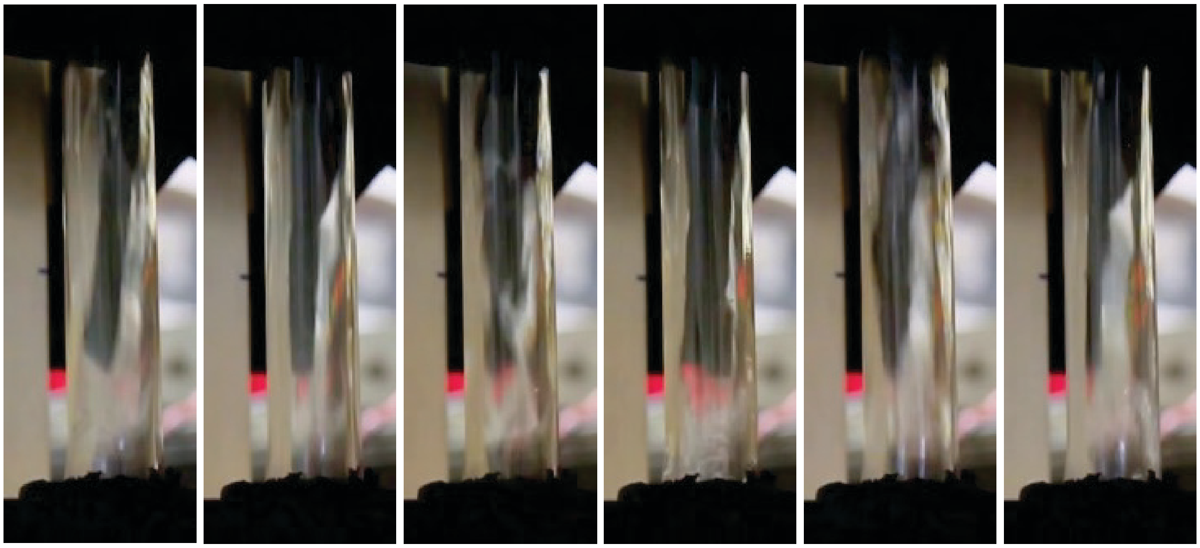

t = 0 s *t = 1 s* *t = 2 s* *t = 3 s* *t = 4 s* *t = 5 s*

Figure 4.2: Sequence of flow visualization pictures at selected times during nucleate boiling in the evaporator for Run # 35: FR = 150 %, $\theta = 0^o$, and q_{in} = 250 W (nominal).

4.2 Overview of Repeatability Tests and Uncertainties in the Experimental Results

Repeatability tests were conducted for 28 of the 50 final runs of the GHP experiments. In this section, summaries of the results obtained for only 10 of these repeatability runs are presented: in Table 4.3 for Runs # 2, 11, 15, 23, and 30; and in Table 4.4 for Runs # 31, 36, 38, 45, and 50. The results obtained from the other 18 repeatability tests were very similar to those presented in Tables 4.3 and 4.4, so they are not presented here.

The results in Tables 4.3 and 4.4 show the following repeatability values for the settings and conditions considered in this work: q_{loss} values are repeatable to within ± 5.20 %; q_{in} values are repeatable to within ± 0.55 %; $\overline{T}_{evap}^{wall}$ values are repeatable to within ± 1.08 %; $\overline{T}_{evap}^{water}$ values are repeatable to within ± 1.14%; $\overline{T}_{cond}^{wall}$ values are repeatable to within ± 0.15 %; $\overline{T}_{cond}^{vapor}$ values are repeatable to within ± 0.82 %; $\overline{p}_{cond}^{vapor}$ values are repeatable to ± 2.46 %; and C_{GHP} values are repeatable to within ± 2.98 %.

Experimental settings and conditions								Experimental results								
Run #	FR [%]	θ [°]	$q_{in,total}$ [W]	T_{WB} [°C]	$T_{\infty,evap}$ [°C]	$T_{\infty,adiab}$ [°C]	$T_{\infty,cond}$ [°C]	q_{loss} [W]	q_{in} [W]	$\overline{T}^{wall}_{evap}$ [°C]	$\overline{T}^{water}_{evap}$ [°C]	$\overline{T}^{wall}_{cond}$ [°C]	$\overline{T}^{vapor}_{cond}$ [°C]	$\overline{p}^{vapor}_{cond}$ [mbar]	C_{GHP} [W/°C]	Boiling in evap
2	50	0	51.48	20.03	24.71	24.09	24.14	0.668	50.82	32.95	24.27	20.65	21.74	28.49	4.128	Geyser
2R	50	0	51.50	20.02	24.86	24.27	24.20	0.602	50.90	32.25	23.99	20.63	21.61	28.25	4.381	Geyser
Mean value of result								0.635	50.86	32.60	24.13	20.64	21.68	28.37	4.255	-
Difference about mean: ±								0.033	0.040	0.350	0.140	0.010	0.065	0.120	0.127	-
Difference about mean: %								5.197	0.079	1.074	0.580	0.048	0.300	0.423	2.973	-
11	100	0	50.62	20.01	25.66	25.09	24.58	1.331	49.29	42.36	38.05	20.72	22.79	54.90	2.281	Geyser
11R	100	0	50.62	19.99	25.78	25.30	24.78	1.307	49.32	42.24	37.98	20.73	22.68	55.33	2.287	Geyser
Mean value of result								1.319	49.31	42.30	38.02	20.73	22.74	55.12	2.284	-
Difference about mean: ±								0.012	0.015	0.060	0.035	0.005	0.055	0.215	0.003	-
Difference about mean: %								0.910	0.030	0.142	0.092	0.024	0.242	0.390	0.131	-
15	100	0	249.4	20.14	28.78	28.14	27.52	2.552	246.9	61.31	49.40	24.14	36.09	108.9	6.641	Nucleate
15R	100	0	249.4	20.12	28.75	27.62	27.22	2.570	246.9	61.23	49.32	24.07	35.96	108.5	6.648	Nucleate
Mean value of result								2.561	246.9	61.27	49.36	24.11	36.03	108.7	6.645	-
Difference about mean: ±								0.009	0.000	0.040	0.040	0.035	0.065	0.200	0.003	-
Difference about mean: %								0.351	0.000	0.065	0.081	0.145	0.180	0.184	0.053	-
23	100	20	150.9	20.03	27.30	29.41	28.01	1.971	149.0	53.86	45.44	22.13	27.41	90.90	4.704	Nucleate
23R	100	20	150.9	20.02	27.59	29.14	27.73	1.921	148.9	53.04	44.63	22.15	27.36	86.62	4.818	Nucleate
Mean value of result								1.946	148.9	53.45	45.04	22.14	27.39	88.76	4.761	-
Difference about mean: ±								0.025	0.050	0.410	0.405	0.010	0.025	2.140	0.057	-
Difference about mean: %								1.285	0.034	0.767	0.899	0.045	0.091	2.411	1.197	-
30	100	30	249.2	20.00	33.32	35.98	29.14	2.486	246.8	65.11	52.82	23.67	33.35	134.2	5.946	Nucleate
30R	100	30	249.4	20.02	33.47	36.07	29.39	2.471	246.9	65.10	52.79	23.65	33.90	134.2	5.961	Nucleate
Mean value of result								2.479	246.9	65.11	52.81	23.66	33.63	134.2	5.954	-
Difference about mean: ±								0.007	0.050	0.005	0.015	0.010	0.275	0.000	0.008	-
Difference about mean: %								0.303	0.020	0.008	0.028	0.042	0.818	0.000	0.126	-

Table 4.3: Summary of the repeatability tests and results for Runs # 2, 11, 15, 23, and 30 of the GHP experiments.

Experimental settings and conditions								Experimental results								
Run #	FR [%]	θ [°]	$q_{in,total}$ [W]	T_{WB} [°C]	$T_{\infty,evap}$ [°C]	$T_{\infty,adiab}$ [°C]	$T_{\infty,cond}$ [°C]	q_{loss} [W]	q_{in} [W]	$\overline{T}^{wall}_{evap}$ [°C]	$\overline{T}^{water}_{evap}$ [°C]	$\overline{T}^{wall}_{cond}$ [°C]	$\overline{T}^{vapor}_{cond}$ [°C]	$\overline{p}^{vapor}_{cond}$ [mbar]	C_{GHP} [W/°C]	Boiling in evap
31	150	0	50.63	20.07	22.85	23.96	23.38	1.778	48.85	46.51	41.69	20.75	22.27	54.52	1.901	Geyser
31R	150	0	50.06	20.06	23.93	25.50	24.58	1.741	48.32	47.25	42.65	20.78	22.24	57.26	1.829	Geyser
Mean value of result								1.760	48.59	46.88	42.17	20.77	22.26	55.89	1.865	-
Difference about mean: ±								0.019	0.265	0.370	0.480	0.015	0.015	1.370	0.036	-
Difference about mean: %								1.051	0.545	0.789	1.138	0.072	0.067	2.451	1.930	-
36	150	10	50.22	20.03	25.37	29.99	26.64	2.033	48.19	53.70	49.14	20.62	21.13	94.42	1.458	Geyser
36R	150	10	50.22	20.04	25.14	30.03	26.49	2.024	48.20	53.48	48.85	20.62	21.41	92.70	1.469	Geyser
Mean value of result								2.029	48.20	53.59	49.00	20.62	21.27	93.56	1.464	-
Difference about mean: ±								0.004	0.005	0.110	0.145	0.000	0.140	0.860	0.006	-
Difference about mean: %								0.222	0.010	0.205	0.296	0.000	0.658	0.919	0.376	-
38	150	10	149.9	20.03	24.14	27.87	24.84	2.313	147.6	55.66	47.47	22.15	24.42	91.38	4.404	Nucleate
38R	150	10	149.9	20.03	23.90	27.95	24.69	2.301	147.6	55.41	47.16	22.19	24.69	89.64	4.443	Nucleate
Mean value of result								2.307	147.6	55.54	47.32	22.17	24.56	90.51	4.424	-
Difference about mean: ±								0.006	0.000	0.125	0.155	0.020	0.135	0.870	0.019	-
Difference about mean: %								0.260	0.000	0.225	0.328	0.090	0.550	0.961	0.441	-
45	150	20	251.1	20.03	25.45	26.34	25.64	2.864	248.3	62.96	50.57	23.76	32.65	109.0	6.342	Nucleate
45R	150	20	251.1	20.02	25.58	26.43	25.78	2.839	248.2	62.87	50.46	23.76	32.70	108.3	6.346	Nucleate
Mean value of result								2.852	248.3	62.92	50.52	23.76	32.68	108.7	6.344	-
Difference about mean: ±								0.013	0.050	0.045	0.055	0.000	0.025	0.350	0.002	-
Difference about mean: %								0.438	0.020	0.072	0.109	0.000	0.077	0.322	0.032	-
50	150	30	250.9	20.03	28.98	35.37	27.66	2.486	248.5	62.98	50.54	23.72	31.85	110.8	6.334	Nucleate
50R	150	30	251.1	20.04	29.79	35.71	28.23	2.442	248.6	62.89	50.42	23.71	31.85	110.1	6.348	Nucleate
Mean value of result								2.464	248.6	62.94	50.48	23.72	31.85	110.5	6.341	-
Difference about mean: ±								0.022	0.050	0.045	0.060	0.005	0.000	0.350	0.007	-
Difference about mean: %								0.893	0.020	0.072	0.119	0.021	0.000	0.317	0.110	-

Table 4.4: Summary of the repeatability tests and results for Runs # 31, 36, 38, 45, and 50 of the GHP experiments.

With the techniques and procedures described in Chapter 3, in this work, the maximum experimental uncertainties were the following: ± 0.05 ^oC in the temperature measurements; ± 0.5 % of reading or 0.67 mbar in the pressure measurements; ± 3.0 μV in the voltage measurements; ± 1.0 mA in the current measurements; and ± 0.125 W in the measurements of total input power to the nichrome wire wrapped around the tube in the evaporator section.

4.3 Variations of GHP Conductance with Fill Ratio and Power Input

The variations of the overall conductance of the GHP (C_{GHP}) with the fill ratio (*FR*) and the nominal values of power input to the evaporator (q_{in}) are shown in Figure 4.3 for the GHP in the vertical orientation ($\theta = 0^o$). As was mentioned in Section 4.1, for *FR* = 50 % the full range of power input to the evaporator (50 W to 250 W, nominal) could be used only with the GHP in the vertical orientation ($\theta = 0^o$); for $\theta \geq 10^o$, the dry-out limit was reached for $q_{in} \geq$ 50 W. Thus, only the $\theta = 0^o$ orientation is considered in this section. The results in Figure 4.3 show that C_{GHP} increases as the power input to the evaporator (q_{in}) is increased for a fixed value of the fill ratio, with the increases in C_{GHP} getting progressively smaller as q_{in} is increased; and for a fixed value of q_{in}, C_{GHP} decreases as the fill ratio is increased, asymptoting to an essential constant value for values of *FR* greater than 120 %. These results are quite similar to those presented and discussed in the published literature (as reviewed in Chapter 1, Section 1.2).

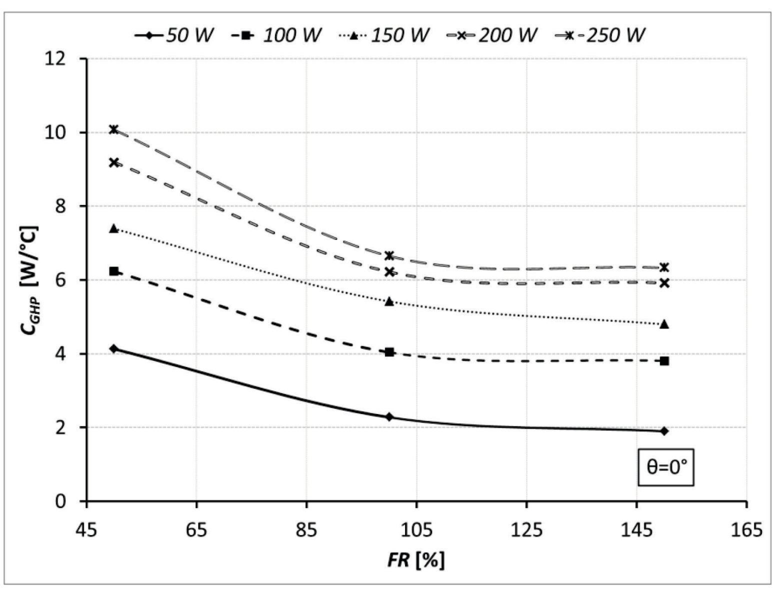

Figure 4.3: Variations of GHP conductance with fill ratio and power input for $\theta = 0^o$.

4.4 Variations of GHP Conductance with Power Input and Tilt Angle

The variations of the overall conductance of the GHP (C_{GHP}) with the power input to the evaporator (q_{in}) and the tilt angle (θ) are shown in Figures 4.4 and 4.5 for *FR* = 100 % and 150 %, respectively. As was mentioned Section 4.1, for *FR* = 50 %, the full range of power input to the evaporator (50 W to 250 W, nominal) could be used only with the GHP in the vertical orientation (θ = 0°); for $\theta \geq$ 10°, the dry-out limit was reached for $q_{in} \geq$ 50 W. Thus, only the results for FR = 100 % and 150 % are presented in this section.

The results in both Figures 4.4 and 4.5 show that C_{GHP} increases as power input to the evaporator (q_{in}) is increased for all values of θ considered, with the increases in C_{GHP} getting progressively smaller as q_{in} is increased for each value of θ. Furthermore, for a fixed value of q_{in}, C_{GHP} decreases as the value of θ is increased. The physical reasoning for this behavior of the GHP have already been presented in the earlier sections of this chapter, so they will not be repeated here.

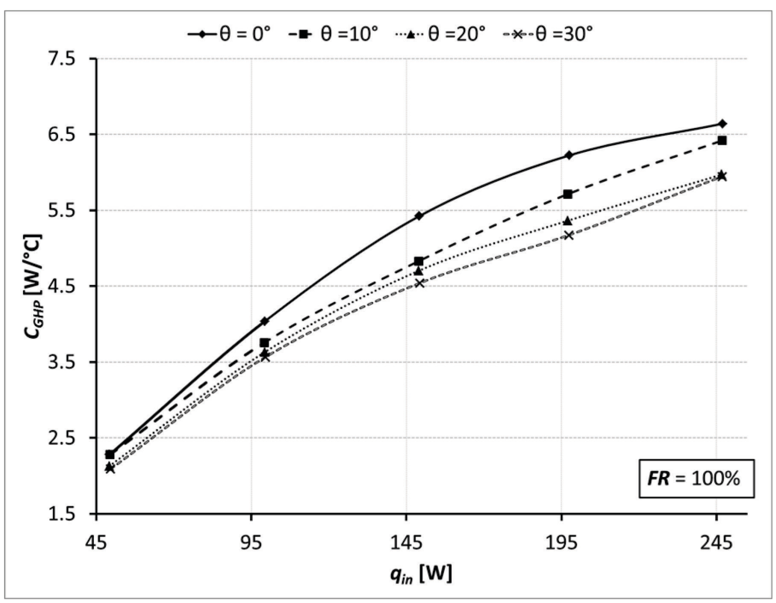

Figure 4.4: Variations of GHP conductance with fill ratio and tilt angle for *FR* = 100 %.

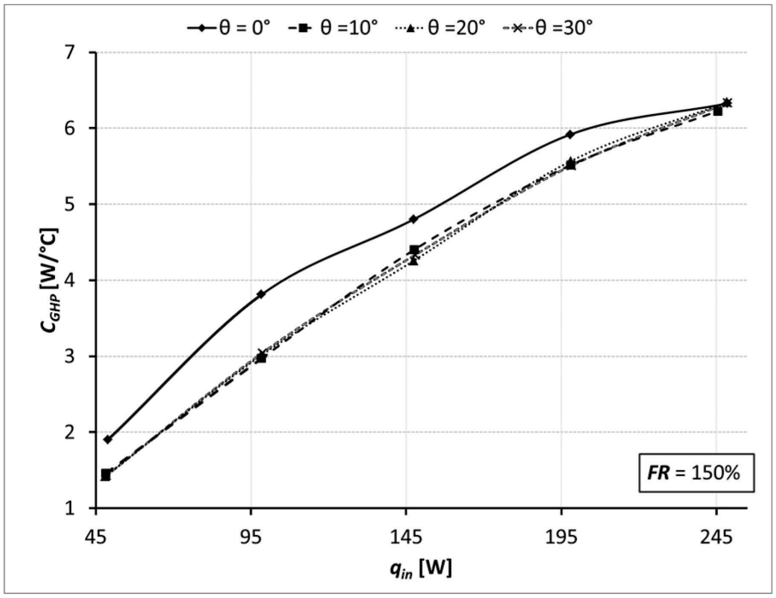

Figure 4.5: Variations of GHP conductance with fill ratio and tilt angle for *FR* = 150 %.

4.5 Variations of Time-Period and Maximum Change of Evaporator-Wall Temperature with Power Input and Tilt Angle during Geyser Boiling

These variations were determined in an approximate manner by examining screen shots of the virtual control panel and display of the experimental data provided by the *National Instruments* LabView program. This program was specially designed, written, and used for data acquisition and control in this work. Examples of such screen shots for conditions corresponding to geyser boiling in the evaporator are shown in Figures 4.6, 4.7, 4.8, and 4.9, for Runs # 11, 12, 31, and 32, respectively. Such screen shots were recorded for all experimental runs in which geyser boiling was encountered (see the summary of the experimental set-up, conditions, and results in Tables 4.1 and 4.2), and they were all similar to those illustrated in Figures 4.6 – 4.9.

It should be noted that the values of t_{period} and $(\Delta T)_{\max}$ were obtained by averaging data from 5-10 candidate oscillations of the measured outer-surface temperatures of the evaporator-tube wall. Another point to note is that in each of the screen shots given in Figures 4.6 – 4.9, the abscissa corresponds to data sets: the elapsed-time between successive data sets was about 4.2 s in the experiments undertaken in this work.

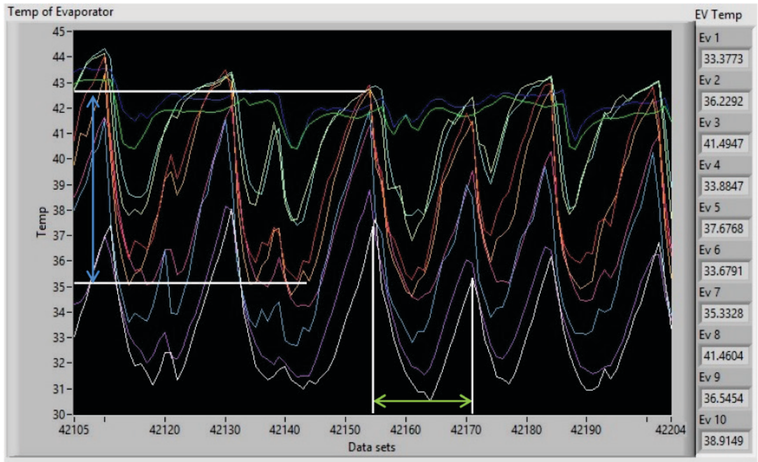

⟷ t_{period} = 56.08 s ⟷ $(\Delta T)_{max}$ = 7.5 °C

Figure 4.6: Variations of temperature at different locations on the outside wall of the evaporator tube for *FR* = 100 %, θ = 0°, and q_{in} = 50 W nominal (Run # 11): the values of t_{period} and $(\Delta T)_{\max}$ represent averages taken over 5-10 oscillations; each data set value corresponds to 4.2 s.

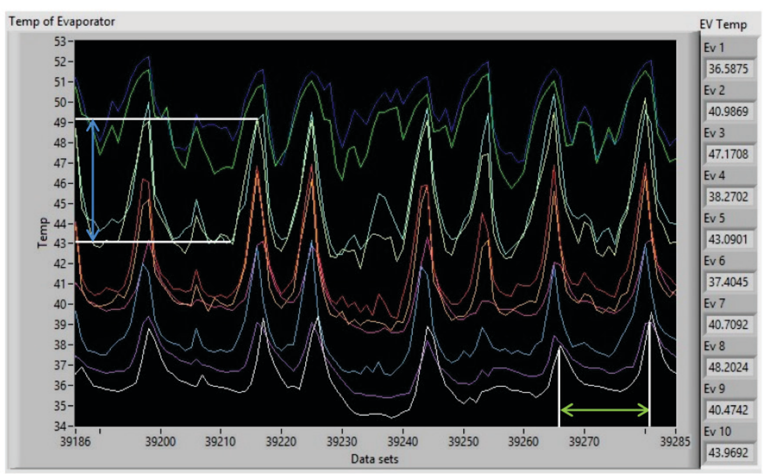

⟷ t_{period} = 28.09 s ⟷ $(\Delta T)_{max}$ = 6.1 °C

Figure 4.7: Variations of temperature at different locations on the outside wall of the evaporator tube for *FR* = 100 %, θ = 0°, and q_{in} = 100 W nominal (Run # 12): the values of t_{period} and $(\Delta T)_{\max}$ represent averages taken over 5-10 oscillations; each data set value corresponds to 4.2 s.

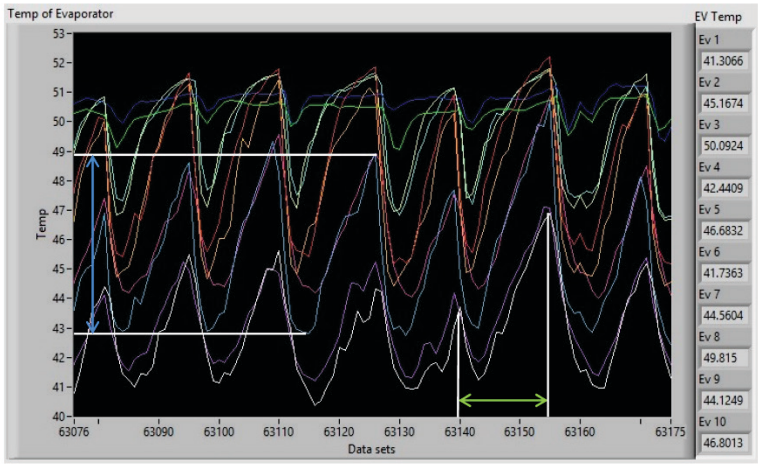

⟷ t_{period} = 43.45 s ⟷ $(\Delta T)_{max}$ = 7.0 °C

Figure 4.8: Variations of temperature at different locations on the outside wall of the evaporator tube for FR = 150 %, θ = 0°, and q_{in} = 50 W nominal (Run # 31): the values of t_{period} and $(\Delta T)_{\max}$ represent averages taken over 5-10 oscillations; each data set value corresponds to 4.2 s.

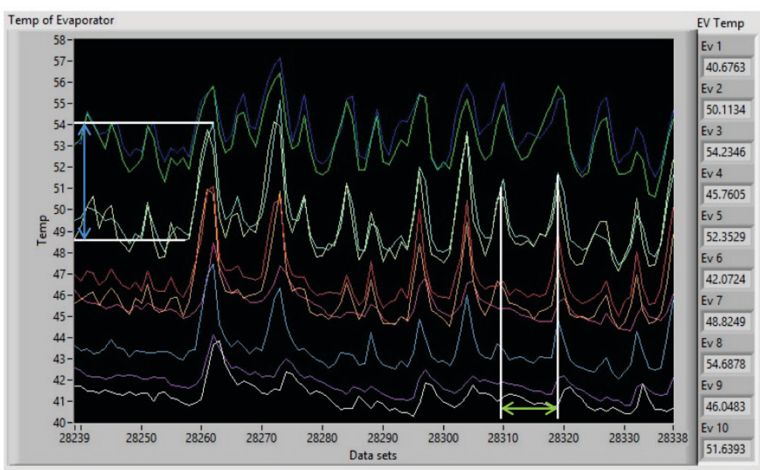

⟷ t_{period} = 26.08 s ⟷ $(\Delta T)_{max}$ = 5.5 °C

Figure 4.9: Variations of temperature at different locations on the outside wall of the evaporator tube for FR = 150%, θ = 0°, and q_{in} = 100 W nominal (Run # 32): the values of t_{period} and $(\Delta T)_{\max}$ represent averages taken over 5-10 oscillations; each data set value corresponds to 4.2 s.

The variations of t_{period} and $(\Delta T)_{\max}$, obtained using the above-mentioned screen shots and procedures, with power input and tilt angle during geyser boiling are displayed in Figures 4.10 and 4.11, respectively, for FR = 100 %; and in Figures 4.12 and 4.13, respectively, for FR = 150 %. Again, such data could not be obtained for FR = 50 % as the dry-out limit was encountered for conditions corresponding to $\theta > 0^{o}$ and $q_{in} > 50$ W (nominal).

The results presented in Figures 4.10 – 4.13 show the following trends:

1) The values of t_{period} decrease with increasing values of q_{in}, as at the higher power inputs, bubbles are generated at increasing number of nucleation sites on the inner surface of the evaporator tube wall, so the geysering occurs with increasing frequency.

2) The values of $(\Delta T)_{\max}$ decrease with increasing values, q_{in}, as with increasing rate of bubble generation (for the reasons given above) there is less time for significant excursions of the temperature of the outer-surface of the evaporator-tube wall.

3) The values of both t_{period} and $(\Delta T)_{\max}$ decrease with increasing values of θ, as with increasing tilt of the GHP from the vertical, the hydraulic head of the water pool in the evaporator decreases, thus increasing the frequency and reducing the intensity of geysering.

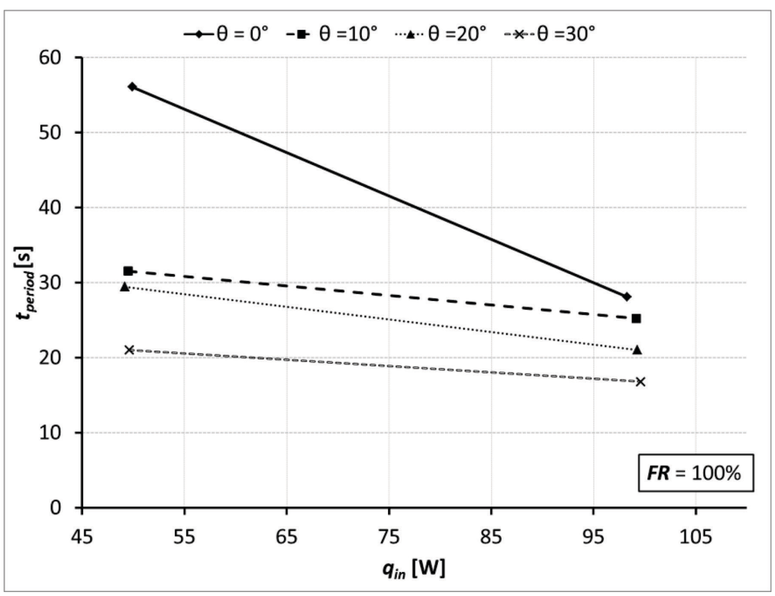

Figure 4.10: Variations of the time-period of the evaporator-wall temperature with power input and tilt angle during geyser boiling for FR = 100 %.

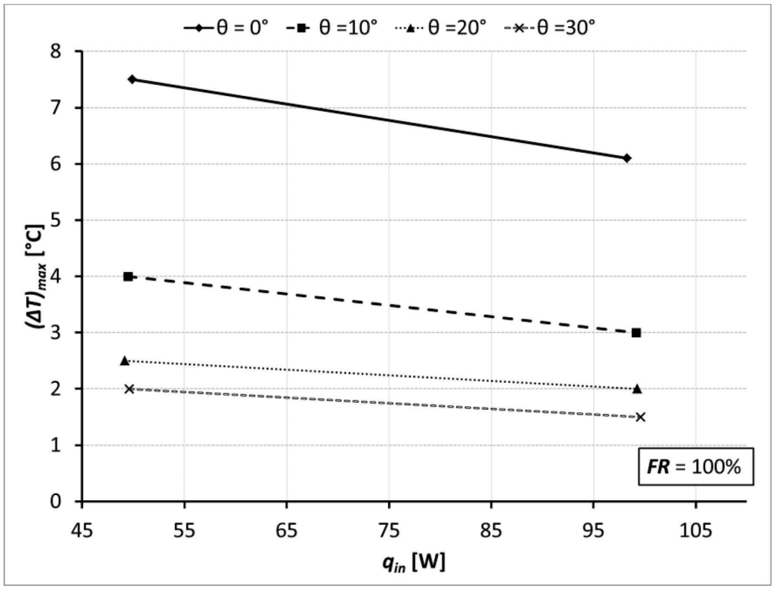

Figure 4.11: Variations of the maximum change of the evaporator-wall temperature with power input and tilt angle during geyser boiling for *FR* = 100 %.

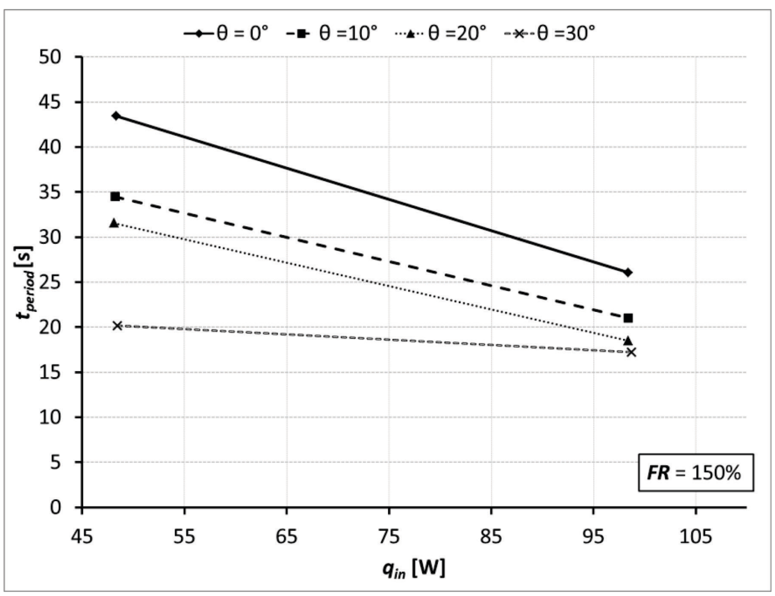

Figure 4.12: Variations of the time-period of the evaporator-wall temperature with power input and tilt angle during geyser boiling for *FR* = 150 %.

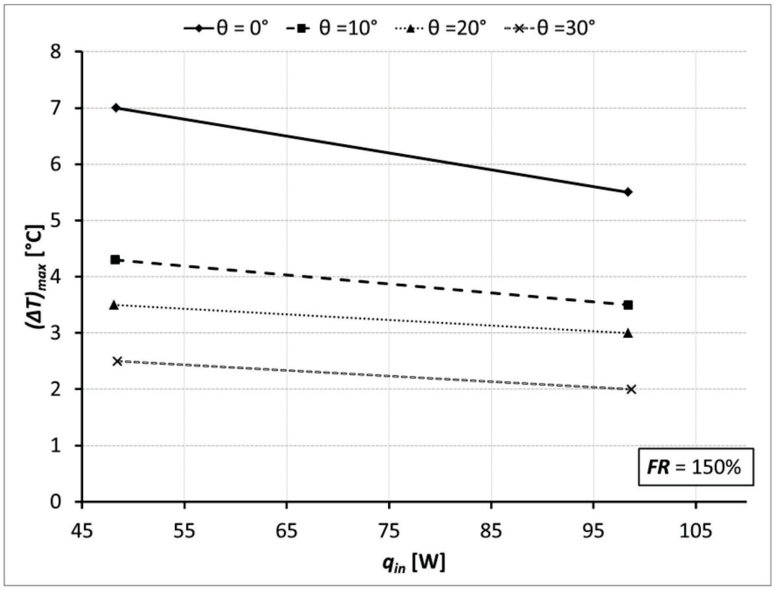

Figure 4.13: Variations of the maximum change of the evaporator-wall temperature with power input and tilt angle during geyser boiling for FR = 150 %.

4.6 Variations of Time-Period and Maximum Change of Evaporator-Wall Temperature with Power Input and Fill Ratio during Geyser Boiling

These results are given in Figures 4.14 and 4.15 below, and followed by the related discussions.

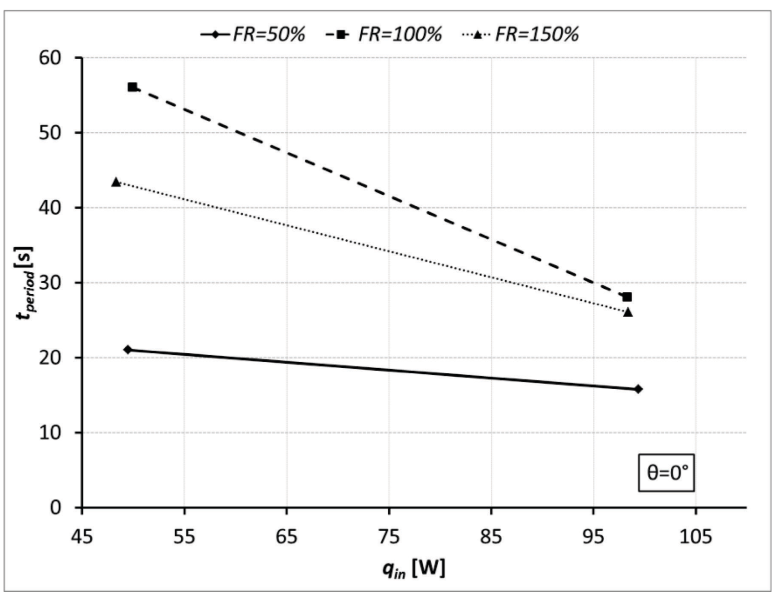

Figure 4.14: Variations of the time-period of the evaporator wall-temperature with power input and fill ratio during geyser boiling for $\theta = 0^{o}$.

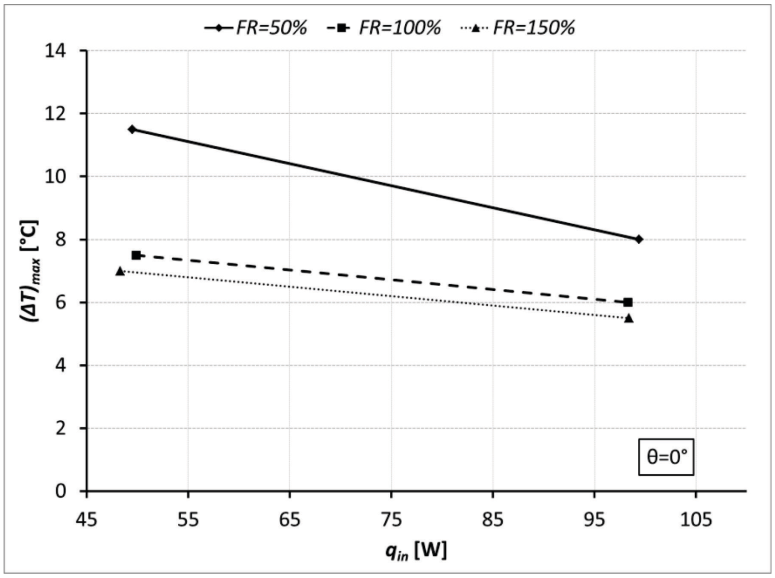

Figure 4.15: Variations of the maximum change of the evaporator-wall temperature with power input and fill ratio during geyser boiling for $\theta = 0^o$.

The variations of t_{period} and $(\Delta T)_{\max}$, obtained using the screen shots and procedures presented in Section 4.5, with power input and fill ratio during geyser boiling are displayed in Figures 4.14 and 4.15, respectively. These results are provided only for $\theta = 0^o$, because (as was discussed earlier) the dry-out limit is encountered for FR > 50 % and q_{in} > 50 W (nominal).

The results presented in Figures 4.14 and 4-15 show the following trends:

1) The values of t_{period} decrease with increasing values of q_{in}, because (as was discussed earlier) at the higher power inputs, bubbles are generated at increasing number of nucleation sites on the inner surface of the evaporator tube wall, so the geyser phenomenon occurs with increasing frequency

2) The values of $(\Delta T)_{\max}$ decrease with increasing values, q_{in}, as with increasing rate of bubble generation (for the reasons given above) there is less time for significant excursions of the temperature of the outer-surface of the evaporator-tube wall.

Chapter 5: Conclusion

This final chapter contains a review of the earlier chapters of this thesis, a summary of the contributions of this work, and some recommendations for extensions of this work.

5.1 Review of the Earlier Chapters of this Thesis

In Chapter 1, the motivation, overall goal, and specific objectives of this work were presented, along with a review of the pertinent published literature.

In Chapter 2, some of the theoretical considerations that were used for developing a basic understanding of the various thermofluid processes that occur within GHPs were discussed briefly. They supplemented the discussions that were already presented earlier in Chapter 1, Section 1.2. The dimensionless geometric parameters and some of the thermofluid parameters that govern GHPs were also presented in Chapter 2, along with their values or ranges applicable to this particular investigation.

Descriptions of the GHP and the experimental set-up that were designed and constructed for this work, and also the related procedures that were used to run the experiments, were presented and discussed in Chapter 3.

In Chapter 4, the experimental results were presented and discussed.

5.2 Main Contributions of this Work

The main contributions of this work are summarized below:

1. A GHP was designed, constructed, and used, along with a supporting experimental set-up, the necessary instrumentation, and calibration
2. Some of the key finding with respect to the design of the GHP and the experimental set-up are the following:
   - Standard *Swagelok* fittings hold vacuum very well for the conditions considered
   - The *Edwards* RV 8 vacuum pump used in this work is capable of handling vacuuming as well as exhausting of the related water vapor (encountered in the experiments), using the gas ballast feature
   - On the vacuum circuit (exhaust) side of the experimental set-up, suitable heating of the tubes, valves, fittings, and vacuum gauges was critically important to

prevent vapor condensation (a simple hair dryer was used to blow hot air past the aforementioned components, and this arrangement worked well)

3. With regard to the characterization of the GHP used in this work, the following findings are worthy of note (the related discussions were provided in Chapter 4):
   - At a fill ratios of $FR \leq 40$ %, the dry-out limit was reached for $q_{in,\,total} > 50$ W (nominal) and $\theta > 0^{o}$
   - With FR = 100 % and 150 %, the GHP ran well for values of $q_{in,\,total}$ between nominal values of 50 W to 250 W, and θ values of 0^{o}, 10^{o}, 20^{o}, and 30^{o}
   - The overall conductance of the GHP, C_{GHP}, increased with increasing values of q_{in} and decreased with increasing values of FR
   - The maximum values of C_{GHP} occurred at $\theta = 0^{o}$ for the GHP and conditions investigated in this work
   - For FR = 50 %, 100 %, and 150 %, geyser boiling occurred for $q_{in,total} \leq 140$ W, and effectively nucleate pool boiling occurred for $q_{in,total} \geq 150$ W

5.3 Recommendations for Extensions of this Work

The following extensions of this work are recommended:

1. GHPs with smaller values of aspect ratio, perhaps ≤ 2, may lead to effective nucleate boiling at lower values of q_{in}. It may also be possible to prevent geyser boiling by introduction metal foams or gauzes inside the evaporator, thereby providing additional nucleation sites for bubbles and/or preventing the agglomeration of bubbles to form bigger bubbles or vapor slugs. It would be useful to undertake experiments to check out these options and their potential benefits.

2. Simple mathematical models, based on empirical correlations for boiling, condensation, and forced convection cooling, and classical thermodynamics, may allow predictions of GHP performance in the nucleate pool boiling regime. It would be very worthwhile to formulate such a model and also benchmark it against the experimental data obtained in this work.

3. It would be useful to try out other working fluids, such as ethanol and refrigerant R134a.

References

Abreu, S. L. and Colle, S. (2004), An experimental study of two-phase closed thermosyphon for compact solar domestic hot-water systems, *Solar Energy*, **76**, 141-145.

Alizadehdakhel, A., Rahimi, M., and Alsairafi, A. A. (2010), CFD modeling of flow and heat transfer in a thermosyphon, *International Communications in Heat and Mass Transfer*, **37**, 312-318.

Amatachaya, P. and Srimuang, W. (2010), Comparative heat transfer characteristics of a flat two-phase closed thermosyphon (FTPCT) and a conventional two-phase closed thermosyphon (CTPCT), *International Communications in Heat and Mass Transfer*, **37**, 293-298.

Azad, E., Bahar, F., and Moztarzadeh, F. (1985), Design of water-to-air gravity-assisted heat pipe heat exchanger, *Journal of Heat Recovery Systems*, **5**, 89-99.

Azad, E. and Geoola, F. (1984), A design procedure for gravity-assisted heat pipe heat exchange, *Journal of Heat Recovery Systems*, **4**, 101-111.

Carey, V. P. (1992), *Liquid-vapor phase change phenomena, an introduction of vaporization and condensation processes in heat transfer equipment*, Taylor & Francis, Washington D.C.

Casarosa, C., Latrofa, E., and Shelginski, A. (1983), The geyser effect in a two-phase thermosyphon, *International Journal of Heat and Mass Transfer*, **26**, 933-941.

Casarosa, C. and Dobran, F. (1988), Experimental investigation and analytical modeling of a closed two-phase thermosyphon with imposed convection boundary conditions, *International Journal of Heat and Mass Transfer*, **31**, 1815-1833.

Chen, S.J., Reed, J.G., and Tien, C.L. (1984), Reflux condensation in a two-phase closed thermosyphon, *International Journal of Heat and Mass Transfer*, **27**, 1587-1594.

Chi, S.W. (1976), *Heat Pipe Theory and Practice: A Sourcebook*, Hemisphere Publishing, Washington D.C.

Cotter, T. P. (1965), *Theory of Heat Pipes*, Los Alamos Scientific Laboratory, Report No. LA-3246-MS, Albuquerque, New Mexico.

Danielewicz, J., Sayegh, M.A., Sniechowska, B., Szulgowska-Zgrzywa, M., and Jouhara, H. (2014), Experimental and analytical performance investigation of air to air two phase closed thermosyphon based heat exchangers, *Energy*, **77**, 82-87.

Dhir, V. and Lienhard, J. (1971), Laminar film condensation on plane and axisymmetric bodies in non-uniform gravity, *ASME Journal of Heat Transfer*, **93**, 97-100.

Dobran, F. (1985), Steady-state characteristics and stability thresholds of a closed two-phase thermosyphon, *International Journal of Heat and Mass Transfer*, **28**, 949-957.

Dobson, M. K. and Chato, J. C. (1998), Condensation in smooth horizontal tubes, *ASME Journal of Heat Transfer*, **120**, 193-213.

Dowden, J., Kapadia, P., Brown, G., and Rymer, H. (1991), Dynamics of a geyser eruption, *Journal of Geophysical Research*, **96**, 18059-18071.

Du, J., Bansal, P., and Huang, B. (2012), Simulation model of a greenhouse with a heat-pipe heating system, *Applied Energy*, **93**, 268-276.

Dunn, P. D. and Reay, D. (2012), *Heat pipes,* Elsevier, New York.

El Hajal, J., Thome, J. R., and Cavallini, A. (2003), Condensation in horizontal tubes, part 1: two-phase flow pattern map, *International Journal of Heat and Mass Transfer*, **46**, 3349-3363.

El-Genk, M. S. and Saber, H. H. (1997), Flooding limit in closed, two-phase flow thermosyphons, *International Journal of Heat and Mass Transfer*, **40**, 2147-2164.

El-Genk, M. S. and Saber, H. H. (1999), Determination of operation envelopes for closed, two-phase thermosyphons, *International Journal of Heat and Mass Transfer*, **42**, 889-903.

Fadhl, B., Wrobel, L. C., and Jouhara, H. (2013), Numerical modelling of the temperature distribution in a two-phase closed thermosyphon, *Applied Thermal Engineering*, **60**, 122-131.

Fadhl, B., Wrobel, L. C., and Jouhara, H. (2015), CFD modelling of a two-phase thermosyphon charged with R134a and R404a, *Applied Thermal Engineering*, **78**, 482-490.

Faghri, A. (1995), *Heat pipe science and technology,* Global Digital Press.

Faghri, A. (2012), Review and advances in heat pipe science and technology, *ASME Journal of Heat Transfer*, **134**, 123001-1-18.

Faghri, A. (2014), Heat pipes: Review, opportunities and challenges, *Frontiers in Heat Pipes*, **5**, 1-48, Global Digital Central.

Farsi, H., Joly, J. L., Miscevic, M., Platel, V., and Mazet, N. (2003), An experimental and theoretical investigation of the transient behavior of a two-phase closed thermosyphon, *Applied Thermal Engineering*, **23**, 1895-1912.

Fox, R.W. and McDonald, A.T. (1985), Introduction to Fluid Mechanics, 3rd Edition, John Wiley, New York.

Gaugler, R.S. (1944), *Heat Transfer Device*, *US Patent 2350348*, Applied December 21, 1942, Published June 1, 1994.

Grooten, M. H. M., Van der Geld, C. W. M., and Van Deurzen, L. G. M. (2008), A study of flow patterns in a thermosyphon for compact heat exchanger applications, in *Proceedings of the Fifth International Conference on Transport Phenomena in Multiphase Systems*, June 30 – July 3, Bialystock, Poland, 1-7.

Grover, G.M. (1966), *Evaporation-Condensation Heat Transfer Device*, *US Patent 3229759*, Applied December 2, 1963, Published January 18, 1966.

Grover, G. M., Cotter, T. P., and Erickson, G. F. (1964), Structures of very high thermal conductance, *Journal of Applied Physics*, **35**, 1990-1991.

Harley, C. and Faghri, A. (1994), Complete transient two-dimensional analysis of two-phase closed thermosyphons including the falling condensate film, *ASME Journal of Heat Transfer*, **116**, 418-426.

Haynes, F.D., Zarling, J.P., and Gooch, G.E. (1992), Performance of a thermosyphon with a 37-meter-long, horizontal evaporator, *Cold Regions Science and Technology*, **20**, 261-269.

Hewitt, G.F. (1998), Boiling, in *Handbook of Heat Transfer*, 3rd Edition, W.M. Rohsenow, J.P. Hartnett, and Y.I. Cho (Eds.), Chapter 15, McGaw-Hill, New York.

Huikata, K., Chen, S.J., and Tien, C.L. (1984), Non-condensable gas effect on condensation in a two-phase closed thermosyphon, *International Journal of Heat and Mass Transfer*, **27**, 1319-1325.

Hussein, H. M. S., El-Ghetany, H. H., and Nada, S. A. (2006), Performance of wickless heat pipe flat plate solar collectors having different pipes cross sections geometries and filling ratios, *Energy Conversion and Management*, **47**, 1539-1549.

Imura, H., Sasaguchi, K., Kozai, H., and Numata, S. (1983), Critical heat flux in a closed two-phase thermosyphon, *International Journal of Heat and Mass Transfer*, **26**, 1181-1188.

Incropera, F.P. and DeWitt, D.P. (2002), *Fundamentals of Heat and Mass Transfer*, Fifth Edition, John Wiley, Hoboken, New Jersey.

Jafari, D., Franco, A., Filippeschi, S., and Di Marco, P. (2016), Two-phase closed thermosyphons: A review of studies and solar applications, *Renewable and Sustainable Energy Reviews*, **53**, 575-593.

Japikse, D. (1973), Advances in thermosyphon technology, *Advances in Heat Transfer*, **9**, 1-111.

Joudi, K. A. and Witwit, A. M. (2000), Improvements of gravity assisted wickless heat pipes, *Energy Conversion and Management*, **41**, 2041-2061.

Jouhara, H. and Robinson, A. J. (2010), Experimental investigation of small diameter two-phase closed thermosyphons charged with water, FC-84, FC-77 and FC-3283, *Applied Thermal Engineering*, **30**, 201-211.

Khazaee, I., Hosseini, R., and Noie, S. H. (2010), Experimental investigation of effective parameters and correlation of geyser boiling in a two-phase closed thermosyphon, *Applied Thermal Engineering*, **30**, 406-412.

Kim, S.J. and No, H.C. (2000), Turbulent film condensation of high pressure steam in a vertical tube, *International Journal of Heat and Mass Transfer*, **43**, 4031-4042.

King, C.R. (1931), Perkins hermetic tube boiler, *The Engineer*, **152**, 405-406.

Kubin, M., Hirs, J., and Plasek, J. (2016), Experimental analysis of steam condensation in vertical tube with small diameter, *International Journal of Heat and mass Transfer*, **94**, 403-410.

Kuncoro, H., Rao, Y.F., and Fukuda, K. (1995), An experimental study on the mechanism of geysering in a closed two phase thermosyphon, *International Journal of Multiphase Flow*, **21**, 1243-1252.

Lee, Y. and Mittal, U. (1972), A two-phase closed thermosyphon, *International Journal of Heat and Mass Transfer*, **15**, 1695-1707.

Li, H., Akbarzadeh, A., and Johnson, P. (1991), The thermal characteristics of a closed two-phase thermosyphon at low temperature difference, *Heat Recovery Systems and CHP*, **11**, 533-540.

Lighthill, M. J. (1953), Theoretical considerations on free convection in tubes, Quart. J. Mech. Appl. Math., 6, 398–439.

Lin, S., Broadbent, J., and McGlen, R. (2005), Numerical study of heat pipe application in heat recovery systems, *Applied Thermal Engineering*, **25**, 127-133.

Lin, T.F., Lin, W.T., Tsay, Y.L., Wu, J.C., and Shyu, R.J. (1995), Experimental investigation of geyser boiling in an annular two-phase closed thermosyphon, *International Journal of Heat and Mass Transfer*, **38**, 295-307.

Ma, C., Wu, X., and Gao, S. (2013), Analysis and applications of a two-phase closed thermosyphon for improving the fluid temperature distribution in well bores, *Applied Thermal Engineering*, **55**, 1-6.

Martin, B. W. (1955), Free convection in an open thermosyphon, with special reference to turbulent flow, *Proceedings of the Royal Society of London A: Mathematical, Physical and Engineering Sciences*, **230**, No. 1183, pp. 502-530.

Marto, P.J. (1998), Condensation, in *Handbook of Heat Transfer*, 3rd Edition, W.M. Rohsenow, J.P. Hartnett, and Y.I. Cho (Eds.), Chapter 14, McGaw-Hill, New York.

Mathioulakis, E. and Belessiotis, V. (2002), A new heat-pipe type solar domestic hot water system, *Solar Energy*, **72**, 13-20.

Mikic, B.B. and Rohsenow, W.M. (1969), A new correlation of pool boiling data including the effect of heating surface characteristics, *ASME Journal of Heat Transfer*, **91**, 245-250.

Moissis, R. and Berenson, P.J. (1963), On the hydrodynamic transitions in nucleate boiling, *ASME Journal of Heat Transfer*, **83**, 221-226.

Murphy, D.W. (1965), An experimental investigation of geysering in vertical tubes, in Advances in Cryogenic Engineering, K.D. Timmerhaus (Ed.), Springer, New York, Chapter I-7, 353-359.

Nguyen-Chi, H. and Groll, M. (1981), Entrainment or flooding limit in a closed two-phase thermosyphon, *Journal of Heat Recovery Systems*, **1**, 275-286.

Noie, S. H. (2005), Heat transfer characteristics of a two-phase closed thermosyphon, *Applied Thermal Engineering*, **25**, 495-506.

Noie, S. H., Sarmasti Emami, M. R., and Khoshnoodi, M. (2007), Effect of inclination angle and filling ratio on thermal performance of a two-phase closed thermosyphon under normal operating conditions, *Heat Transfer Engineering*, **28**, 365-371.

Nukiyama, S. (1966), The maximum and minimum values of the heat Q transmitted from metal to boiling water under atmospheric pressure, *International Journal of Heat and Mass Transfer*, **9**, 1419-1433 (originally published in 1934, in the Journal of the Japan Society of Mechanical Engineers, **37**, 367-374).

Nusselt, W. (1916), Die oberflachenkoondensation des wasserdampfes (rough translation of German to English: The surface condensation of water vapor), *Z. Ver. Deut. Ing.*, **60**, 541-546.

Pashkevich, R.I. and Muratov, P.V. (2015), Film condensation in a large diameter tube with upward flow, *International Journal of Heat and Mass Transfer*, **81**, 804-810.

Payakaruk, T., Terdtoon, P., and Ritthidech, S. (2000), Correlations to predict heat transfer characteristics of an inclined closed two-phase thermosyphon at normal operating conditions, *Applied Thermal Engineering*, **20**, 781-790.

Perkins, J. (1836), *United Kingdom Patent 7059*, Published April 1836.

Peterson, G.P. (1998), Heat Pipes, in *Handbook of Heat Transfer*, 3rd Edition, W.M. Rohsenow, J.P. Hartnett, and Y.I. Cho (Eds.), Chapter 12, McGaw-Hill, New York.

Reay, D., McGlen, R., and Kew, P. (2013), *Heat pipes: Theory, design and applications,* Butterworth-Heinemann, New York.

Reed, J.G. and Tien, C.L. (1987), Modeling of the two-phase closed thermosyphon, *ASME Journal of Heat Transfer*, **109**, 722-730.

Rohsenow, W.M. (1952), A method of correlating heat transfer data for surface boiling of liquids, *Transactions of the ASME*, **74**, 969-976.

Rohsenow, W.M. (1973), Boiling, in *Handbook of Heat Transfer*, W.M. Rohsenow and J.P. Hartnett (Eds.), Chapter 13, McGraw-Hill, New York.

Rohsenow, W.M. (1985), Film condensation, *in Handbook of Heat Transfer Fundamentals*, W.M. Rohsenow, J.P. Hartnett, and E.N. Ganić (Eds.), 2nd Edition, Chapter 11, 1-36, McGraw-Hill, New York.

Seban, R.A. and Hodgson, J. (1982), Laminar film condensation in a tube with upward vapor flow, *International Journal of Heat and Mass Transfer*, **25**, 1291-1300.

Seban, R.A. and Faghri, A. (1984), Film condensation in a vertical tube with a closed top, *International Journal of Heat and Mass Transfer*, **27**, 944-948.

Shabgard, H., Robak, C. W., Bergman, T. L., and Faghri, A. (2012), Heat transfer and exergy analysis of cascaded latent heat storage with gravity-assisted heat pipes for concentrating solar power applications, *Solar Energy*, **86**, 816-830.

Shiraishi, M., Kikuchi, K., and Yamanishi, T. (1981), Investigation of heat transfer characteristics of a two-phase closed thermosyphon, *Journal of Heat Recovery Systems*, **1**, 287-297.

Shiraishi, M., Terdtoon, P., and Murakami, M. (1995), Visual study on flow behavior in an inclined two-phase closed thermosyphon, *Heat Transfer Engineering*, **16**, 53-59.

Terdtoon, P., Chailungkar, M., Ritthidej, S., and Shiraishi, M. (1997), Effects of Bond numbers on internal flow patterns of an inclined, closed, two-phase thermosyphon at normal operating conditions, *Experimental Heat Transfer*, **10**, 233-251.

Thome, J.R. (2003), On recent advances in modeling two-phase flow and heat transfer, *Heat Transfer Engineering*, **24**, 46-59.

Thumm, S., Philipp, Ch., and Gross, U. (2001), Film condensation of water in a vertical tube with countercurrent vapour flow, *International Journal of Heat and Mass Transfer*, **44**, 4245-4256.

Tien, C. L. (1975), Fluid mechanics of heat pipes, *Annual Review of Fluid Mechanics*, **7**, 167-185.

Tsai, T. E., Wu, H. H., Chang, C. C., and Chen, S. L. (2010), Two-phase closed thermosyphon vapor-chamber system for electronic cooling, *International Communications in Heat and Mass Transfer*, **37**, 484-489.

Wadowski, T., Akbarzadeh, A., and Johnson, P. (1991), Characteristics of a gravity-assisted heat pipe-based heat exchanger, *Heat Recovery Systems and CHP*, **11**, 69-77.

Wang, J.C.Y. and Ma, Y. (1991), Condensation heat transfer inside vertical and inclined thermosyphons, *ASME Journal of Heat Transfer*, **113**, 777-780.

Wangnippanto, S. (1994), Study of evaporation and condensation performance in thermosyphon, *Doctoral dissertation*, KMITT, Thailand (in Thai).

Whalley, P.B. (1996), *Two-Phase Flow and Heat Transfer*, Oxford Science Publications, Oxford University Press, Oxford, U.K.

Xu, J. and Goering, D. J. (2008), Experimental validation of passive permafrost cooling systems, *Cold Regions Science and Technology*, **53**, 283-297.

Yang, F., Yuan, X., and Lin, G. (2003), Waste heat recovery using heat pipe heat exchanger for heating automobile using exhaust gas, *Applied Thermal Engineering*, **23**, 367-372.

Zhang, X. and Che, H. (2013), Reducing heat loss of fluids in heavy oil wellbore using two-phase closed thermosyphon sucker rod, Energy, **57**, 352-358.

Zhou, X. and Collins, R.E. (1991), Measurement of condensation heat transfer in a thermosyphon, *International Journal of Heat and Mass Transfer*, **34**, 369-376.

Zuo, Z. J. and Gunnerson, F. S. (1995), Heat transfer analysis of an inclined two-phase closed thermosyphon, *ASME Journal of Heat Transfer*, **117**, 1073-1075.